Spring 1967

Energy transfer and electron conduction in the fluid transpiration arc column

Pin-Seng Tschang
New Jersey Institute of Technology

Copyright Warning & Restrictions

The copyright law of the United States (Title 17, United States Code) governs the making of photocopies or other reproductions of copyrighted material.

Under certain conditions specified in the law, libraries and archives are authorized to furnish a photocopy or other reproduction. One of these specified conditions is that the photocopy or reproduction is not to be "used for any purpose other than private study, scholarship, or research." If a, user makes a request for, or later uses, a photocopy or reproduction for purposes in excess of "fair use" that user may be liable for copyright infringement,

This institution reserves the right to refuse to accept a copying order if, in its judgment, fulfillment of the order would involve violation of copyright law.

Please Note: The author retains the copyright while the New Jersey Institute of Technology reserves the right to distribute this thesis or dissertation

Printing note: If you do not wish to print this page, then select "Pages from: first page # to: last page #" on the print dialog screen

67-14,249

TSCHANG, Pin-Seng, 1934-
ENERGY TRANSFER AND ELECTRON CONDUCTION IN THE FLUID TRANSPIRATION ARC COLUMN.

Newark College of Engineering, D. Eng. Sc., 1967
Physics, electronics and electricity

University Microfilms, Inc., Ann Arbor, Michigan

ENERGY TRANSFER AND ELECTRON CONDUCTION IN THE FLUID TRANSPIRATION ARC COLUMN

BY

PIN-SENG TSCHANG

A DISSERTATION

PRESENTED IN PARTIAL FULFILLMENT OF

THE REQUIREMENTS FOR THE DEGREE

OF

DOCTOR OF ENGINEERING SCIENCE IN ELECTRICAL ENGINEERING

AT

NEWARK COLLEGE OF ENGINEERING

Newark, New Jersey

1967

To

MY PARENTS

for

THE UPBRINGING

and

to

SHIRLEY

for

PATIENCE and ENCOURAGEMENT

ABSTRACT

The energy relaxation and electrical conductivity of an electron gas in one atmosphere argon arc discharge has been examined theoretically and observed quantitatively in an experimental arrangement. The plasma column utilized for study is the type generated in a fluid transpiration arc equipment in which the argon working fluid is injected through a porous graphite anode. The rate of forced convection is such as to insure significant electron-heavy particle nonequilibrium in the sample volume of interest. A simple model of a developing arc column with internal heat generation indicates that, with typical rates of argon injection realized in practice, the development of the column in the axial direction from a constant radial profile to a nearly fully-developed profile requires several cm, of which the first cm or so may be characterized as quasi one-dimensional in z. This region is large enough to allow transient probings and spectrometric observations the results of which can then be compared in a straight forward manner with a theoretical one-dimensional model. An examination of the various relaxation times in a three-component fluid (electron-ion-neutral) reveals that the self-relaxation times are short and the electron-heavy particle relaxation times

are not negligible compared with the transit times through the nonequilibrium volume. It is therefore proper to employ the usual two-temperature macroscopic model equations obtained from the Boltzmann equation. Accordingly, the electrical conductivity and the two-temperature volume rates of energy transfer have been obtained. The diagnostic techniques utilized include (1) Hall-effect magnetic field probe for current density, (2) floating electrostatic probe for electric field, (3) spherical thermocouple heat transfer probe for heavy particle temperature, and, (4) continuum intensity measurement for electron density and temperature. High-speed motion pictures give qualitative measure of the plasma volume and its reaction to a material probe.

The results indicate that while somewhat higher electrical conductivities are observed the volume rates of energy transfer show fairly wide discrepancy between theory and experiment. Thus, although electron energy loss is observed to be due to volume transfer to the heavy particles the familiar current density compatibility relation, $J = n_e e\sqrt{3k(T_e - T_s)/m_s}$ appears not to hold. This is ascribed to the possibility that the collision frequency for momentum transfer and the collision frequency for energy transfer may not be the same. In particular, the observed collision frequency for energy

transfer between electron and ion appears to be one fifth of that magnitude predicted by current theories. It is suggested that a modified theory is needed for the particular condition of low n_D (the number of electrons within a Debye sphere) for $n_e \approx 2 \times 10^{16}$ cm^{-3} and $T_e \approx 10^4$ ^oK.

APPROVAL OF DISSERTATION

ENERGY TRANSFER AND ELECTRON CONDUCTION

IN THE FLUID TRANSPIRATION ARC COLUMN

BY

PIN-SENG TSCHANG

FOR

DEPARTMENT OF ELECTRICAL ENGINEERING

NEWARK COLLEGE OF ENGINEERING

BY

FACULTY COMMITTEE

APPROVED: _____ CHAIRMAN

_____

_____

_____

NEWARK, NEW JERSEY
FEBRUARY, 1967

ACKNOWLEDGEMENTS

The author is indebted to Dr.M.Zambuto for critical reading of the dissertation and for suggesting numerous improvements, to Dr.C.Sheer for advice and encouragement, to Mr.M.Gelband for competent and valuable laboratory assistance, and to Mr.C.Stojanoff for discussions particularly on spectroscopy and for his design of the photomultiplier tube setup.

The experimental work and the preparation of the dissertation were performed under contracts AF49(638)-1395 for the Mechanics Division of the Air Force Office of Scientific Research, and, AF33(615)-3165, AF33(615)-1141 for the ThermoMechanics Laboratory of the Aerospace Research Laboratories, Wright-Patterson AFB, Ohio. The work was carried out in the Electronics Research Laboratories of Columbia University. The active cooperation of the ERL staff, under the direction of Prof.L.H.O'Neill, is gratefully acknowledged.

The Newark College of Engineering Research Foundation furnished partial financial assistance in the early exploratory phase of this dissertation research when the author was teaching in the College.

TABLE OF CONTENTS

LIST OF FIGURES

FIGURE Page

FIGURE Page

LIST OF TABLES

Chapter 1

INTRODUCTION

During the past decade, the efforts to extend ordinary fluid and particle dynamics into the regime of the ionized state have produced a vast output of new works in magnetofluiddynamics, ion propulsion, thermonuclear fusion as well as a greatly intensified renewal of interests in laboratory gas discharges, atmospheric discharges, particle dynamics and gas transport processes.

The behavior of an ionized gas is truly complex. For, all the complexities of ordinary gas, viz. as a consequence of its deformability, compressibility, shear(viscosity), energy transport(thermal conduction, convection), variable state properties(density, energy states), etc. are manifolded by the circumstance of ionization. That is, in ionized media we must also consider the interacting charged particles, their interplay with electrostatic and magnetic fields, multiplication of types of particles and various quantum effects etc.

The complexity of ionized gases is of such a degree that a treatment general enough to be valid under all of the possible conditions of an ionized gas

would be impossible. To make the problem manageable the discussion is limited to ranges of possible conditions, so that for purposes of analysis a differentiation between "domains" of ionized gas states is made, generally on the following bases:

High energy	-	Low energy
Fully ionized	-	Weakly ionized
Quantum	-	Classical
Kinetic formulation	-	Phenomenological formulation
Continuum fluid	-	Rarefied(free-molecule) gas
Multi-component gas	-	Single-component gas
Plasma(electrically neutral)	-	Non-plasma
Steady state	-	Transient
Strong EM interaction	-	Weak EM interaction

Also, theoretical approaches and experimental approaches to the problem are generally considered separately and their interrelations subsequently investigated and verified.

Hopefully, restriction to a partial domain of the ionized state would render the specific problem at hand sufficiently tractable to be solved but not so simple as to lose relevance to the general cases. The danger of departing from such a balance is ever present in

researches in ionized gases.

In this dissertation we have directed our investication to some properties of a one atmosphere argon arc column which may be characterized as:

> A direct current, steady state, partly-ionized, moderately dense classical plasma of medium energy and considered to obey a continuum fluid, kinetic formulation with its multicomponents partially in nonequilibrium, and, subject to a weak electrostatic force and a negligible magnetic field.

There appears to be no unique definition available of an arc discharge and we shall not try to supply one. For the moment, it is convenient to consider an arc as a low-voltage and self-sustained quasi steady-state gas discharge of high temperature and capable of conducting large currents. In contrast, the glow discharge occurs generally in a low temperature gas with higher voltage and lower currents. The spark discharge, on the other hand, is unsteady and of even higher voltage.

The region occupied by arc discharge in the ionized gas domain is depicted in Fig.1. The electron energy is typically one or more ev(1 ev corresponds approximately to $7700^{o}K$ in thermal kinetic energy)

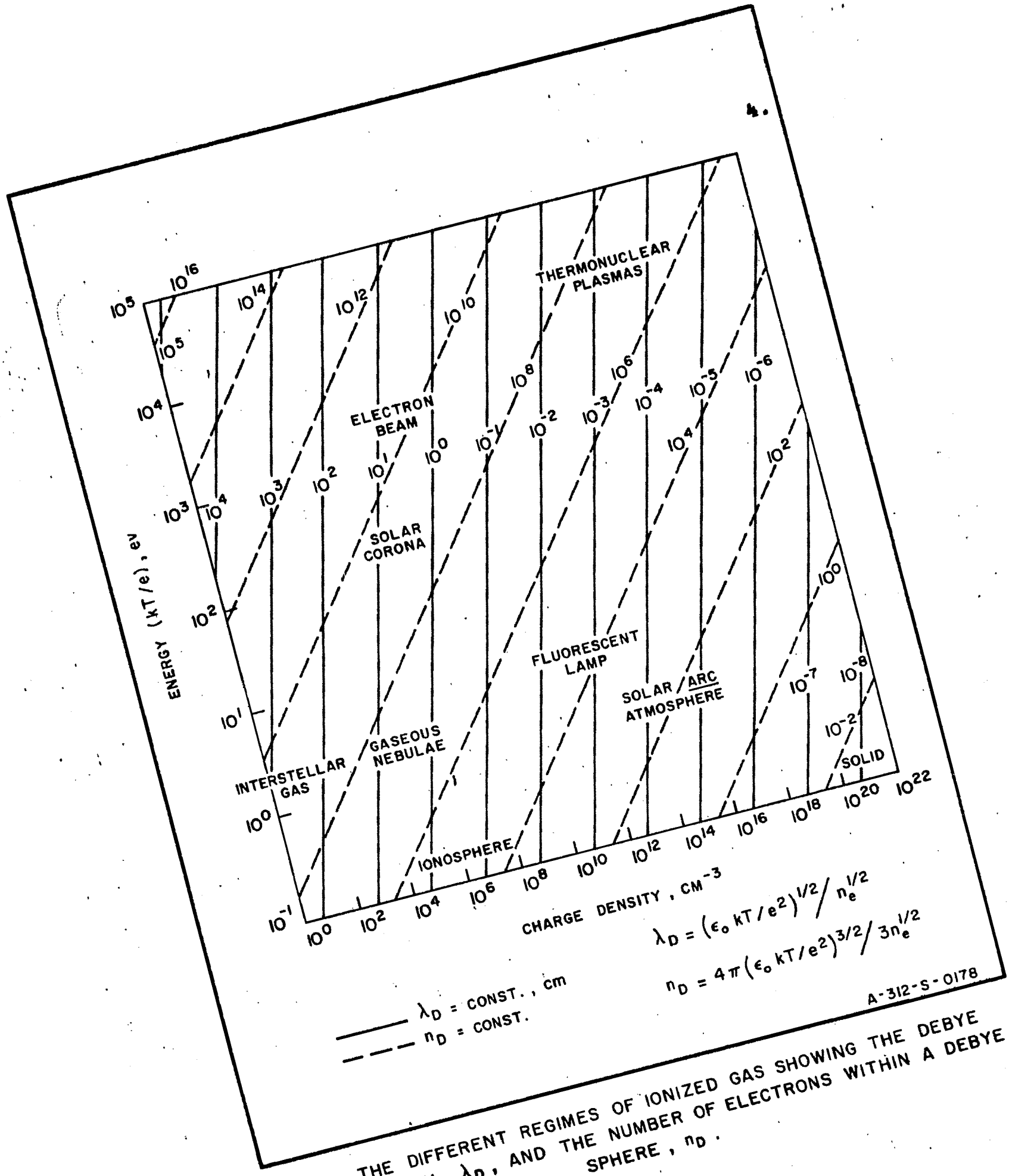

FIG. 1 THE DIFFERENT REGIMES OF IONIZED GAS SHOWING THE DEBYE LENGTH, λ_D, AND THE NUMBER OF ELECTRONS WITHIN A DEBYE SPHERE, n_D.

and, the electron density somewhere between 10^{16} and 10^{17} cm^{-3}.

While this magnitude of energy is very small in comparison with that of fusion plasmas it is significantly higher than that released in any chemical reactions. Remarkable also, is the relatively high charge concentration easily achieved in an arc. These are the main reasons for the great importance of arc technology of which more will be said later.

From the Debye lengths indicated in Fig.1, we see that for an arc of ordinary dimensions(e.g. 1 cm^3) the Debye length of around 10^{-5} cm is exceedingly small and, accordingly, most of the arc column is in a plasma state.

Though the arc region that has been singled out of the vast domain of ionized gas may seem small, arc phenomena involve so many physical laws that the overall picture remains highly complex.

To be sure, the physical laws related to arcs are, for the most part, reasonably well established. One might be tempted to say that knowledge in arcs is represented by the sum of the individual disciplines involved. One would therefore expect that advances in these disciplines should naturally lead to greater understanding

in arc physics. An example of this is the application of the theory of gravitational particle dynamics developed in astrophysics to the interaction of swarms of charged particles in plasmas. The same may seem to hold for experimentation as, for instance, in the case of spectroscopic techniques so nicely passed on by astrophysicists.

But, where so many disciplines are involved, the converse is also true. All too frequently, one is confronted during investigation by obstacles not necessarily in the main line of research which nevertheless are quite effective in delaying accomplishments. Thus, one who is interested in solving the arc equations will find that reliable transport coefficients are lacking. Sometimes, conceptual difficulties arise and one is not quite sure what equations to use or what experimental techniques to rely on.

In the face of such uncertainties there is a tendency to resort to refinements of pure theory which may have little practical relevance, or, to practice empiricism contributing little to clarification of theory.

In order to avoid this pitfall in this dissertation we shall strictly adhere to the following line of app-

roach:

(1) Production of a "laboratory-controlled" type of arc in which the physical laws involved act under conditions amenable to a manageable theoretical form.

(2) Development of a suitable theoretical model from which predictions are made about measurable quantities.

(3) Development of experimental techniques for reliable and sufficiently precise measurements of the above quantities.

(4) Comparison of theoretical prediction to experimental results and conclusions about the degree of validity of the theory.

Present day arc research is mainly concerned with three principal areas of interest, namely, the arc interaction with:

(1) Material boundary

(2) Magnetic field

and, (3) Fluid flow considerations.

In the first category belong the electrode phenomena, important for the maintainance of the discharge, and the effects of lateral material walls in stabilizing and enhancing arc performance. The application of

magnetic field, of course, leads to the wide field of magnetofluiddynamics.

The importance of fluid flow concepts can best be emphasized by pointing out that electrons and ions (essential ingredients of an arc) may be considered as fluid components. Their interaction with a third fluid, e.g. the neutral atoms of the ambient atmosphere, plays an important role in arc behavior. This is true even though this third fluid may not be intentionally introduced. For instance, we see that the appearance of a curvature in a long arc column is due to the gravitational (natural) convection of the surrounding gas, which is usually present despite the wishes of the investigator.

Conversely, the forced convection of a "working fluid" through the arc zone results in a whole genre of arc phenomena with widespread implications in many branches of technology. For example, forced convection is an important factor in arc heaters, MFD accelerators and generators, circuits breakers, etc.

In accordance with our premises, we shall address ourselves to the effects of arc behavior under a fluid flow by forced convection. To simplify matters, we investigate the arc column, away from any material

boundary, and, in the absence of an applied magnetic field.

In Chapter 2 several types of conventional arcs will be described together with the concept of the Fluid Transpiration Arc(FTA) and the manner in which it can be used to allow controlled fluid convection in an arc.

In Chapter 3 a detailed review of available arc column theories is presented. From the results we determine what further simplifications are available to us because of the geometry and characteristics of the FTA. We then investigate the physical limits withinwhich such simplifications are valid, and re-write the basic equations specifically for the special case considered. This will give us a more manageable form of the basic equations.

Results from the equations will be discussed and compared with (A) available data in the literature, and, (B) a number of specific measured characteristics of the arc having to do with the transfer of macroscopic momentum and energy observables. The two-temperature model of electrical conduction in the arc column is presented.

In Chapter 4 the various needed diagnostic methods

are described.

In Chapter 5 the results of diagnostics are presented.

In Chapter 6 we examine the extent of agreement between theory and experiment.

Finally, in Chapter 7 we present the findings of this dissertation. These indicate a qualitative agreement between the theoretical and experimental aspects of our work but point to the evidence of somewhat higher electrical conductivity and that one of the long held (but up to now not directly verified) processes of energy transfer between charged particles does not yield the correct rate in our arc regime.

In closing, we might mention that in spite of the limited domain occupied by arc phenomena in the vast spectrum of ionized gases the technological significance of arc techniques in the modern world is exceedingly great(see Reference 46).

The intense radiation emitted by arcs was utilized very early for image projection and in searchlights.

Because of their close resemblance with solar atmosphere phenomena(see Fig.1) arcs are being used extensively as solar simulators.

Arc heaters are powerful and efficient devices for obtaining ultra high temperature materials testing and for chemical synthesis.

The potentialities of arc jet thrustors for certain space flight missions have also been recognized.

Of late, efforts to raise the power output of gas laser tend to make use of plasma phenomena closer and closer to arc discharge of the nonequilibrium type.

This research is motivated by the following hope: If arcs have shown such versatility in the face of admitted paucity in knowledge of basic arc physics, a true understanding of this phenomenon would open up the prospect of much wider utilization in science and industry, to a degree that can hardly be foreseen. With such a prospect the very considerable labor expended towards the acquisition of basic data is amply justified.

Chapter 2

BACKGROUND OF PRESENT INVESTIGATION

Let us first look at some conventional arc configurations as shown in Fig.2. The top figure shows a horizontal arc under the influence of a vertical buoyant force. The electric field is generally in the same direction as the arc column and causes the drift of electrons and ions towards the anode and cathode, respectively, giving rise to the self-magnetic field, $\vec{B}$.

To be self-sustaining the arc must produce electrons near the cathode and ions near the anode. These are generated either by thermal ionization or ionization due to the high electric fields that exist in these electrode "fall" spaces.

The arc contracts towards the cathode fall zone and the resulting current density gradient produces a magnetic pressure gradient that effectively propels the constituents away from the cathode in the form of a plasma jet; a phenomenon known as the Maecker effect (see Reference 23).

A similar jet can also be produced at the anode. This occurs, for example in the high intensity arc,

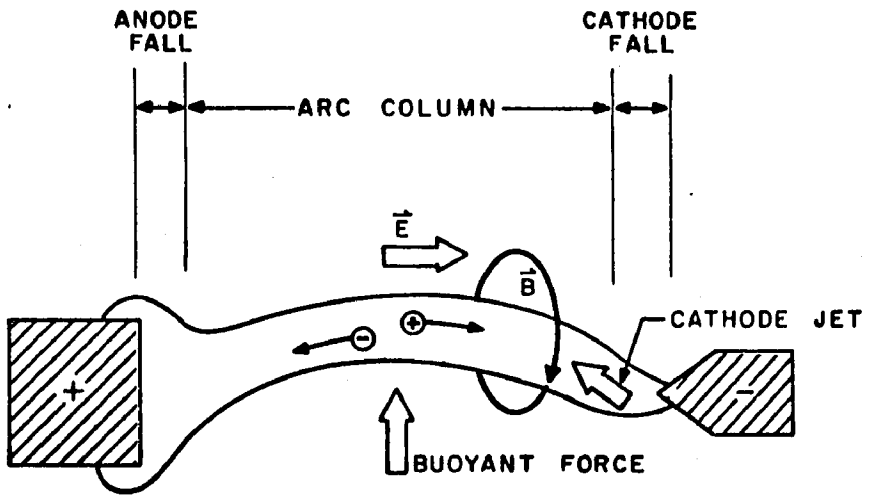

(a) HORIZONTAL ARC

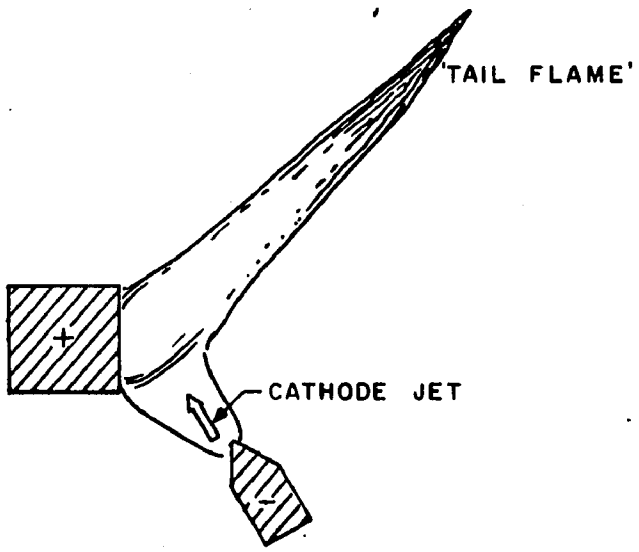

(b) ARC WITH A PRONOUNCED 'TAIL FLAME'

A-334-S-0035

FIG. 2 FEATURES OF SOME CONVENTIONAL ARCS

or "Beck arc" as it is sometimes called. In this type of arc the effect is produced by increasing the arc current until the thermal loading at the anode is too great to be dissipated by conduction and radiation. This results in enough additional energy to supply the latent heat required for the vaporization of the anode material. Under these conditions a vapor jet blowing away from the anode is generated, the vapor necessarily streaming through the arc column where it profoundly influences the arc characteristics. Of course, the anode material is consumed in this type of arc, but the condition can be maintained in steady state indefinitely by feeding the anode forward at the appropriate rate, and end-wise joining of new anodes as they are consumed.

When the electrodes of a high intensity arc are maintained in a collinear configuration, the anode and cathode jets collide and can cause large scale fluctuations in the arc, generally aggravating the difficulties of experimental studies. By using the off-set geometry shown in Fig.2(bottom) the anode and cathode jets can be made to merge smoothly to produce the characteristic "tail flame" of the high intensity arc. Even in this case, however, owing to the configurational asymmetry required for smooth operation and the high

current densities required for anode evaporation, the flow field of anode vapor is distorted and turbulent even quite close to the anode surface.

The main point is, in these foregoing examples (and in nearly all other arc arrangements) where fluid convection dominates the behavior of the arc, the lack of a simple geometry requires complications in the theoretical representation and renders the interpretation of experimental data quite difficult.

Ideally, a one-dimensional arc should be sought or, at least, a vastly scaled-up arc zone isolated for study so that there is some local region within which only one-dimensional changes are involved. Unfortunately, one-dimensional arcs do not exist and scaling up the arc so as to enlarge a more or less uniform zone to a convenient size for study is usually limited by power ceiling and materials problems, not to mention the notoriously non-linear and little understood arc scaling laws.

In the past, most arc research involving forced convection has been conducted with rotationally symmetric devices in which the arc column is stabilized by means of a constraint of one form or another which serves to immobilize the column against the forces of

vigorous convection. This can take the form of a narrow, water-cooled channel through which the column must pass. The channel walls maintain a cool, non-conductive boundary layer, forcing the conduction column to remain on the channel axis while appreciable amounts of fluid are flowing through the channel. This is generally called the "wall-stabilized" arc.

Alternately, the column may be stabilized by fluid-mechanical means by establishing the column on the axis of a cylindrical chamber into which the fluid is fed tangentially to set up a strong vortex, the column being constrained by the centripetal pressure field to remain on the vortex axis. The device is known as a "vortex-stabilized" arc.

Stabilization against convection may also be accomplished by an electromagnetic constraint, in which a D.C. column is spun rapidly in a strong magnetic field, or in which an electrodeless discharge is established in the form of an eddy current sheet by induction in the interior of a coil energized by high frequency A.C.

The resulting arcs exhibit good rotational symmetry. In the case of the wall- or vortex-stabilized arcs, a "fully-developed" arc column may under some conditions be obtained characterized by cylindrical

symmetry as well. In the latter case only radial changes are involved and the system is to some degree tractable to analysis(see Reference 22). However, even in these instances, the radial gradients are so steep that considerable difficulty is encountered in the severe radial variations of the transport properties (Reference 20). As a result such analyses are either highly approximate or involve prohibitively laborious machine computation.

In principle one can rely on probe and spectroscopic observations to obtain empirically the radial distributions of plasma properties. But, because of the smallness of arc core and the sharpness of radial gradients in practical arc systems, considerable error is usually incurred because of the fact that perturbations produced by probe insertion extend over a region comparable to that of the arc itself. Also, it is nearly impossible to determine experimentally the radial fluxes except those that reach the walls. In addition, the flow field of the hot ionized gas within a confining tube is always difficult to measure experimentally or to estimate on the theoretical basis.

As a result of these and many other difficulties it is little wonder that in the long history of arc research comparatively little in the way of arc

discharge mechanisms has been uncovered, or definitively analyzed.

In 1958, a new type of plasma generator(convective arc system) was introduced by Sheer et al(References 50, 51). This possesses a number of features that appear to alleviate some of the difficulties mentioned above for the earlier systems. This system therefore seems to represent a more suitable device with which to study interaction phenomena between the working fluid and the arc discharge.

Essentially, the technique consists of injecting the fluid directly into the discharge via transpiration through a porous anode structure at the anodic boundary of the discharge. The anode material is convectively cooled by the injected fluid and therefore not consumed, as in the high intensity arc. The rate of working fluid injection can therefore be varied(above the minimum required for anode cooling) independently of the arc current over a wide range, and, after penetrating the high gradient anode sheath, flows collinearly with the arc current for a considerable distance into the column with a fairly uniform mass flow distribution radially. Several versions of this so-called Fluid Transpiration Arc(FTA) have been constructed and operated in the Electronics Research Laboratories of

Columbia University. A representative photograph of such an arc is shown in Fig.3. Construction details are indicated in Fig.4.

The FTA has many interesting features. In the first place, it has clearly separate anode and cathode columns which apparently interact in only a limited mixing region.

Secondly, the FTA can be operated stably without external constraints of any kind; in short, the anode and cathode jets are self-stable. The operational stability has been found to persist, especially for the anode column, despite vigorous convection - up to 2 $gm/sec\text{-}cm^2$.

For this reason the FTA may be considered as a "free-burning" plasma generator, in which stability is insensitive to forced convection, despite the absence of external constraints. As a result of this property, it is easily accessible to probings and spectroscopic observations throughout the entire discharge volume.

Thirdly, since the transpirant is introduced into the column through micro-pores of the anode(average pore size $\sim$30 microns) the local mass flow in the column is relatively uniform and can be estimated even if actual measurement should prove not feasible. This

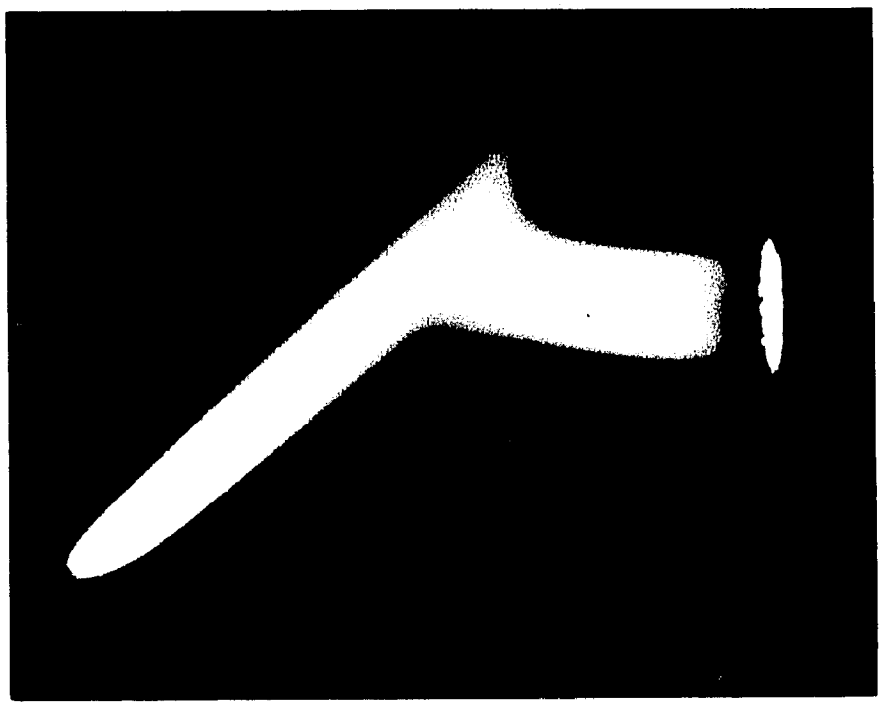

(a)

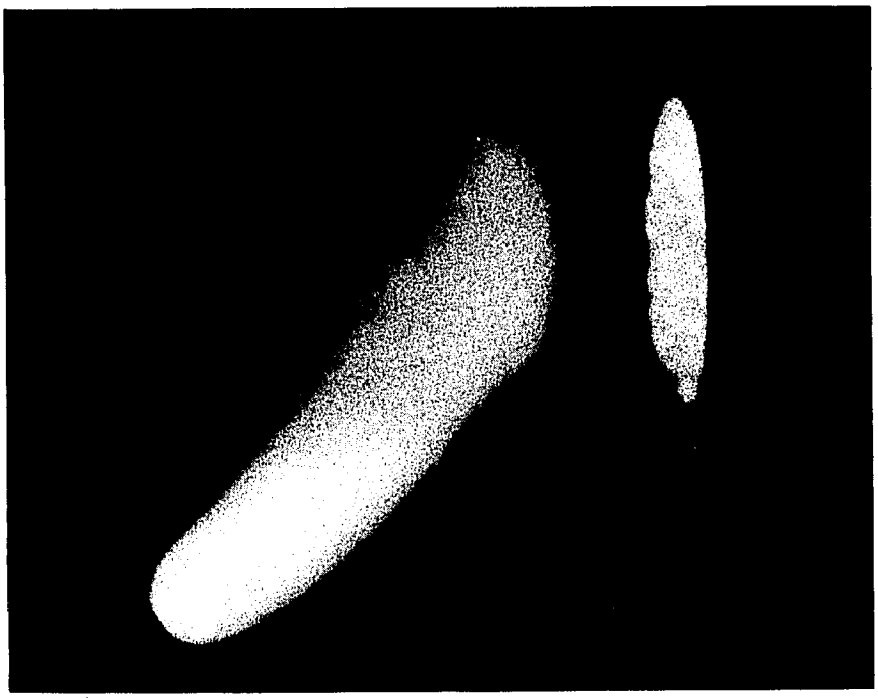

(b)

Fig.3 Photographs of the Fluid Transpiration Arc

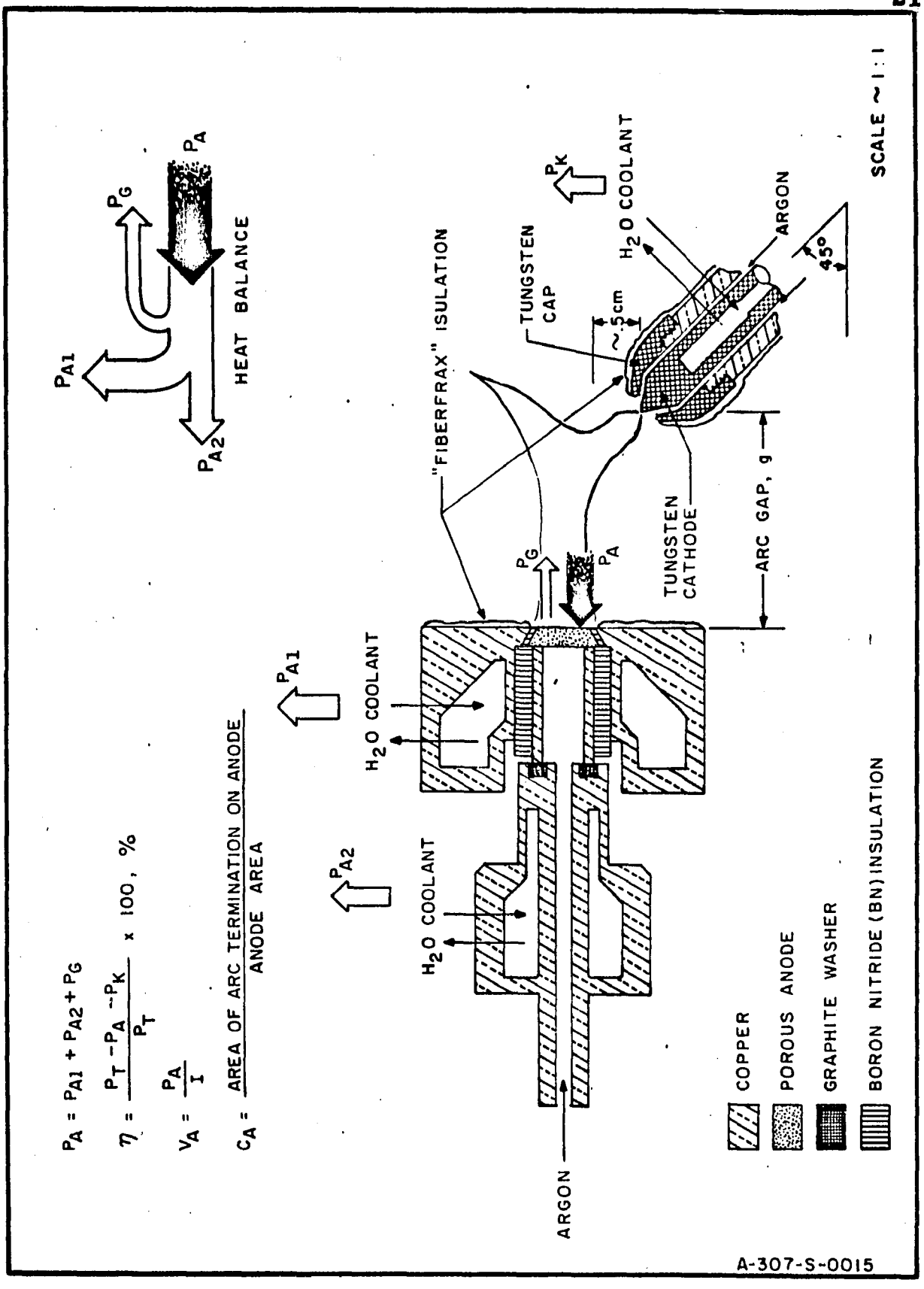

FIG. 4 SCHEMATIC DIAGRAM OF FLUID TRANSPIRATION ARC AND TERMINOLOGY OF CALORIMETRY PARAMETERS

DRAWN	CHECKED	APPROVED

last attribute is one of the most important experimental features on which our study is based.

For our study, we have concentrated on that portion of the positive column extending from the anode to a distance about 1 cm away.

In a preliminary published paper(Reference 60) we noted that the current density distribution in this region seemed to be quite uniform radially. Since at atmospheric densities the electrical conductivity depends primarily on temperature it appears that in this region the temperature, and other temperature-dependent properties, should also be radially uniform. Consequently, changes in arc properties should be largely one-dimensional, along the z-axis. Theoretical considerations relative to a one-dimensional column will be given in Chapter 3.

By means of the forced convection the gas in the region of interest is made relative cool. In Fig.3, for example, a cool dark space is seen extending to a considerable distance from the anode. If the electrons are assumed to be in equilibrium with the gas then it can be shown theoretically that only a negligible amount of conduction should be possible. The fact that electrical conduction persists suggests that the conducti-

vity might correspond to that given by ionization equilibrium at an electron temperature appreciably higher than the gas temperature. This zone, therefore, appears to be suitable for the study of the so-called two-temperature conduction law. Such nonequilibrium condition will be theoretically investigated in Chapter 3.

Chapter 3

THEORIES OF ARC COLUMN

In order to develop a suitable theoretical background for the present study we shall first consider the theories of conventional(spatially nonuniform) arc column in local thermodynamic equilibrium(LTE) and derive some results which will be used in later discussions. Then we shall examine the theory of the nonequilibrium column leading to the two-temperature model which will also be utilized in evaluating the system under study.

3.1 The Fully Developed Column

In this section we treat the simplest case, i.e. we derive the energy equation of a fully developed arc column at moderate pressure and without radial convection. The term "fully developed" signifies the condition $\frac{\partial}{\partial z} = 0$. This is found, for instance, in that portion of a long arc sufficiently far away from the electrodes, where energy transport is in the radial direction only. We assume, because of axial symmetry, $\frac{\partial}{\partial \theta} = 0$. Also, radiative transfer is neglected. However, because of the $\frac{\partial}{\partial z} = 0$ stipulation, axial convection is allowed but would not appear in the energy equation, which is:

$$r^{-1}\frac{d}{dr}(\lambda r\frac{dT}{dr}) + \sigma E^2 = 0 \qquad \text{(Eq.1)}$$

where $\sigma = \sigma(T)$ is the electrical conductivity, and $\lambda = \lambda(T)$ is the thermal conductivity. It is characteristic of a fully developed column that E, the electric field, is a constant*. This is simply the heat conduction equation according to Fourier's law of heat conduction, with a Joule heating source term, σE^2.** In its general form, where σ and λ are temperature-dependent, Eq.1 is without closed form solution.***

It is convenient to use a new variable, the heat potential:

$$\phi = \int_{T_c}^{T} \lambda(T)dT \qquad (T_c \text{ constant})$$

wherein $\frac{d\phi}{dr} = \frac{d\phi}{dT}\frac{dT}{dr} = \lambda(T)\frac{dT}{dr}$ which is substituted in

*Experimental measurements described later(see Figs.27 and 53) show that in the system under study E is approximately radially invariant.

**In arc literature, Eq.1 is generally referred to as the Elenbaas-Heller equation.

***See Carslaw and Jaeger, "Conduction of Heat in Solids", 2nd Ed., Oxford(1959). p.12.

Eq.1 to give

$$\frac{d^2\phi}{dr^2} + r^{-1}\frac{d\phi}{dr} + \sigma E^2 = 0 \quad ; \quad \sigma = \sigma(\phi)$$

or,

$$\frac{d^2\phi}{dx^2} + x^{-1}\frac{d\phi}{dx} + \sigma = 0 \qquad \text{(Eq.2)}$$

where $x = Er$.

It turns out(see Reference 55) that for many gases the function $\sigma(\phi)$ can be represented by a finite number of piecewise-linear functions of ϕ, i.e.

$$\begin{aligned}
\sigma(\phi) &= A_o\phi + B_o \quad ; \quad \phi_1 \leq \phi \leq \phi_o \\
&= A_1\phi + B_1 \quad ; \quad \phi_2 \leq \phi \leq \phi_1 \\
&= \ldots \\
&= A_n\phi + B_n \quad ; \quad \phi_{n+1} \leq \phi \leq \phi_n
\end{aligned}$$

which allows step-by-step construction of the solution $\phi = \phi(x)$.

With the piecewise-linear representation of $\sigma(\phi)$, the complete solution of Eq.2, for $A_n > 0$, is

$$\phi(x) = -B_n/A_n + C_n J_o(x\sqrt{A_n}) + D_n Y_o(x\sqrt{A_n}) \qquad \text{(Eq.3)}$$

For $A_n = 0$ and $A_n < 0$, equally simple solutions can be obtained in terms of elementary and modified Bessel functions. These are of no interest here since for the noble gases, ϕ is a monotonic function of x. In Eq.3 J_o and Y_o are the zero-order Bessel functions of the first and second kind, respectively.

By specifying the arc axis temperature, T_o (and ϕ_o), and imposing the zero slope boundary condition, we have,

$$x = 0 : \quad \phi = \phi_o$$

$$\frac{d\phi}{dx} = 0$$

$$D_o = 0 \quad (Y_o(0) \text{ unbounded})$$

$$C_o = \phi_o + B_o/A_o$$

Hence, in the first region:

$$\phi_1 \leqslant \phi \leqslant \phi_o \quad ; \quad x_1 \geqslant x \geqslant 0$$

$$\phi(x) = -B_o/A_o + (\phi_o + B_o/A_o) J_o(x\sqrt{A_o}) \qquad \text{(Eq.4)}$$

and x_1 is given by:

$$J_o(x_1\sqrt{A_o}) = (A_o\phi_1 + B_o)/(A_o\phi_o + B_o) = \sigma(\phi_1)/\sigma(\phi_o)$$

In the second region,

$$\phi_2 \leqslant \phi \leqslant \phi_1$$

$$\phi(x) = -B_1/A_1+C_1J_o(x\sqrt{A_1})+D_1Y_o(x\sqrt{A_1}) \qquad \text{(Eq.5)}$$

From Eq.4, ϕ_1, x_1 and, $\left.\frac{d\phi}{dx}\right|_1$ are known and we have from the conditions of continuity of ϕ and $\frac{d\phi}{dx}$ @ $x = x_1$,

$x = x_1$:

$$\phi=-B_o/A_o+(\phi_o+B_o/A_o)J_o(x_1\sqrt{A_o})=-B_1/A_1+C_1J_o(x_1\sqrt{A_1})$$
$$+D_1Y_o(x_1\sqrt{A_1}) \qquad \text{(Eq.6)}$$

$$\frac{d\phi}{dx}=(\phi_o+B_o/A_o)\sqrt{A_o}J_1(x_1\sqrt{A_o})=\sqrt{A_1}\left[C_1J_1(x_1\sqrt{A_1})+D_1Y_1(x_1\sqrt{A_1})\right]$$
$$\text{(Eq.7)}$$

where J_1 and Y_1 are the first-order Bessel functions and from Eqs. 6 and 7, C_1 and D_1 are obtained:

$$C_1=\Delta^{-1}\left[(\phi_1+B_1/A_1)Y_1(x_1\sqrt{A_1}) - (\phi_o+B_o/A_o)(A_o/A_1)^{\frac{1}{2}}\right.$$
$$\left.J_1(x_1\sqrt{A_o})Y_o(x_1\sqrt{A_1})\right]$$

$$D_1=\Delta^{-1}\left[(\phi_o+B_o/A_o)(A_o/A_1)^{\frac{1}{2}}J_1(x_1\sqrt{A_o})J_o(x_1\sqrt{A_1}) -\right.$$

$$(\phi_1+B_1/A_1)J_1(x_1\sqrt{A_1})\Big]$$

where

$$\Delta = J_o(x_1\sqrt{A_1})Y_1(x_1\sqrt{A_1})-J_1(x_1\sqrt{A_1})Y_o(x_1\sqrt{A_1})$$

Equation 5 will hold in the region

$$x_2 \geqslant x \geqslant x_1$$

where x_2 is obtained from

$$\phi_2 = -B_1/A_1+C_1J_o(x_2\sqrt{A_1})+D_1Y_o(x_2\sqrt{A_1})$$

In the above fashion construction of the solution $\phi(x)$ may proceed further until the entire range of interst in ϕ has been covered.

The thermal conductivity of partially ionized argon at one atmosphere has been computed by Ahtye (Reference 1) and is shown in Fig.5, from which ϕ has been computed and plotted in Fig.6 against values of σ computed in Section 3.4. Here, as in all later work, the critical temperature T_c has been chosen to be 6000^oK. Below this temperature, argon can be taken to be electrically nonconducting.

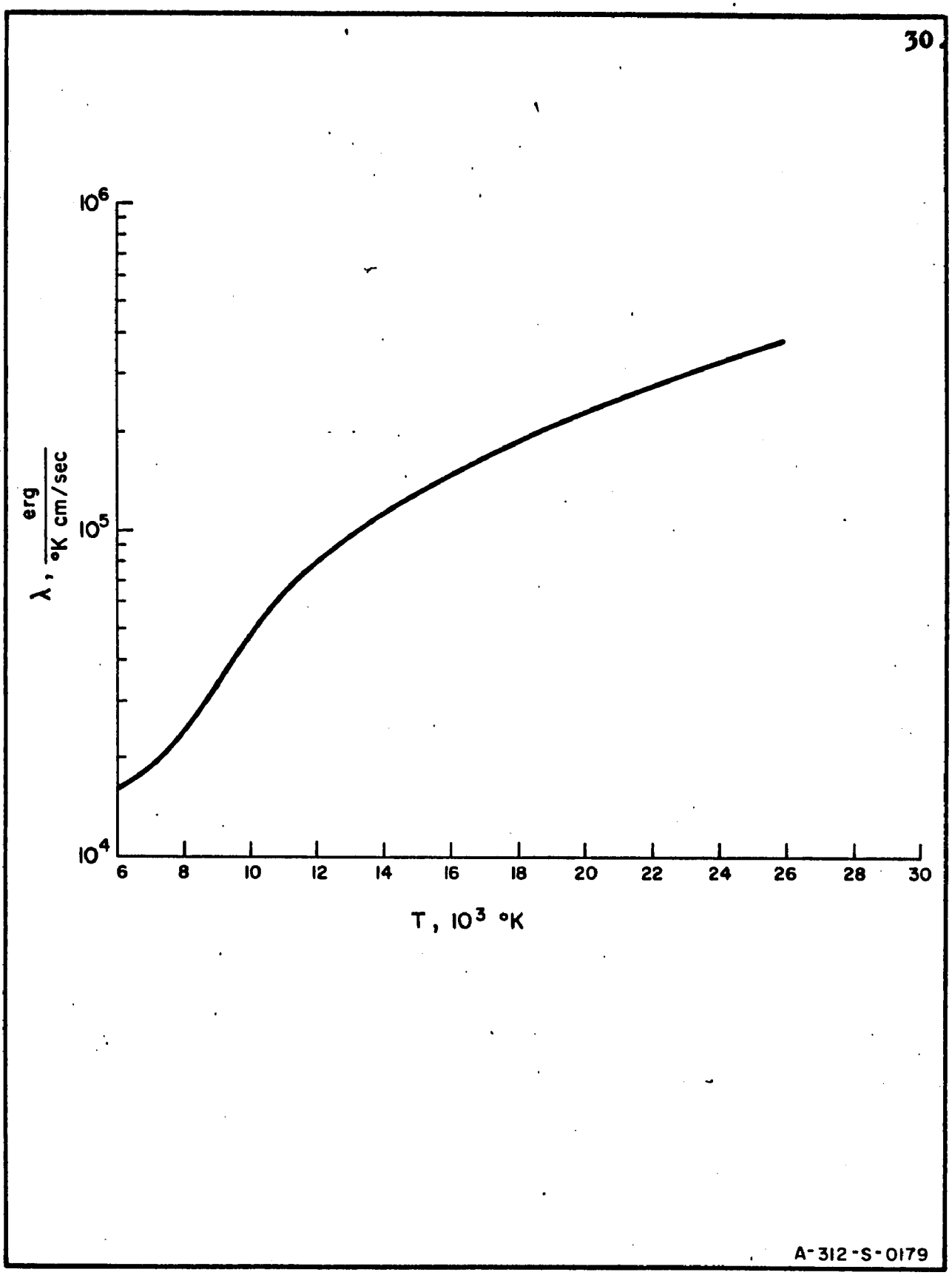

FIG. 5 TRANSLATIONAL THERMAL CONDUCTIVITY OF ARGON AT ONE ATMOSPHERE FROM AHTYE , Reference 1. (1 erg = 10^{-7} JOULE)

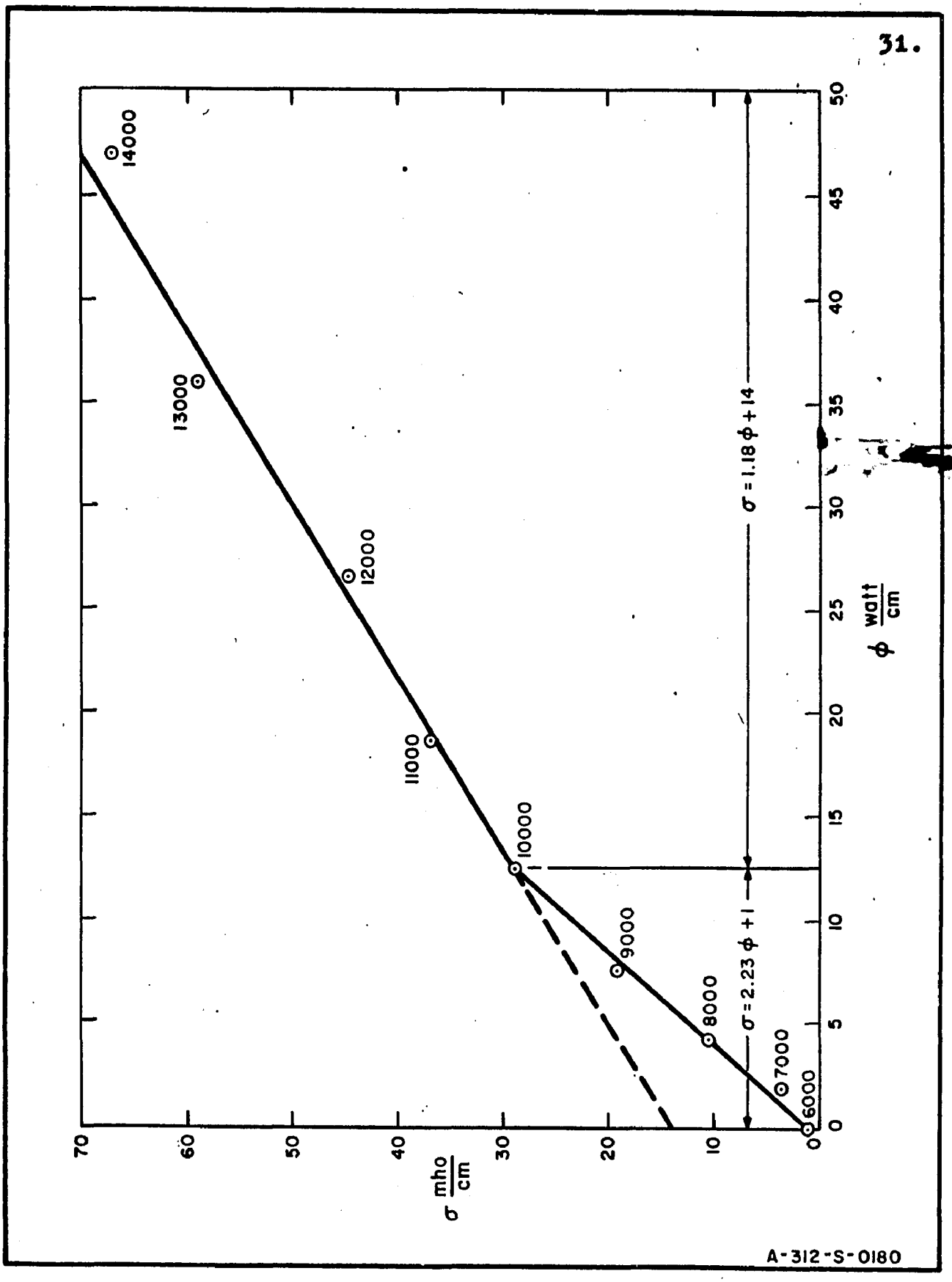

FIG. 6 ARGON ELECTRICAL CONDUCTIVITY vs. HEAT POTENTIAL, 1 ATM.

For our purposes, we see that only two straight lines are needed to represent σ from 6000 to 13000°K.

$$\sigma = 1.18\phi + 14.0 \quad ; \quad 12.5 \leqslant \phi \leqslant 36.0$$

$$= 2.23\phi + 1.0 \quad ; \quad 0 \leqslant \phi \leqslant 12.5$$

$$T_c = 6000^{\circ}K$$

Solutions for T_o = 9000, 10000, 11000, and 12000°K have been obtained and the radial temperature distributions plotted in Fig.7. It is striking to note that the column radius, r_c, defined as:

$$T(r_c) = T_c = 6000^{\circ}K$$

is rather insensitive to changes in the axis temperature.

The total current, I_c, carried by the column can be directly obtained by integration:

$$I_c = 2\pi \int_0^{r_c} r\, \sigma(r) E\, dr$$

Hence,

$$I_c = \frac{2\pi}{E}\left\{ \int_0^{x_1\sqrt{A_o}} (\phi_o + B_o/A_o)\, x\, A_o J_o(x\sqrt{A_o})\, dx\sqrt{A_o} + \right.$$

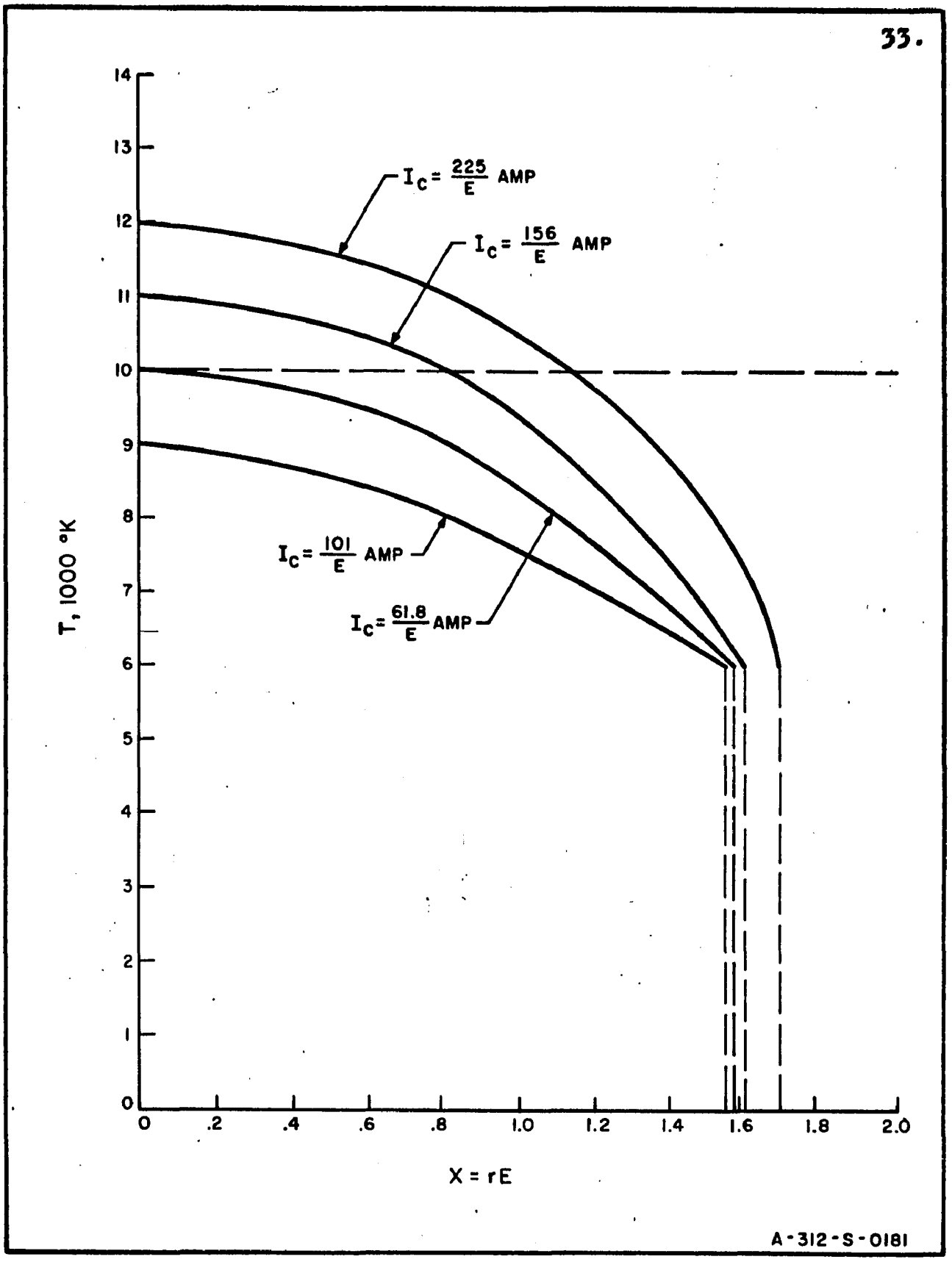

FIG. 7 COMPUTED RADIAL TEMPERATURE DISTRIBUTIONS FOR FULLY DEVELOPED ARC COLUMNS AT 1 ATM. ARGON

$$\left.\int_{x_1\sqrt{A_1}}^{x_2\sqrt{A_1}} \left[C_1 J_o(x\sqrt{A_1}) + D_1 Y_o(x\sqrt{A_1})\right] x\sqrt{A_1}\, dx\sqrt{A_1}\right\}$$

$$I_c = \frac{2\pi}{E}\Big\{(\phi_o + B_o/A_o) J_1(x_1\sqrt{A_o})\, x_1\sqrt{A_o} + C_1\Big[x_2\sqrt{A_1} J_1(x_2\sqrt{A_1}) - x_1\sqrt{A_1} J_1(x_1\sqrt{A_1})\Big] + D_1\Big[x_2\sqrt{A_1} Y_1(x_2\sqrt{A_1}) - x_1\sqrt{A_1} Y_1(x_1\sqrt{A_1})\Big]\Big\} \qquad \text{(Eq.7)}$$

From the computations as summarized in Table 1 we see that in the temperature range of interest the total column current increases nearly four fold while the centerline temperature varies from 9000 to 12000°K, but the effective column radius, r_c, undergoes only a small increase($< 12\%$). Since in a fully developed column E is independent of r (see Appendix A) we can define the effective column conductivity as:

$$\sigma_c = I_c / \pi r_c^2 E.$$

Values of σ_c in Table 1 indicate a marked increase with centerline temperature.

TABLE 1

COMPUTED RADIUS, CURRENT AND σ_c

FOR A FULLY DEVELOPED ARGON ARC COLUMN

T_o, ^oK	r_c/E, cm/v/cm	I_c/E, amp/v/cm	σ_o, mho/cm
9,000	1.55/E	61/E	8.1
10,000	1.57/E	101/E	13.1
11,000	1.63/E	156/E	18.7
12,000	1.73/E	225/E	24.0

3.2 The Developing Column

The developing column refers to that portion of a long column sufficiently close to the point at which gas is injected that local thermodynamic equilibrium has not become fully established. In particular, axial gradients are appreciable in this region and the simplification $\frac{\partial}{\partial z} = 0$ does not apply. The details of treating departure from LTE are given in Section 3.3 and here we examine the feasibility of the hope expressed earlier of isolating a special portion of the convection controlled arc displaying properties particularly favorable for study.

This sample volume should possess the following characteristics:

(1) Quasi one-dimensional change in properties.

(2) Sufficiently large in volume to allow probings without serious perturbation.

If we picture a section of the column as a source of internally generated power, Q_E, then in steady state this power must be dissipated axially(Q_z), radially(Q_r), and, radiatively(Q_{rad}) as illustrated Fig.8. Thus,

$$Q_E = Q_z + Q_r + Q_{rad}$$

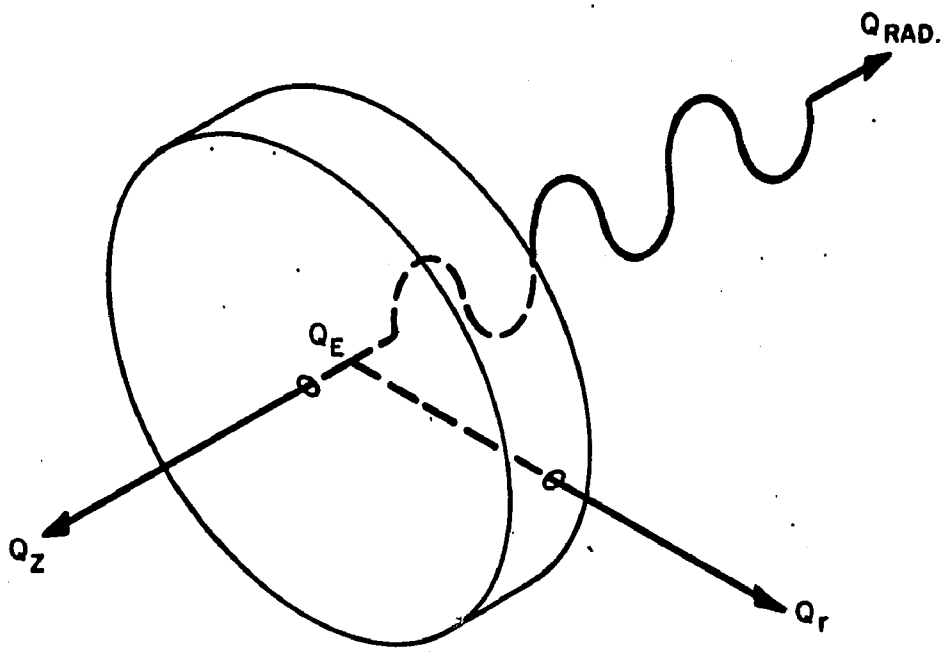

A-312-S-0182

FIG. 8 ENERGY BALANCE IN A SECTION OF THE DEVELOPING ARC COLUMN

or,

$$Q_E = \frac{-\partial}{\partial z}(\lambda \frac{\partial T}{\partial z}) + \dot{m} c_p \frac{\partial T}{\partial z} - r^{-1} \frac{\partial}{\partial r}(\lambda r \frac{\partial T}{\partial r}) + Q_{rad} \qquad \text{(Eq.8)}$$

where $\dot{m}$ is the mass flow rate density and c_p is the specific heat at constant pressure. The convection term $(\dot{m} c_p \frac{\partial T}{\partial z})$ as well as the axial conduction term must now be included since $\frac{\partial}{\partial z} \neq 0$.

One can see intuitively that for a fixed Q_E and Q_{rad}, the relative importance of axial change versus radial change hinges upon the magnitude of the parameter $(\lambda/\dot{m} c_p)$. If this number is large then radial change predominates and if this number is small then axial change predominates.

It is important to know quantitatively just what constitutes largeness and this requires the solution of Eq.8, subject to the appropriate boundary conditions, and cannot be decided solely on the basis of the magnitude of the parameter. Indeed, it can be shown that in most instances both Q_z and Q_r are important fractions of Q_E.

The introduction of the heat potential, ϕ, as before, and the enthalpy:

$$h = \int_{T_c}^{T} c_p dT$$

will be found helpful. Using these variables, Eq.8 becomes

$$\frac{\partial^2 \phi}{\partial r^2} + r^{-1}\frac{\partial \phi}{\partial r} + \frac{\partial^2 \phi}{\partial z^2} + (Q_E - Q_{rad}) - \dot{m}\frac{\partial h}{\partial z} = 0 \qquad \text{(Eq.9)}$$

As in Eq.1, for arc discharge Q_E is set equal to $(\sigma' E^2)$ and then σ' is approximated by an expression of the form

$$\sigma' \cong A_{\sigma'}\phi + B_{\sigma'}$$

Similarly, h (see Fig.62, data from B.D.Adcock) can be related to ϕ in an approximate fashion by

$$h \cong A_h \phi \ .$$

For argon, h is plotted against ϕ in Fig.9 from which we obtain the value

$$A_h = 250 \text{ cm-sec/gm}$$

good from 6000 to 11000°K.

When these substitutions are made we have

$$\frac{\partial^2 \phi}{\partial r^2} + r^{-1}\frac{\partial \phi}{\partial r} + \frac{\partial^2 \phi}{\partial z^2} + E^2(A_{\sigma'}\phi + B_{\sigma'}) - A_h \dot{m}\frac{\partial \phi}{\partial z} = Q_{rad} \qquad \text{(Eq.10)}$$

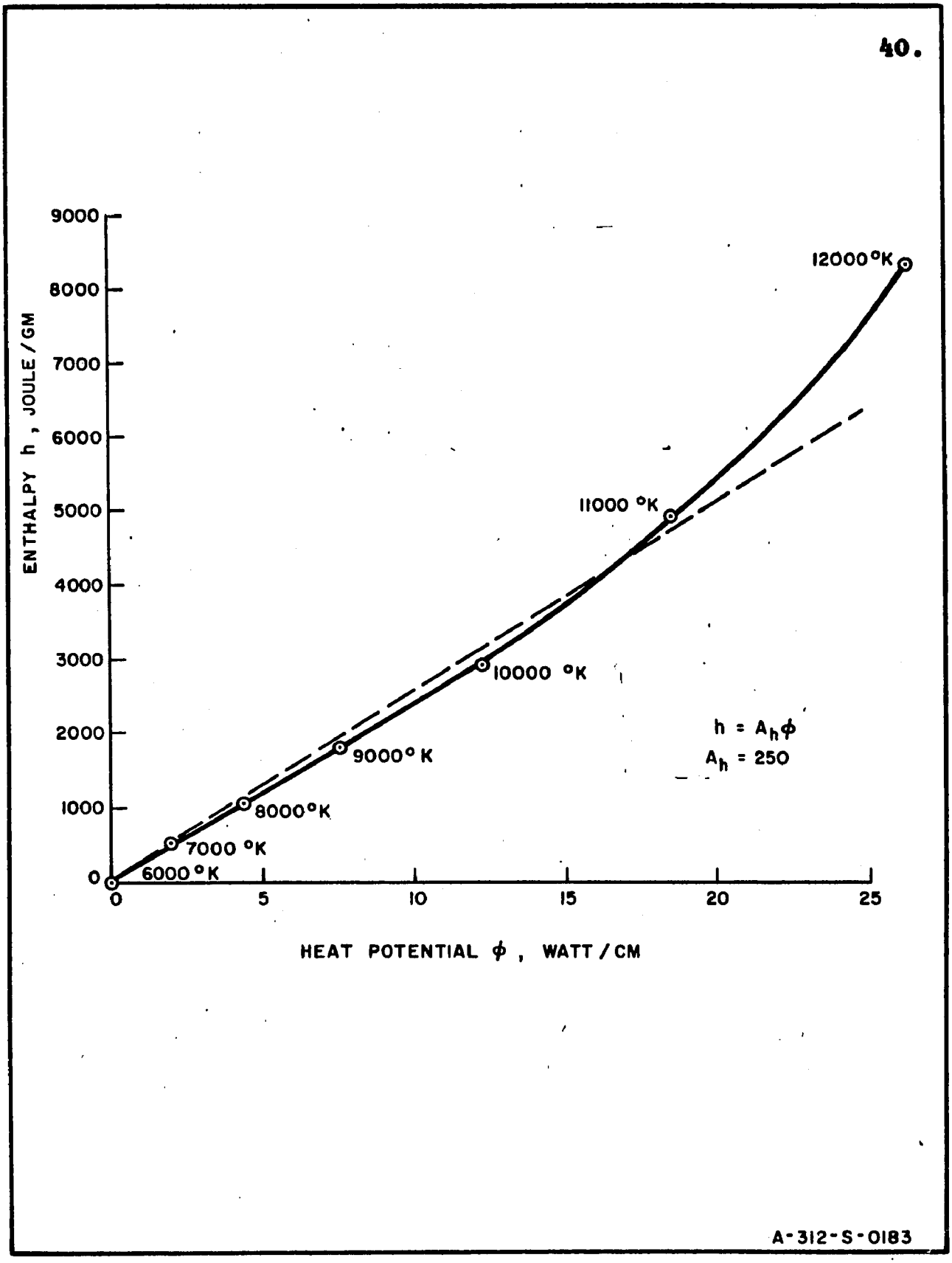

FIG. 9 ENTHALPY vs. HEAT POTENTIAL FOR 1 ATM. ARGON

in which we can show *a posteriori* that the axial conduction term $(\frac{\partial^2 \phi}{\partial z^2})$ is completely negligible. Hence,

$$\frac{\partial^2 \phi}{\partial r^2}+r^{-1}\frac{\partial \phi}{\partial r}+E^2(A_\sigma \phi+B_\sigma)-A_h \dot{m}\frac{\partial \phi}{\partial z} = Q_{rad} \qquad \text{(Eq.11)}$$

which has all the appearance of a classical diffusion equation with $(\frac{\partial}{\partial z})$ in place of the familiar $(\frac{\partial}{\partial t})$.

Unfortunately, there is an important difference. Namely, E is generally varying with z according to the Kirchhoff's law of current continuity,

$$I_c = \int_0^{r_c} 2\pi r \sigma E dr = \text{constant}$$

from which it is obvious that in sections where the average σ is high E will be low and vice versa. This subsidiary condition, of course, does not arise when $\frac{\partial}{\partial z} = 0$. In the general case an integro-differential equation presents itself with dim prospect for solution.*

*It should be pointed out that Stine and Watson (Reference 55) have succeeded in taking care of the z-dependent E by allowing only one radial characteristic solution to an equation similar to Eq.11. This is the zero-order Bessel function $J_0(\sqrt{A_\sigma}Er)$. Their special case is of no interest to us since we are interested in "flat top" radial solutions which can only be formed with a combination of characteristic solutions.

If it can be assumed, as experimentally indicated, that the total internal heat addition may be adequately represented by a constant Q_o then the relative roles played by radial conduction and axial convection in dissipating this amount can be obtained by solving

$$\frac{\partial^2 \phi}{\partial r^2} + r^{-1}\frac{\partial \phi}{\partial r} + Q_o - A_h \dot{m}\frac{\partial \phi}{\partial z} = 0 \qquad \text{(Eq.12)}$$

A separation of variables can be made by the substitution of $\phi(r,z) = u(r)\exp(-\alpha^2 z)$ and $\rho = r/r_c$ in Eq.12 giving

$$\frac{d^2u}{d\rho^2} + \rho^{-1}\frac{du}{d\rho} + \beta^2 u + Q_o r_c^2 = 0 \qquad \text{(Eq.13)}$$

$$\beta^2 = \alpha^2 A_h \dot{m} r_c^2$$

which is seen to be the zero-order Bessel equation.

Because $\phi(0,z)$ is finite and $\phi(r_c,z)$ is zero, the complete complementary function for Eq.13 is:

$$u_c = \sum_{n=1}^{\infty} a_n J_o(\beta_n \rho)$$

where the β_n's are the zeroes of J_o.

$$\beta_1 = 2.402, \quad \beta_2 = 5.5 \quad , \quad \ldots$$

Hence,

$$\phi_c = \sum_{n=1}^{\infty} a_n J_o(\beta_n \rho) \exp(-\alpha_n^2 z)$$

$$\alpha_n^2 = \beta_n^2 / A_h \dot{m} r_c^2$$

The particular solution, ϕ_p is

$$\phi_p = Q_o r_c^2 (1 - \rho^2)/4$$

Hence,

$$\phi = \phi_p + \phi_c = Q_o r_c^2 (1 - \rho^2)/4 + \sum_{n=1}^{\infty} a_n J_o(\beta_n \rho) \exp(-\alpha_n^2 z).$$

By virtue of the orthogonal properties of J_o, the coefficients a_n's can be evaluated @ z = 0,

$$a_n = \frac{\int_0^1 \rho \left[\phi(\rho, 0) - (1-\rho^2) r_c^2 Q_o/4\right] J_o(\beta_n \rho) d\rho}{\int_0^1 \rho J_o^2(\beta_n \rho) d\rho}$$

In our arc geometry, the transpiring gas leaves the porous anode plane surface with a uniform radial distribution of temperature. Therefore $\phi(\rho, 0)$ may be taken to be constant, say, zero. In which case

$$a_n = -2r_c^2 Q_o / \beta_n^3 J_1(\beta_n)$$

and,

$$\phi = (r_c^2 Q_o/4)\left[(1-\rho^2) - 8\sum_{n=1}^{\infty} \frac{J_o(\beta_n \rho)\exp(-\alpha_n^2 z)}{\beta_n^3 J_1(\beta_n)}\right]$$

(Eq.14)

Since the values of the α's are:

$$\alpha_1^2 = 2.4^2/A_h \dot{m} r_c^2$$

$$\alpha_2^2 = 5.5^2/...$$

$$\alpha_3^2 = 8.65^2/...$$

$$\alpha_4^2 = 11.8^2/...$$

$$\alpha_5^2 = 14.9^2/...$$

...

the terms in Eq.14 with n greater than 1 damp out very rapidly with increasing z, in relation to the dominant, n = 1, term. When $\alpha_1^2 z$ is small and $\exp(-\alpha_1^2 z)$ close to unity, the higher n terms must be retained.

Some values of $(4\phi/r_c^2 Q_o)$ as function of ρ have been computed with different values of $\alpha_1^2 z$ as parameters. The results are plotted in Fig.10 and from it we obtain a quantitative picture of the extent of the quasi one-dimensional region that was sought after.

We see that for $\alpha_1^2 z = 0.1$, this region extends to approximately $\rho = 0.8$. As the gas moves down stream (z increases) the effects of radial gradient propagate towards the center. Thus, for $\alpha_1^2 z = 0.4$, only the region from the center to $\rho = 0.4$ remains essentially flat. For this value of $\alpha_1^2 z$ and for $A_h = 250$, $\dot{m} = 0.2$, $r_c = 0.5$,

$$z = 0.4 A_h \dot{m} r_c^2 / 2.4^2 \cong 0.9 \text{ cm}$$

whence we conclude that as far down stream as 0.9 cm the one-dimensional streamtube concept can be accepted as valid.

Since $\dot{m} = 0.2$ is the low end of the forced convection range*, and, a 0.4 cm diameter by 0.9 cm long sample volume quite ample for probings and optical measurements, we are satisfied that on theoretical grounds our proposed scheme for studying the forced

---

*We have, of course, assumed that fluid flow is uniform and only in the axial direction. These appear to be borne out experimentally. See Chapter 6.

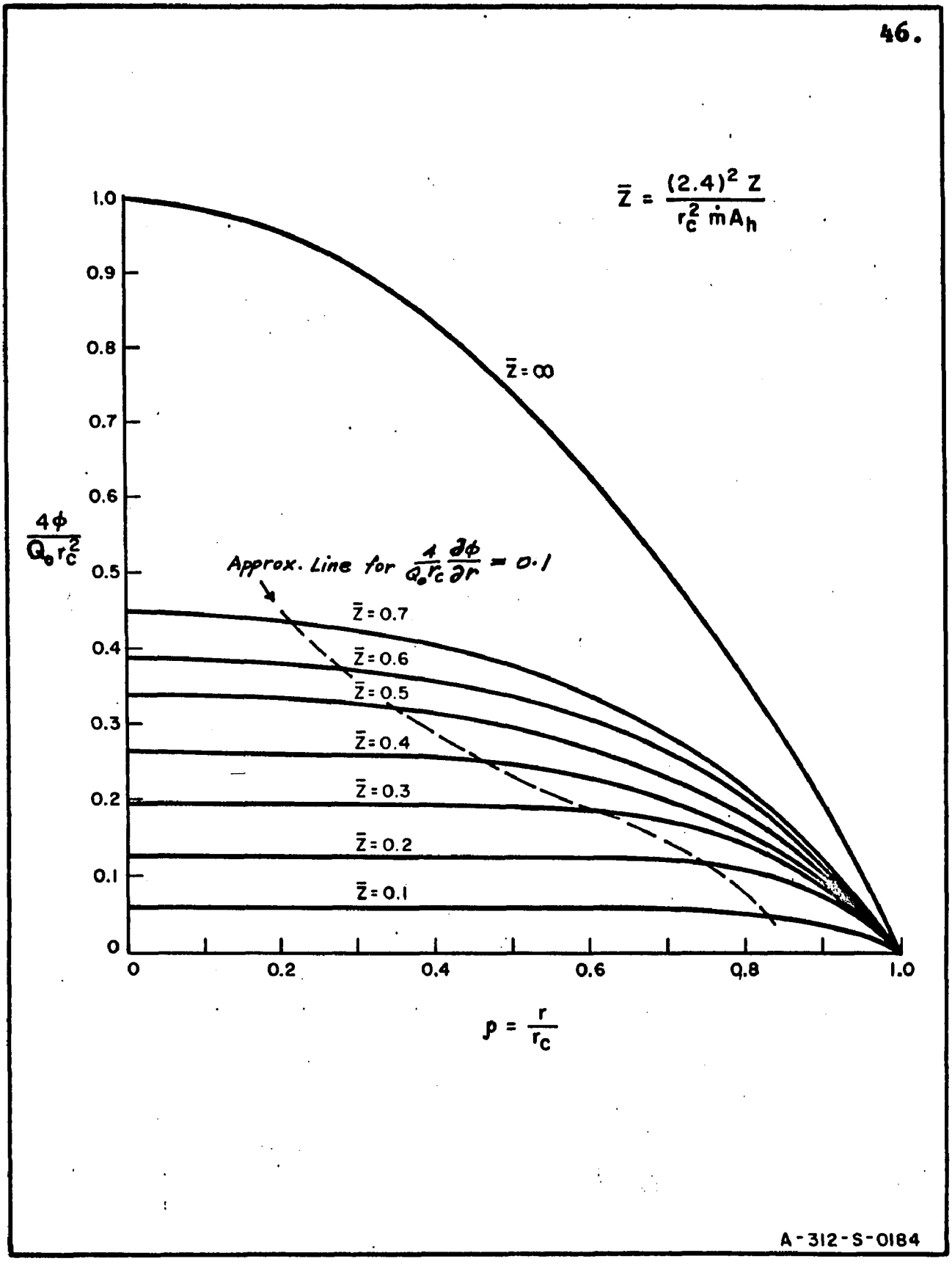

FIG. 10 COMPUTED RADIAL DISTRIBUTIONS OF Ø AT VARIOUS AXIAL DISTANCE FOR 1 ATM. ARGON ARC WITH INTERNAL HEAT SOURCE Q_o

convective arc zone comprising the first cm of length of the positive column of the FTA seems quite feasible.

Incidentally, from Fig.10 the prior assumption that axial heat conduction is negligible can be easily justified. In addition, this is confirmed by experimental evidence to be presented later(see Fig.54).

3.3 The Nonequilibrium Column

3.3.1 Basic equations. We now proceed to obtain some relations that govern the motion and energy of the electron working fluid in a one-dimensional model of a gaseous conducting column.

For many applications where the charged particle density and the neutral particle density are sufficiently high, the electron-ion plasma and the neutrals can be considered as components forming a continuum fluid obeying fluid dynamic equations not so different from those for ordinary fluids. To make use of these equations, however, the transport coefficients(thermal conductivity, viscosity, diffusion coefficient, electrical conductivity, etc.) must be known.

Experimental determinations of these quantities are currently either lacking or incomplete. Consequently, theoretical computations must frequently be employed. These invariably utilize the kinetic theory of gases thoroughly expounded in the classical treatises of Chapmen and Cowling(Reference 11) and Hirschfelder, Curtis and Bird(Reference 31).

The very complex nature of kinetic theory calculations precludes a self-contained discussion, even one

introductory in scope, from being included in this dissertation. Suffice it to state that this is a well established discipline which has been successfully applied to the study of ordinary fluids. This is well in evidence in the aforementioned references, whose treatments show much promise of fruitful extension to ionized gases; the present investigation being partly an attempt to apply the theory in the latter regime.

In the following, the equations pertinent to our goals will be given and discussed in sufficient detail to convey their significance, and, not the least, to define the notations.

Starting from somewhat different origins, there exist what appear to be eventually equivalent kinetic equations for describing the behavior of a large collection of particles. Central to all these is the one-particle distribution function

$$f(\vec{v},\vec{r},t)$$

giving the distribution of the various particles in velocity, space, and in time, which, altogether form a seven-dimensional space. The kinetic equation we chose is the well-known Boltzmann equation expressing the principle of the conservation of probability measure in

such a space. This is generally written as

$$\frac{\partial f_1}{\partial t} + \vec{v}\cdot\frac{\partial f_1}{\partial \vec{r}} + \frac{\vec{E}}{m_1}\cdot\frac{\partial f_1}{\partial \vec{v}} = \left(\frac{\partial f_1}{\partial t}\right)_c \qquad \text{(Eq.15)}$$

where $\vec{r} = \{x,y,z\}$

$\vec{v} = \{v_x, v_y, v_z\}$

$$\vec{a}\cdot\frac{\partial}{\partial \vec{b}} \equiv a_x\frac{\partial}{\partial b_x} + a_y\frac{\partial}{\partial b_y} + a_z\frac{\partial}{\partial b_z}$$

$\vec{E}/m_1$ = external field force per unit mass

t = time

$\left(\frac{\partial f_1}{\partial t}\right)_c$ = rate of change of f_1 due to effects of collision, the subscript 1 being used to identify a certain species of particles as, for example, the electrons.

As might be expected, the interparticle dynamics is contained in the term $\left(\frac{\partial f_1}{\partial t}\right)_c$ which is given by the binary form appropriate to gases where collision between two particles predominates:

$$\left(\frac{\partial f_1}{\partial t}\right)_c = \sum_{i=1}^{n}\iint\left(f_1' f_i' - f_1 f_i\right) g\,\sigma_{1i}(g,\theta)\,d\Omega\,d\vec{v}_i \qquad \text{(Eq.16)}$$

where $f_i' \equiv f(\vec{v}_i', \vec{r}, t)$ and $\vec{v}_i'$ signifies the velocity of the ith species after a collision. The unprimed quantities refer to condition before collision. The meaning of the differential collision cross section $\sigma_{1i}(g,\theta)$ is explained in the following:

When two particles with masses m_1 and m_2, and initial velocities $\vec{v}_1$, $\vec{v}_2$ approach each other from a great distance they eventually enter the force field of one another and undergo an elastic "collision"(or, more properly, an encounter)* through their interparticle potential V(r), ($r \equiv |\vec{r}_2 - \vec{r}_1|$), as a result of which they end up with velocities $\vec{v}_1'$ and $\vec{v}_2'$.

This type of encounters is more easily studied in a coordinate system referred to the center-of-mass of the two particles combined(see Reference 16, Chs.1 and 2) if one is interested only in momentum and energy exchange between the two particles. In this case the problem is reduced to the motion of <u>one</u> particle of mass $m_o = m_1 m_2/(m_1+m_2)$ moving under a potential V(r), with velocity(i.e. relative velocity)

$$\vec{g} = \vec{v}_2 - \vec{v}_1$$

---

*Here we consider only elastic collisions, i.e. those resulting in no change of internal energy states, whichare also not accompanied by radiative transfer.

The trajectory is depicted in Fig.11 which also defines the polar coordinates and the impact parameter b of the two colliding particles. If V(r) is known then the scattering angle

$$\theta = \theta(g,b)$$

can be determined.

Now, imagine a parallel stream of N_i particles per cm^3 with relative velocity g incident on a target particle. As shown in Fig.12, the individual trajectories will vary because the incident particles have varying impact parameters. $\sigma_{1i}(g,\theta)$ is defined by:

$gN_i \sigma_{1i} d\Omega$ = Number of particles with speed g scattered into the solid angle element $d\Omega$, θ radian from the reference axis.

where g is in cm/sec, N_i in cm^{-3}, $d\Omega$ in steradian and σ_{1i} has the dimension of cm^2/ster. and is called the differential collision cross section.

With this in mind, it can be shown that in Eq.16

$$d\vec{v}_1 d\vec{r} \iint f_1 f_i g \sigma_{1i} d\Omega d\vec{v}_i$$

is just the number of particles scattered, per unit time, out of the element $d\vec{v}_1 d\vec{r}$, and

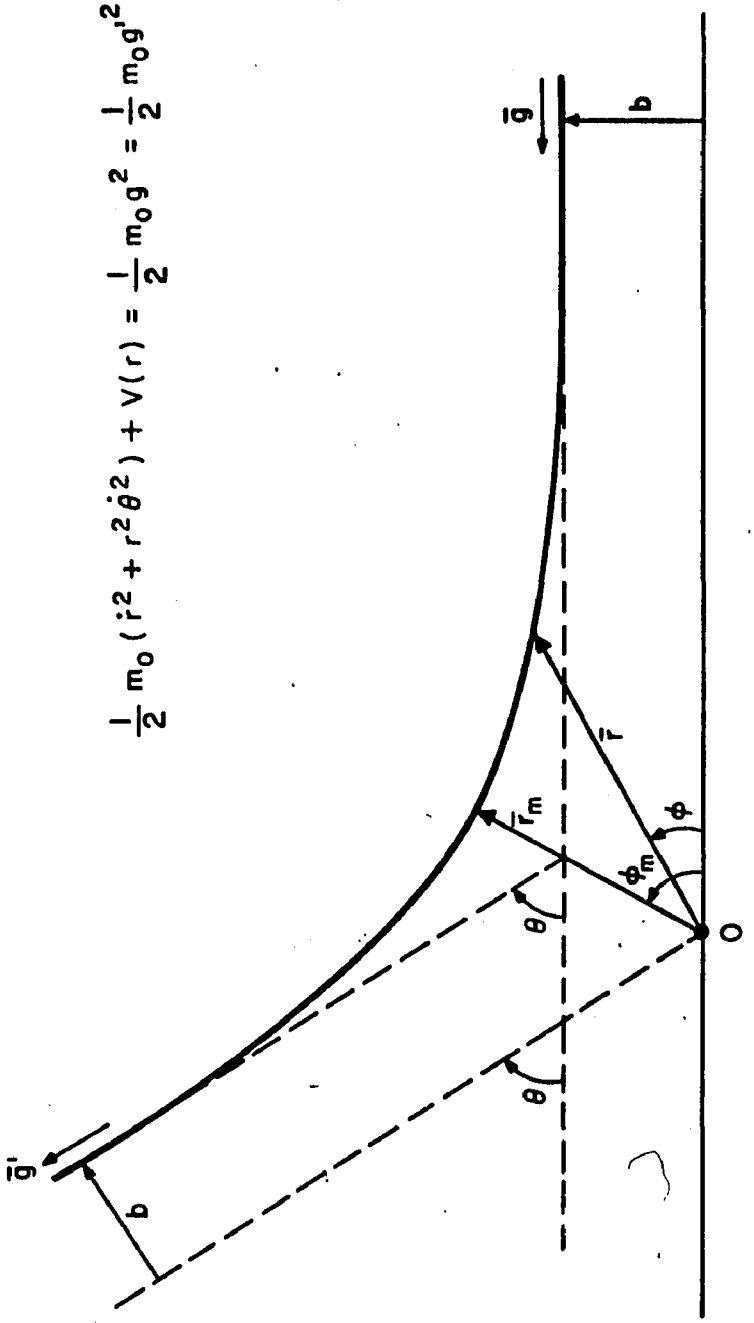

A-312-S-0185

FIG. II EQUIVALENT TRAJECTORY OF A TWO-BODY ENCOUNTER

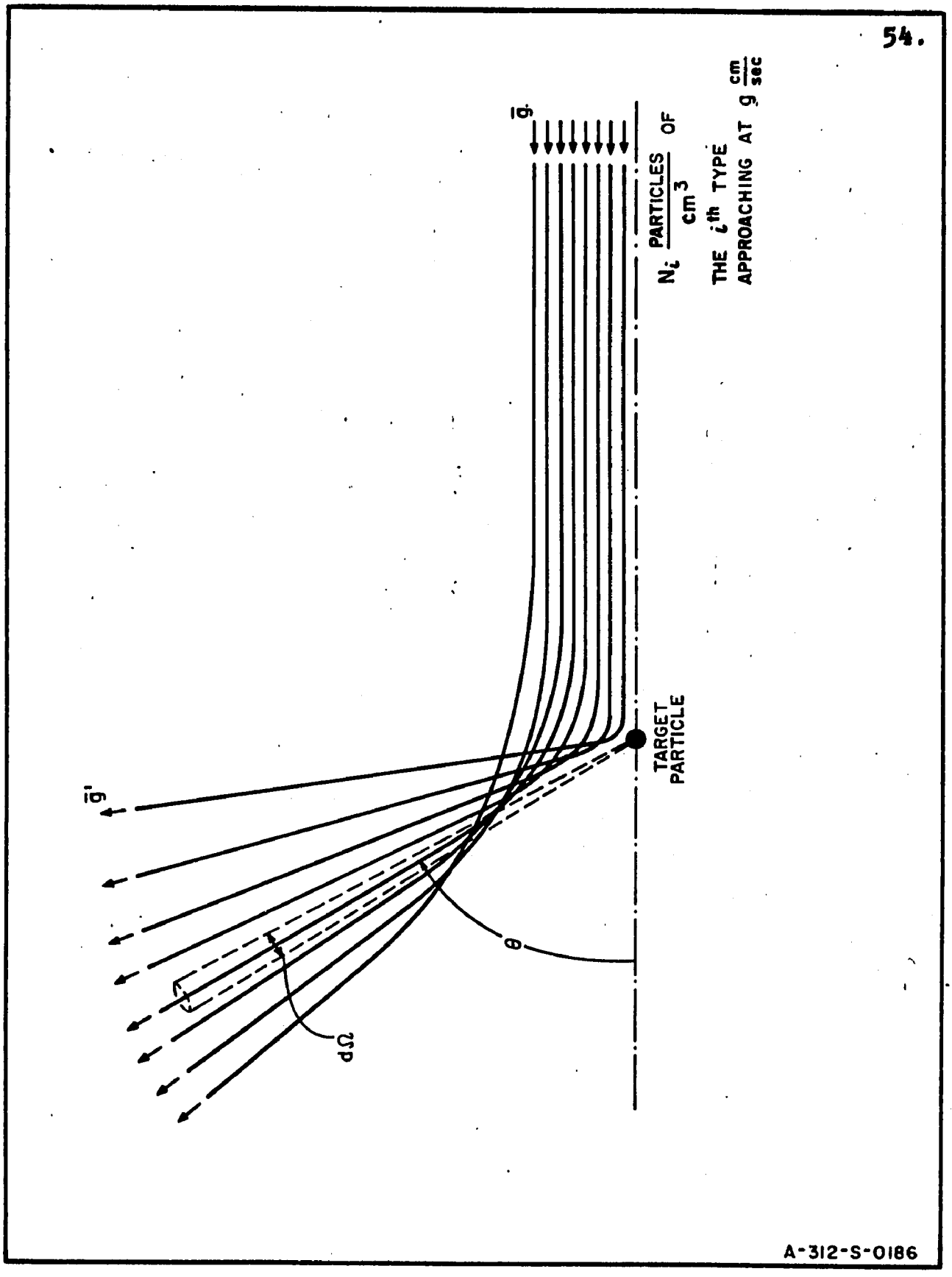

FIG. 12 SCATTERING OF PARTICLES BY A TARGET

$$d\vec{v}_1 d\vec{r} \int\int f_1' f_i' g \, \sigma_{1i} \, d\Omega \, d\vec{v}_i$$

is the number of particles scattered into the element, by the ith species. The difference of these summed over all species(i.e. Eq.16) is the net rate of change of type 1 particles in $d\vec{v}_1 d\vec{r}$, due to collisions.

Many types of interparticle potential V(r) are known theoretically, e.g. the Coulomb potential, and they can be directly introduced into the kinetic calculations. Others that are not as well known may also be treated provided that measured values of their collision cross sections are available. Examples of both will be seen later on.

The concept of a collision cross section is not limited to the elastic processes. Inelastic collision such as ionization by electron impact can also be similarly treated. Since the latter is usually much less frequent the very substantial increase in complexity of $\left(\frac{\partial f_1}{\partial t}\right)_c$ when it is directly included does not seem to warrant the effort. Effects of inelastic processes may be inserted later into the macroscopic equations derived from the Boltzmann equation.

Knowledge of f amounts to complete information on

the gas as a whole. This is, in fact, much more than needed. In general, one is interested in not more than the following three moments of f :

$$n(\vec{r},t) = \int f(\vec{v},\vec{r},t)\,d\vec{v} \qquad \text{(Eq.17)}$$

$$\langle \vec{v} \rangle = \vec{v}_i(\vec{r},t) = \int \vec{v} f(\vec{v},\vec{r},t)\,d\vec{v} \qquad \text{(Eq.18)}$$

$$\left\langle \text{Kinetic Energy} \right\rangle = \tfrac{1}{2}m\int v^2 f(\vec{v},\vec{r},t)\,d\vec{v} \qquad \text{(Eq.19)}$$

which are the macroscopic density, mean velocity and mean kinetic energy, respectively.

For gases in thermal equilibrium, a very special state but one apparently reached in many practical systems, the distribution function is:

$$f^o = n(m/2\pi kT)^{3/2}\exp\left\{-m(\vec{v}-\vec{v}_o)^2/2kT\right\} \qquad \text{(Eq.20)}$$

where T is the temperature and k the Boltzmann constant.

Equation 20 is, of course, the Maxwellian distribution function corresponding to number density n, mean velocity v_o, and, mean thermal kinetic energy* 3kT/2, a well known result of statistical mechanics (see Reference 59, Ch.IV).

* $\tfrac{1}{2}m\int(\vec{v}-\vec{v}_o)^2 f\,d\vec{v}$.

A nonequilibrium gas when not acted upon by external forces, will, as time goes on, relax to a Maxwellian distribution. The time required to achieve this state is termed the relaxation time. The relaxation is naturally dictated by the nature of the interparticle collisions; forceful and frequent collisions give rise to rapid relaxation, and vice versa.

When the particles are acted upon by external forces, their distribution function will in general not be Maxwellian but may still be stationary.

If the departure from Maxwellian is not too large (i.e. $\left|\frac{f-f^o}{f^o}\right| \ll 1$) then some form of perturbation method can be used. For instance,(see Reference 31, Ch.7) in a first approximation:

$$f = f^o + f^o \varphi \qquad \text{(Eq.21)}$$

where the perturbation function φ can then be solved for in accordance with the Boltzmann equation. Since f is a multi-dimensional function of considerable complexity φ is usually further approximated by a finite polynomial series(Sonine, Hermite polynomials, as the case may be). Using only a few terms of the expansion, methods for computing all the transport properties of gases(and gas mixtures) have been established and all

that is needed is the knowledge of the interparticle force.

It can be shown that it is the asymmetry about, or displacement from the origin in φ which accounts for transport phenomena. In a homogeneous gas in which diffusion, heat flux, and viscosity play no role, φ will be either zero or an isotropic function, at least in respect to velocity, depending on whether thermal equilibrium exists or not.

In a multi-component homogeneous gas such as our electron-ion-neutral gas in the presence of a weak* external electric field $\vec{E}$, the electrons and ions will attain drift velocities in opposite directions. Because of the much smaller electron mass, the electrom mobility is much greater than the ion mobility; this results in the arc current being primarily an electron current (in the column)

$$\vec{J} = \vec{J}_e + \vec{J}_i \cong en_e\vec{U}_e.$$

Since $\vec{E}\cdot\vec{J}$ is the power extracted from the external electric field, it follows that most of the power is transmitted first to the drifting electrons.

*More will be said shortly on what constitutes a weak electric field.

We shall see that the electrons should quickly thermalize(i.e. acquire equipartition of kinetic energy in accordance with the Maxwellian distribution) through collisions among themselves.

In Section 3.3.3 a comparison of the various computed equipartition times will be made. The electron-electron relaxation time, for example, is about 10^{-11} sec. A typical value for E is 10 v/cm and the maximum electron drift velocity U_e (for J=500 amp/cm^2) is about $5x10^5$ cm/sec. Therefore, $5X10^6$ ev/sec is gained by an electron from the field but 1ev/10^{-11}sec = 10^{11} ev/sec can be transmitted to the other electrons. From this we see that all electrons must be essentially in equilibrium. Hence, we can speak of an electron temperature, T_e.

Similarly, the self relaxation times of the heavy species will also be shown to be small in comparison with the cross relaxation times. Again, the heavy species will possess a temperature.

Furthermore, because the electrons are rather inefficient* in imparting kinetic energy to the heavy

*The energy transferred in each collision is proportional to m_e/M, the ratio of electron mass to heavy particle mass. This for argon is about 1/73500 and is indeed very small, when compared with that involving equal masses. However, as Allis(Reference 2) aptly points out, many such collisions may render the net rate appreciable.

species, considering a typical transit time through the sample volume it may not be long enough for electron-heavy particle relaxation to be completed. Thus we come to the concept of a simple two-temperature non-equilibrium.

In this connection, we observe that the mean thermal velocity given by

$$\langle v \rangle = (8kT/\pi m)^{\frac{1}{2}}$$

is 2×10^5 cm/sec for argon atoms and 6×10^7 cm/sec for the electrons at a temperature 10^4 ^{0}K. These velocities are much greater than the typical drift velocities of the respective species for $E \approx 10$ v/cm .

In the case of the electrons the existence of a drift velocity of such a small magnitude represents a small anisotropy in the electron distribution function. Hence, in the interest of tractability, we take it to be of the form given by Eq.20. That is,

$$f_e = n_e (m_e/2\pi kT_e)^{3/2} \exp\left\{\frac{-m_e(\vec{v}_e - \vec{U}_e)^2}{2kT_e}\right\} \quad \text{(Eq.22)}$$

where $\vec{U}_e$ is essentially the electron drift velocity relative to the heavy particles.

In Section 3.4 we show that the electrical conductivity of a fully ionized plasma computed from Eq.22 differs from that given by a more rigorous theory by about a factor of 2. Hence, Eq.22 is probably only approximately correct when it comes to the U_e representation.

However, one of our main purposes is to determine the transfer of random kinetic energy. That Eq.22 should be adequate in this respect may be seen with the aid of Fig.13 which demonstrates the relative flatness of f_e (large random velocity, small mass) and the delta-like feature of f_a and f_i (small random velocity, large mass). The f_e that would prevail with non-zero U_e is also shown for comparison. The displacement from the origin of the maximum of the actual electron distribution function had to be graphically exaggerated to be seen. Since it is the relative thermal motion of the electrons with respect to the heavy particles that determines the random kinetic energy transfer the shapes of the various distributions as depicted in Fig.13 lead us to believe that with a minute U_e the very small departure from an isotropic distribution in f_e should have but negligible effects on energy transfer from the electrons to the heavy particles.

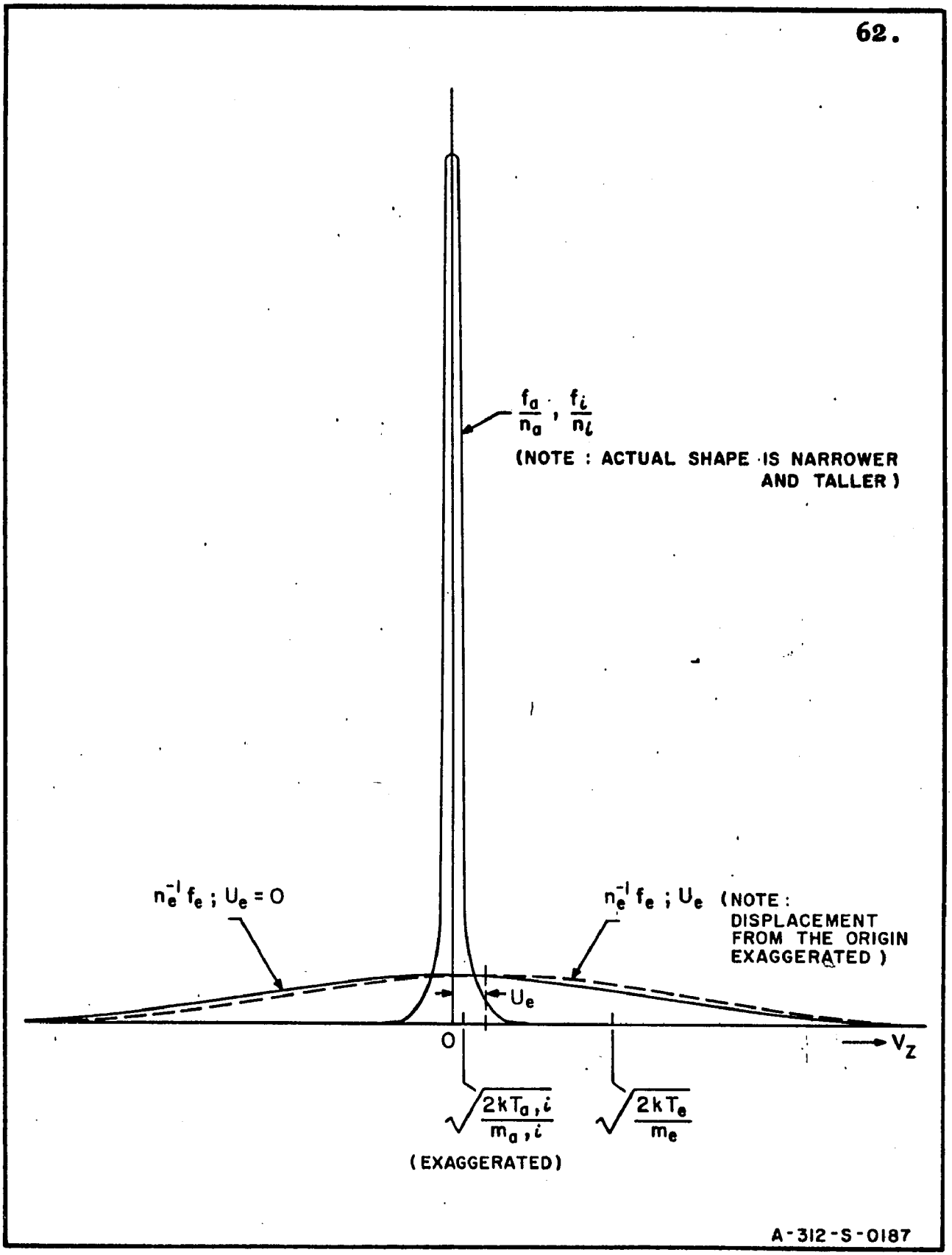

FIG. 13 SKETCHES OF DISTRIBUTION FUNCTIONS

We wish to point out that Cahn(Reference 10) in an elaborate calculation has shown that in a discharge where $n_e > 10^{12}$ cm^{-3} the electron distribution should be Maxwellian. Recently, Lyman(Reference 38) has also come to the same conclusion specifically for a low voltage electrical discharge.

In the well-known work of Spitzer and Härm(Reference 54) in computing the electrical conductivity of a fully ionized gas the perturbation of f_e is assumed to be:

$$f^{o}D(x) \cos \theta$$

where D(x) is the isotropic part of φ and $x = v(m_e/2kT_e)^{\frac{1}{2}}$ is the nondimensional speed, θ the angle between the velocity vector and the direction of the applied electric field. A small portion of their numerical results is shown in Table 2. The third column, D(x), is for

$$A = -0.002, \quad n_e = 10^{16} \text{ cm}^{-3} \quad \text{and} \quad E = 10 \text{ v/cm}.$$

From it we can see clearly the extremely small departure from the Maxwellian distribution.

The parameter

$$A = -EkT_e/\pi e^3 n_e \ln\Lambda \quad \text{(esu)}$$

TABLE 2

EXCERPTS FROM SPITZER AND HÄRM NUMERICAL RESULTS

(REFERENCE 54)

x	D(x)/A	D(x) for A=-0.002
0.1	0.0008	0.0000016
0.32	0.08	0.00016
1.04	1.65	0.0033
3.20	26.0	0.052

$$A = \frac{-EkT_e}{\pi e^3 n_e \ln\Lambda} \qquad \text{(esu)}$$

$\ln\Lambda$ is a slowly varying function of order 10

can be used as a criterion for the validity of the weak field assumption. According to the above example, 10 v/cm easily passes the test.

Once the form of the distribution functions has been chosen they can then be inserted into the appropriate Boltzmann equations and the moments corresponding to momentum and kinetic energy taken to yield the macroscopic equations of transfer of momentum and kinetic energy, respectively.

This is done in accordance with standard methods from the kinetic theory of gases(Reference 11, 31) and, though very tedious, does not present any fundamental difficulty. This very problem, in fact, has already been treated in several recent works(Reference 40, 57, 7). As it turned out, even for the Maxwellian distribution function the evaluation of the collision integrals becomes exceedingly tedious for which the interested reader may refer to the cited references for the details.

Using subscripts e, i, and a to denote electron, ion, and neutral atom, respectively, the macroscopic equations of transfer of momentum and kinetic energy in a three-component fluid are: (see Reference 40, 57)

$$m_e n_e \frac{D\vec{U}_e}{Dt} = n_e e\vec{E} + \nabla p_e - \sum_s m_e n_e \nu_{es}(\vec{U}_e - \vec{U}_s) \qquad \text{(Eq.23)}$$

$$m_e n_e \frac{DT_e}{Dt} = \frac{2}{3} T_e \frac{D(n_e m_e)}{Dt} - \sum_s m_e n_e \nu_{es} \left[\frac{2m_e}{m_e+m_s}(T_e - T_s) - \frac{2}{3k} \frac{m_s m_e}{m_s+m_e} |\vec{U}_e - \vec{U}_s|^2 \right] \qquad \text{(Eq.24)}$$

where

$$\nu_{es} = \frac{4\pi(m_s m_e)^{7/2}}{3m_e(2\pi k)^{3/2} k} \frac{\int_0^\infty \sigma_M^{es} g^5 e^{-Kg^2} dg}{(m_s+m_e)(m_s T_e + m_e T_s)^{5/2}} \cdot n_s$$

$$K = m_e m_s / 2k(T_e m_s + T_s m_e)$$

$$\sigma_M^{es}(g) \equiv \int (1-\cos\theta)\, \sigma_{es}(g,\theta)\, d\Omega$$

where $\vec{U}$ is the mean velocity, n the particle density, m the particle mass, e the electronic charge, $\vec{E}$ the electric field, p the scalar pressure, k the Boltzmann

constant, g the relative velocity of impacting bodies, T the temperature, $\frac{D}{Dt}$ the convective derivative, σ_M^{es} the momentum transfer cross section, ν_{es} the collision frequency, and, s = e, i, a for electron, ion and neutral atom, respectively.

Equations 23 and 24 are written for the electrons and they are, in general, complemented by two other sets of equations for the ions and the atoms.

For our purposes, considerable simplification is possible. First, only one spatial coordinate will be involved; $\nabla = \frac{d}{dz}$. Next, in dealing with stationary state only, the convective derivative

$$\frac{D}{Dt} = \underbrace{\frac{\partial}{\partial t}}_{0} + U_e \frac{d}{dz}$$

In addition, it can be easily shown that in our application, $\vec{U}_i$ and $\vec{U}_a$ may be assumed to be zero in comparison with $\vec{U}_e$. By virtue of the smallness of $m_e/m_{i,a}$ only T_e remains, excepting the term involving $(T_e - T_s)$ in Eq.24. Finally, the electron inertia term on the left hand side of Eq.23 can be shown to be completely negligible; that is to say, the lightweight electron fluid is resistance- and not inertia-limited.

Carrying out the above stated simplifications,

one obtains:

$$n_e eE = -\frac{dp_e}{dz} + \sum_s m_e n_e \nu_{es} U_e \qquad \text{(Eq.25)}$$

$$m_e n_e U_e \frac{dT_e}{dz} = \frac{2m_e T_e}{3} U_e \frac{dn_e}{dz} - \sum_s m_e n_e \nu_{es} \left[\frac{2m_e}{m_s}(T_e - T_s) - \frac{2}{3k} m_e U_e^2 \right] \qquad \text{(Eq.26)}$$

$$\nu_{es} = \frac{1}{3}\sqrt{\frac{2}{\pi}}\left(\frac{m_e}{kT_e}\right)^{5/2} \cdot n_s \cdot \int_0^\infty \sigma_M^{es} g^5 e^{-Kg^2}\, dg$$

$$K = m_e/2kT_e$$

We remind ourselves that Eqs.25 and 26 are strictly the results of manipulating the Boltzmann equation in which inelastic processes are not taken into account. This is quite permissible in the case of momentum transfer since the weak field regime that we are in insures that the low value of drift momentum will not give rise to inelastic process.

There is less *a priori* certainty about this for the energy equation because of the possibility of electron-ion recombinations. Now, recombination processes in such dense and active discharge are most certainly very complicated in view of the multiplicity of competing and cascading processes.

Certainly, however, with each electron-ion pair recombined the ionization energy eE_i (E_i = ionization potential) must be released. In pure radiative recombination this energy is carried off by a photon. If the plasma is not optically thin the photon may be reabsorbed and reemitted many times before being lost to the surroundings. More likely, the electron and ion will recombine to form an excited atom, either radiatively, or, through a three-body collision in which the electron potential energy difference is imparted to the second electron, thus allowing the first electron to be captured into a lower energy state.

In this fashion a fraction of eE_i will be transferred to the free electron gas. This energy we denote by eE^* ($E^* \leq E_i$). Since E_i is 15.755 v for argon and one ev is equivalent to the kinetic energy of a particle at 7730^{o}K it appears that, even if only a small fraction of E_i is dumped into the electron gas, this might constitute a sizeable energy flow. Recently,

Gusinow et al(Reference 28) have given a value of $E^* \approx 1.5$ v for argon.

As for radiative energy loss, Emmons' radiometric measurements in arcs(Reference 21) indicate $\sim$100watt/cm^3 @ 10000^{o}K and $\sim$300 watt/cm^3 @ 11000^{o}K, as compared with several kw for the elastic collisional energy loss (see Tables 6,7). Therefore since in the nonequilibrium zone T_e is around 10000^{o}K radiative loss will be a small fraction of the elastic collisional energy loss. Emmons indicates that radiative loss can be explained by continuum radiation theories. This has also been indicated by Sheer(private communication; see Appendix B).

One way of including E^* is to add a term:

$$-\left(\frac{3}{2}T_e + \frac{eE^*}{k}\right)\left(\frac{\partial n_e}{\partial t}\right)_{\text{Recomb.}}$$

to the left hand side of Eq.24. Equation 26 is then amended accordingly, viz.

$$m_e U_e\left[\frac{3}{2}n_e\frac{dT_e}{dz} - T_e\frac{dn_e}{dz}\right] + \left(\frac{3}{2}T_e + \frac{eE^*}{k}\right)\left(\frac{\partial n_e}{\partial t}\right)_{\text{Recomb.}} =$$

$$\sum_s m_e n_e \nu_{es}\left[\frac{3m_e}{m_s}(T_e - T_s) - \frac{m_e U_e^2}{k}\right] \qquad \text{(Eq.27)}$$

We now have in Eqs.25 and 27 a reasonably tractable description of the arc zone in question. It is not a complete description, however, since the number of dependent variables outnumbers the number of equations; i.e., variables

$$n_e, \quad T_e, \quad E, \quad U_e \quad T_s \quad n_s$$

versus two equations, to which we now add the charge conservation equation

$$\nabla \cdot n_e \vec{U}_e = -\left(\frac{\partial n_e}{\partial t}\right)_{\text{Recomb.}}$$

In Fig.14 we indicate the derivation for a quasi one-dimensional, i.e. a streamtube, situation and the result is:

$$(n_e U_e)^{-1}\left(\frac{\partial n_e}{\partial t}\right)_{\text{Recomb.}} = \frac{1}{n_e}\frac{\partial n_e}{\partial z} + \frac{1}{U_e}\frac{\partial U_e}{\partial z} + \frac{1}{A}\frac{\partial A}{\partial z} \qquad \text{(Eq.28)}$$

where A = cross sectional area of the column, A=A(z), and z is the axial coordinate.

Rather than dealing at once with a system of three sets of equations for the three species, we may assume T_s to be given(e.g. experimentally determined) and that

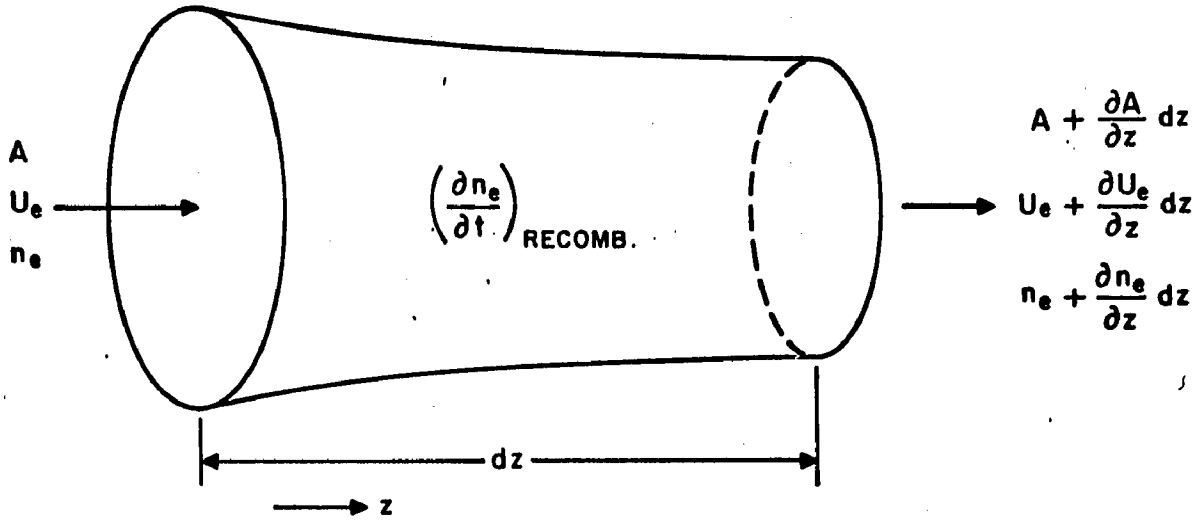

$$\left(n_e + \frac{\partial n_e}{\partial z}\right)\left(U_e + \frac{\partial U_e}{\partial z}\, dz\right)\left(A + \frac{\partial A}{\partial z}\, dz\right) - n_e U_e A = -\left(A + \frac{1}{2}\frac{\partial A}{\partial z}\, dz\right)\left(\frac{\partial n_e}{\partial t}\right)_{RECOMB}$$

AFTER RETAINING ONLY THE FIRST ORDER DIFFERENTIALS AND REARRANGING,

$$\frac{-1}{n_e U_e}\left(\frac{\partial n_e}{\partial t}\right)_{RECOMB} = \frac{1}{n_e}\frac{\partial n_e}{\partial z} + \frac{1}{U_e}\frac{\partial U_e}{\partial z} + \frac{1}{A}\frac{\partial A}{\partial z}$$

A-312-S-0188

FIG. 14 A SECTION OF STREAMTUBE

$n_i = n_e$(i.e. single ionization and quasi neutrality) and that the atom density is given by the perfect gas law:

$$n_a + 2n_e = p/kT_a$$

Now, only one more equation relating n_e to T_e will be required. Preferably this should be in the form of an algebraic function, i.e. in analogy to the usual equation of state concept, without involving another set of differential equations. This will be discussed in the next section.

3.3.2 Calculation of electron concentration. The physical picture of the ionization of a gas by the various processes is very complicated. Thus, the electron concentration is determined by the condition under which the net rate of ionization equals the net rate of deionization(ion-electron recombination and possibly ion diffusion - see Section 3.3.4 below).

The ionization processes may include the following:

(1) $A + e + E_i \longrightarrow A^+ + 2e$ (ionization by electron impact)

(2) $A + h\nu \longrightarrow A^+ + e$ (photoionization)

(3) $A + A + E_i \longrightarrow A + A^+ + e$ (ionization by atom impact)

(4) $A^+ + A \longrightarrow A + A^+$ (charge transfer)

(5) $A + e + E_{ex} \longrightarrow A^* + e$ (excitation by electron impact)

(6) $A^+ + e \longrightarrow A + h\nu$ (radiative recombination)

(7) $A^+ + e + X \longrightarrow A + X + KE$ (three-body recombination)

... etc.

In principle then, from a knowledge of the rate coefficients, the net rate of change of each species can be solved for.

As an example, considering only the reactions (1), (2), (3), (6) and (7) we have the following equations:

$$\frac{dn_e}{dt} = \alpha_1 n_e n_a + \alpha_2 n_a n_\lambda + \alpha_3 n_a^2 - \alpha_6 n_e^2 - \alpha_7 n_e n_a n_x$$

$$\frac{dn_a}{dt} = -\alpha_1 n_e n_a - \alpha_2 n_a n_\lambda - 2\alpha_3 n_a^2 - \alpha_5 n_e n_a + \alpha_6 n_e^2 + \alpha_7 n_e n_a n_x$$

$$\frac{dn_x}{dt} = \ldots$$

$n_e = n_i$ for single ionization; $n_\lambda = \ldots$

where the α's are the rate coefficient. $\alpha = \alpha(T)$.

In steady state, the time derivatives are set to zero and only a system of algebraic equations results. If the coefficients are known solution of this system will yield the concentration of different types of particles at equilibrium. In practice, this is a formidable task, made virtually impossible by the gross lack of knowledge about many of the coefficients, especially those for the photon processes and the recombination processes.

The above indicates the difficulties encountered if the computation of particle densities is approached from the point of view of kinetic theory. This is because the application of kinetic theory requires complete and accurate particle description.

The statistical mechanics approach to the problem often proves more tractable. In accordance with elementary quantum mechanics, there exist discrete energy states for a particle, and, when there is thermal equilibrium, the probability, $P(\epsilon_i)$, that the particle occupies the energy state, ϵ_i, when the total energy and the volume of the whole system are fixed, is the Maxwell-Boltzmann equilibrium distribution:

$$P(\epsilon_i) = \text{constant} \cdot e^{-\epsilon_i/kT}$$

When the energy is identical for several quantum states, then,

$$P(\epsilon_i) = \text{constant} \cdot g_i \, e^{-\epsilon_i/kT}$$

where g_i, the number of states with energy ϵ_i, is known as the order of degeneracy.

The partition function Z evaluates the probability that all of the allowable degenerate states of energy ϵ_i are occupied and is defined as:

$$Z = \sum_i g_i \, e^{-\epsilon_i/kT}$$

It is often more aptly called the "sum of states".

In general, there is more than one type of energy state. When the energy states of different types are independent of one another, the total probability is the product of the probabilities corresponding to the different independent types of energies. Thus, when translational, rotational, vibrational, and electronic excitation levels are relevant,

$$Z = Z_{tr} Z_{rot} Z_{vib} Z_{elec} \cdot$$

For argon atoms or argon ions, only the translational

and electronic excitations need to be considered,* and we have

$$Z = Z_{tr} Z_{elec} \cdot$$

Z_{tr} is the partition function corresponding to the three degrees of translational motion, and can be shown to be: (see Reference 18, p.374)

$$Z_{tr} = (2\pi mkT)^{3/2} V/h^3$$

where m is the particle mass, V the volume, and h the Planck constant.

Let us consider the reaction

$$A + E_i \rightleftharpoons A^+ + e$$

where E_i is the ionization potential. From the definition of the partition function and equilibrium considerations(see Reference 18, p.380) one obtains

$$N_e N_i / N_a = Z_e Z_i / Z_a$$

---

*Only molecules with two or more atoms have rotational and vibrational excitation. Neutral argon rarely forms molecules. Argon ions tend to form clusters, but only at very low temperatures. We are, of course, referring only to conditions in arcs.

where N stands for number of particles.

Assuming that each species possesses temperature (see Section 3.3.3), the partition function for the electrons is

$$Z_e = 2(2\pi m_e kT_e)^{3/2} V/h^3$$

where the factor 2 is due to the two possible spin states.

Similarly, for the ions and the neutral atoms

$$Z_i = (2\pi m_i kT_i)^{3/2} V Z_{i_{elec}} / h^3$$

and, $$Z_a = (2\pi m_a kT_a)^{3/2} V Z_{a_{elec}} /h^3$$

Therefore,

$$\frac{N_e N_i}{N_a} = \frac{2(2\pi m_e kT_e/h^2)^{3/2} V (2\pi m_i kT_i/h^2)^{3/2} V Z_{i_{elec}}}{(2\pi m_a kT_a/h^2)^{3/2} V Z_{a_{elec}}}$$

or,

$$\frac{n_e n_i}{n_a} = 2(2\pi m_e kT_e/h^2)^{3/2} \left(\frac{m_i T_i}{m_a T_a}\right)^{3/2} \frac{Z_{i_{elec}}}{Z_{a_{elec}}} \qquad \text{(Eq.29)}$$

where n stands for particle density, cm^{-3}.

From Eq.29, assuming quasi neutrality ($n_e=n_i$) and given the electronic excitation partition functions for the ions and the neutral atoms, n_e can be computed. This is done in Section 3.3.3.

There are two important factors affecting the validity of equilibrium concentration calculation from statistical mechanics. The first has already been mentioned, namely, thermal nonequilibrium. The second is the loss of charged particles by diffusion, i.e. arising from spatial inhomogeneity. This is elaborated in Section 3.3.4.

3.3.3 Nonequilibrium considerations. Although it is difficult to state with any certainty the exact condition under which departure from thermal equilibrium is truly characterized by assignment to each species its own temperature, even with as simple a system as $A - A^+ - e$, yet there exists a definite scale in relaxation times favoring the equilibration of one reacting pair over that of another.

Based on available theories of energy equilibration (Reference 53 for Coulomb interactions, Reference 40 for equivalent hard-sphere interactions), Table 3 has been

TABLE 3

RELAXATION TIMES FOR TYPICAL ARC CONDITIONS

$t_{\alpha\beta}$, Formula	Condition	$t_{\alpha\beta}$, sec / $t_{\alpha\beta}/t_{ee}$
$t_{ee} = \dfrac{11.4\ T_e^{3/2}}{n_e (1836)^{\frac{1}{2}} \ln\Lambda}$	$n_e = 10^{16}\,cm^{-3}$ $\ln\Lambda \sim 10$ $T_e = 10^4\ ^oK$	10^{-11} 1
$t_{ii} = \dfrac{11.4(40)^{\frac{1}{2}}\ T_i^{3/2}}{n_i\ \ln\Lambda}$	$n_i = 10^{16}\,cm^{-3}$ $\ln\Lambda \sim 10$ $T_i = 10^4\ ^oK$	6×10^{-10} 60
$t_{ia} = \dfrac{6.72\times10^{-2}}{n_a\ \sigma'_{CT}\ T_i^{\frac{1}{2}}}$ (mks)	$n_a = 10^{24}\ m^{-3}$ $\sigma'_{CT} = 10^{-18}\ m^2$ $T_i = 10^4\ ^oK$	7×10^{-10} 70
$t_{aa} = \dfrac{6.72\times10^{-2}}{n_a\ \sigma'_{aa}\ T_a^{\frac{1}{2}}}$ (mks)	$n_a = 10^{24}\ m^{-3}$ $\sigma'_{aa} = 3\times10^{-19} m^2$ $T_a = 10^4\ ^oK$	2.5×10^{-9} 250
$t_{ei} = \dfrac{5.87\times40(1836)^{\frac{1}{2}}T_e^{3/2}}{n_e\ \ln\Lambda}$	$n_e = 10^{16}\,cm^{-3}$ $\ln\Lambda \sim 10$ $T_e = 10^4\ ^oK$	10^{-7} 10,000
$t_{ea} = \dfrac{271\times1.16\times10^{-2}}{n_a\ \sigma_{ea}\ T_e^{\frac{1}{2}}}$ (mks)	$n_a = 10^{24}\ m^{-3}$ $\sigma_{ea} = 10^{-20}\ m^2$ $T_e = 10^4\ ^oK$	3.2×10^{-6} 320,000

constructed which gives the expressions for $t_{\alpha\beta}$ (α, β = e,i,a) and the numerical values under typical arc conditions.

A striking feature to note is the extremely short t_{ee} and the 1 to 320000 ratio between t_{ee} and t_{ea}. Since the electron transit time through the sample volume is about 2×10^{-6} sec and that for the heavy particles is 500×10^{-6} sec it follows that on the basis of the computed relaxation time scale one would expect the electrons to most rapidly attain a defined temperature(10^{-11} sec), then the ions(60×10^{-11} sec), and finally the atoms(250×10^{-11} sec).

After these early epochs of self-relaxation the fastest of the cross-relaxation then sets in to be followed by the next and so forth.

It is, of course, the cross-relaxations that we are mostly concerned with. In this regard, it is interesting to note that the i-a equilibration(70×10^{-11} sec) is an extremely fast one due to the high probability of a charge transfer process. This is one of the important reasons for assuming the ion ground state to be in essential equilibrium with the atoms. The fact that the e-a equilibration rate is on the bottom of the scale(320000×10^{-11} sec) provides the justification in postulating a nonequilibrium state characterized by

two temperatures, namely, T_e and T_a(or T_g).

There is, of course, still T_i to be considered in order that Eq.29 may be used to determine the charge concentration.

For a long time workers in the field of gaseous electronics have been puzzled by the discrepancy of as much as two orders of magnitude that existed between observed values of recombination rate and that predicted by the quantum theory of radiative recombination. The explanation, until very recently, was thought to lie in the mechanism of dissociative recombination,

$$KE + A_2^+ + e \longrightarrow A^* + A^*$$

wherein a molecular ion is dissociated with high probability by electron impact into two excited atoms, the ionization energy and the electron kinetic energy being translated into excitation energies. This point of view was reinforced by the observed presence of A_2^+ in gas discharges(Reference 37) and the extraordinarily low ionic mobility sometimes observed. Recently, D'Angelo (Reference 15) has suggested the following three-body recombination as being active in dense plasmas:

$$A^+ + e + e \longrightarrow A^* + e + KE$$

These, as well as the ionization by electron impact, are all functions of T_e, but this alone does not provide the full justification. The key lies in what become of the excited atoms. They may be re-ionized by electron impact,

$$KE + A^* + e \longrightarrow A^+ + 2e$$

or, excited to high level by electron impact,

$$KE + A^* + e \longrightarrow A^{**} + e$$

or, de-excited by electron impact(superelastic collision)

$$A^* + e \longrightarrow A + e + KE$$

or, de-excited by emission of radiation,

$$A^* \longrightarrow A + h\nu \quad .$$

It has been shown by Byron, Stabler, and Bortz(Reference 9) that for hydrogen atoms in excited states, the rate of radiative de-excitation from a state with principal quantum number n to the next lower decreases very rapidly with the value of n, while the collisional de-excitation rates increase rapidly with the value of

n. This results in a marked minimum in the total rate (sum of radiative plus collisional) at a certain principal quantum number n^*. Since changes involving $\Delta n > \pm 1$ are either forbidden or much less probable, the minimum at n^* acts as the weakest link in a chain reaction and effectively limits the overall rate of de-excitation. In this way, the states above n^* are in essential equilibrium with the electrons, leaving those below to be in equilibrium with the ground state atoms. The same argument could be applied to the ions and the picture emerges of the electrons and a small number of highly excited atoms and ions partitioned off by the minimum rate gap from the lower state atoms and ions.

This prolonged reasoning now tells us that Eq.29 should be evaluated by assuming $T_i = T_a \neq T_e$ for the ground states, and $T_i = T_a = T_e$ for the higher excited states.

For argon, Bond(Reference 5) has given the following partition functions:

$$Z_{i_{elec}} = 4 + 2e^{-2062/T} + 2e^{-156560/T} + 8e^{-190550/T} + \ldots$$

and,

$$Z_{a_{elec}} = 1 + 60e^{-162500/T} + \ldots$$

Using the above partition functions and taking $m_i = m_a$, $T_i = T_a$, Eq.29 can now be put into use,

$$\frac{n_e n_i}{n_a} \cong 2\, e^{-eE_i/kT_e}(2\pi m_e kT_e/h^2)^{3/2}\frac{4+2e^{-2062/T_e}}{1+60e^{-162500/T_e}}$$

where, of course, the partition function energies have been referred to one origin(at atom ground state).

For quasi-neutral plasma($n_e \simeq n_i$), and leaving off higher order terms in the partition functions,*

$$\frac{\alpha^2}{1-\alpha} \cong \frac{3.27\times10^{-7}T_a}{p_{ai}}\,\frac{2(4+2e^{-2062/T_e})}{1+60e^{-162500/T_e}}T_e^{3/2}\; e^{-183000/T_e}$$

$$= \frac{\beta^2}{\beta+1} \qquad \text{(Eq.30)}$$

where $\alpha = n_e/(n_e+n_a)$ is the fractional ionization

$$\beta = n_e/n_a$$

$$p_{ai} = (n_a+n_i)kT_a$$

*For arc temperatures encountered higher order terms are quite insignificant. It appears that some equations similar to Eq.30 are found in the literature that do not seem to have the correct degeneracy factors, and, probably can give quite different results.

3.3.4 Loss of charged particles by diffusion.

Consider a cylindrical element of the arc column as shown in Fig.15 where the main stream of electrons and ions are moving axially in an electric field and in opposite directions. Because of the charge density gradient between the column and its surroundings, the electrons diffuse out radially and drag along the much slower ions. In a steady state, the radial electron flux must equal the radial ion flux and the overall diffusion rate is given by the ambipolar diffusion coefficient, D_a, which is approximately twice the value of the ion diffusion coefficient. Even though ambipolar diffusion does not result in recombination within the arc column its tendency to upset the charge concentration equilibrium can be seen as follows:

Charge conservation requires

$$\nabla \cdot \vec{J}_i = \frac{\partial J_{ir}}{\partial r} + \frac{\partial J_{iz}}{\partial z} = - \frac{\partial n_i}{\partial t}$$

$$\nabla \cdot \vec{J}_e = \frac{\partial J_{er}}{\partial r} + \frac{\partial J_{ez}}{\partial z} = - \frac{\partial n_e}{\partial t} = + \frac{\partial n_i}{\partial t} \qquad \text{(Eq.31)}$$

where J_{ir} and J_{er} are the ambipolar diffusion current

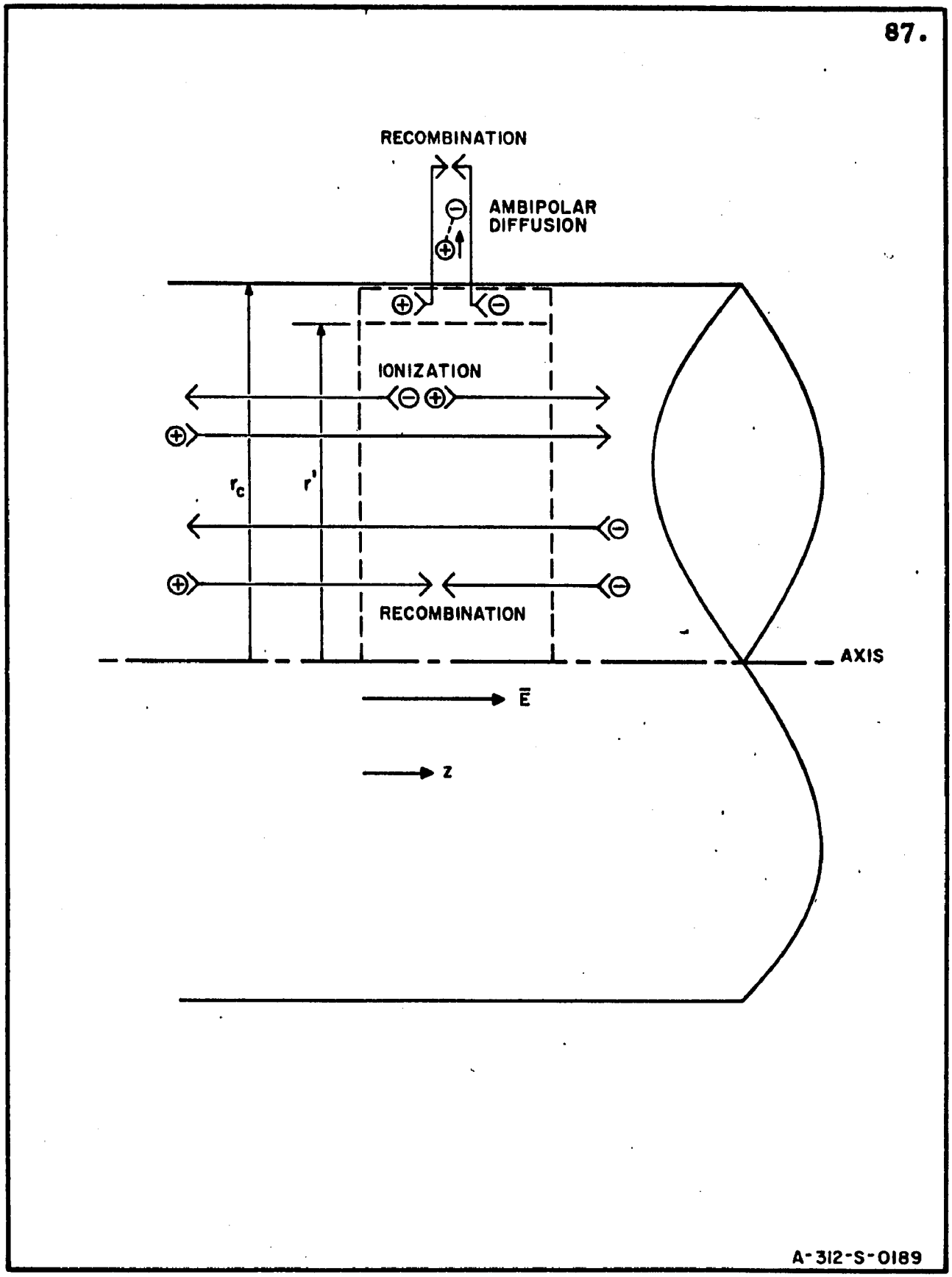

FIG. 15 CHARGED PARTICLE BALANCE IN AN ARC COLUMN.

densities, hence,

$$J_{ir} = J_{er} \ .$$

Consequently,

$$\frac{\partial J_{iz}}{\partial z} + \frac{\partial J_{ez}}{\partial z} = 0 \qquad \text{(Eq.32)}$$

and therefore,

$$J_{iz} + J_{ez} = \text{constant}$$

$$I_{iz} + I_{ez} = \text{constant}.$$

Now, multiplying Eq.31 by $2\pi r$ and integrating from 0 to r_c, the radius of the arc boundary, we have

$$2\pi r_c J_{i,er}(r_c) - 2\pi \int_0^{r_c} J_{i,er}\,dr + \frac{dI_{i,ez}}{dz} = \frac{-\partial}{\partial t} 2\pi \int_0^{r_c} r n_{e,i}\,dr$$

(Eq.33)

If $J_{i,er}$ is negligible within the column except in the interval $\Delta r = r_c - r'$, then

$$2\pi \int_0^{r_c} J_{i,er}\,dr \cong 2\pi \int_{r'}^{r_c} J_{i,er}\,dr \cong 2\pi\, J_{i,er}(r_c)\,\Delta r$$

and it appears as a second order term compared with $2\pi r_c J_{i,e}(r_c)$ and may therefore be neglected. Equation 33 may then be interpreted as:

$$\text{(Ambipolar diffusion flux/unit length)} + \frac{dI_{i,ez}}{dz}$$

$$= \text{(Recombination/unit length)}.$$

In consequence of Eq.32, $\frac{dI_{i,ez}}{dz}$ will be nearly zero if the applied electric field is the principal driving force of the electron and ion currents such as when the axial density gradients are small. Under this condition the effects of ambipolar diffusion losses are equivalent to recombination within the arc column. The previous calculation of electron concentration must therefore be subject to the condition that ambipolar losses be small.

To establish a criterion for its smallness we compute the diffusion flux in the radial direction. Whereas within the arc zone the electrons continually receive energy from the applied electric field and then pass it on to the other constituents of the arc, outside the arc column the electrons are in decay - receiving no energy but losing their initial energy and recombining with the ions.

The appropriate equation for the decaying plasma is: (see Reference 4)

$$\nabla^2 n = \frac{\alpha}{D_a} n^2$$

where α is the electron-ion recombination coefficient (normalized for two-body recombination) and D_a is the ambipolar diffusion coefficient. In a cylindrical coordinate system, and assuming $\frac{\partial}{\partial\theta} = \frac{\partial}{\partial z} = 0$,

$$\nabla^2 n = \frac{d^2 n}{dr^2} + \frac{1}{r}\frac{dn}{dr} = \frac{\alpha}{D_a} n^2$$

which is a nonlinear differential equation possessing no known closed solution. If the first derivative term can be neglected, as when r is appreciable, then the resulting(still nonlinear) equation may be integrated to yield:

$$n = \frac{1}{\left(\frac{r-r_c}{\sqrt{6D_a/\alpha}} + \frac{1}{\sqrt{n_c}}\right)^2} \qquad \text{(Eq.34)}$$

where r_c is the radius of the active column with charge density n_c. In Eq.34, in contrast with the usual calcu-

lations of arc radial profile, no material boundary condition is applied. Instead, we have imposed the condition

$$n = 0 \quad @\ r = \infty$$

which, in turn, implies also $\frac{dn}{dr} = 0$ @ $r = \infty$ as a consequence of the positiveness of the quantity n. The radial flux is now simply

$$- D_a \frac{dn}{dr} = 2(D_a \alpha /6)^{\frac{1}{2}} n_c^{3/2}$$

which for typical values of $D_a \cong 1$ cm^{2}sec^{-1}, $\alpha \cong 10^{-10}$ cm^{3}sec^{-1} and $n_c \cong 10^{15}$ cm^{-3}, the loss is roughly 10^{17} particles/cm^{2}sec.

This order of loss rate may seem startlingly high when one compares it with the rate of ionization by electron impact which can be shown to be: (see Appendix C)

$$\Gamma_i = \frac{4 n_a n_e A B \bar{c}}{\sqrt{\pi}} \left[\frac{E_i}{2B} + \bar{c}^2 \right] \exp(-E_i / B\bar{c}^2) \qquad \text{(Eq.35)}$$

which gives a rate only comparable to the diffusion loss.

However, the values of cross section data used in Eq.35 were obtained from ordinary atomic measurements at low density and room temperatures where multi-step

ionization involving excited states was not accounted for. The production of excited states in argon, e.g. at 9000^{o}K, is about 500 times that of ionization and in high density plasmas is most likely going to lead to ionization from excited states yielding a total rate of ionization orders of magnitude greater than that indicated by this simple calculation.

Because of the lack of precise data on a multi-step ionization process we will not pursue this line any further but will henceforth assume it to overshadow the diffusion loss mechanism.

To the support of this assumption, we cite the fact that a 10^{17} per second loss rate would amount to only 16 milliamp of current and would seem to be insignificant amount in comparison with the 100,000 milliamp or so of arc current.

3.4 Equations for the Two-Temperature Column

With Eqs.25, 27, 28, and 30 we shall see what is to be expected of the two-temperature plasma. These equations will not be solved in the usual sense primarily because of the uncertainties in boundary conditions and in the values of some of the parameters. However, using empirical results we shall check their consistency.

From the momentum equation (Eq.25) we observe that the drift velocity U_e is proportional to

$$\left(E - \frac{1}{en_e} \frac{dp_e}{dz} \right)$$

or $(E+E_p)$ where

$$E_p = \frac{-kT_e}{e} \left(\frac{dT_e}{T_e dz} + \frac{dn_e}{n_e dz} \right)$$

is the equivalent field intensity (v/cm) due to inverse temperature and concentration gradients.

For an isothermal plasma,

$$E_p = \frac{-kT_e}{e} \frac{dn_e}{n_e dz}$$

in agreement with the well-known Einstein relation:

$$D_e/\mu_e = kT_e/e \quad . \quad (\mu_e = \text{mobility})$$

A very important property of the arc column, one that is easily correlated with experimental results, is the ordinary electrical resistivity which may be derived from Eqs.25 and 26:

$$\eta = \frac{E}{J} = \frac{\sum_s m_e \nu_{es}}{e^2 n_e}$$

To evaluate it one needs only σ_M^{ie} and σ_M^{ea} .

Since electrons and ions interact through Coulomb force and it is well-known that this gives rise to an infinite momentum transfer cross section, various means have been used to render it finite(as seems only reasonable). An often adopted approach(see Reference 49) is to limit the sphere of interaction to within a shielding length, λ_D, which is the radius of the so-called "Debye sphere":

$$\lambda_D = (\epsilon_o kT_e/n_e e^2)^{\frac{1}{2}}$$

This yields:

$$\sigma_M^{ei} = e^4 \ln\Lambda / 4\pi \epsilon_o^2 m_e^2 g^4$$

where the Coulomb logarithm is:

$$\ln\Lambda = \ln\left[12\pi (\epsilon_o k T_e / e^2)^{3/2} / n_e^{\frac{1}{2}}\right]$$

From the above, we obtain the electron-ion collision frequency:

$$\nu_{ei} = \frac{n_e e^4 \ln\Lambda}{3\epsilon_o^2 (2\pi k)^{3/2} m_e^{\frac{1}{2}}} \cdot \frac{1}{T_e^{3/2}} \qquad \text{(Eq.36)}$$

and, from which the electron-ion resistivity:

$$\eta_{ei} = m_e \nu_{ei} / e^2 n_e$$

$$= \frac{m_e^{\frac{1}{2}} e^2 \ln\Lambda}{3\epsilon_o^2 (2\pi k)^{3/2}} \cdot \frac{1}{T_e^{3/2}}$$

$$= 128.5 \ln\Lambda / T_e^{3/2} , \quad \text{ohm-m} \quad \text{(Eq.37)}$$

Equation 37 is identical to the formula given by Spitzer and Härm(Reference 54), except that their numerical factor in front is 65.3 - almost half of ours.

This is, in part, due to the form of the f_e assumed which is not expected to give as accurate a result in drift velocity(i.e. electrical conductivity) as in kinetic energy transfer. For this reason, the more or less accepted results of Spitzer and Härm(the 65.3 factor) will be used instead.

The electron-atom interaction force is not so well known as the Coulomb force. It is well known from the measurements of Ramsauer and Kollath(Reference 8) and subsequent works that the cross sections for argon, krypton and xenon increase with decrease in electron energy, reach a maximum around 10 ev, then sharply decrease to a minimum which for argon is around 0.5 ev. The transparency to low energy electrons is usually explained quantum mechanically by the diffraction of the electron wave by certain feature of the argon potential(Reference 30). However, others(Reference 27) thought it could be explained classically. At any rate, the argon minimum occurs precisely in the energy range of most interest to us(i.e. in the range of 3000 to 12000^{o}K) and no really reliable measurements of the cross section have been made in this energy range. In the usual practice, an equivalent hard-sphere(i.e. energy-independent) cross section of the order of 10^{-16} cm^2 is used.

Recently, Engelhardt and Phelps* reported the cross section from 0.02 to 20 ev. which they obtained through fitting of drift velocity data. Their results are reproduced in Fig.16. Since we are interested in σ_M^{ea} only in so far as it affects the integral for the collision frequency ν_{ea}, that is:

$$M_{ea} = \int_0^\infty \sigma_M^{ea}\, g^5\, e^{-Kg^2}\, dg.$$

This integral has been numerically evaluated by us for a range of electron temperatures. The results are shown in Fig.17 where the values of integrals using several hard-sphere cross sections are also included. It is interesting to note that the behavior for the two types of cross sections are rather different. For the hard-sphere the integral varies as T_e^3 while for the Engelhardt and Phelps cross section the integral may be represented accurately by:

$$M_{ea} = 9.81\times10^{14}(T_e/10000)^{4.3} \quad \text{(mks)} \qquad \text{(Eq.39)}$$

for $2000^\circ K \leq T_e \leq 12000^\circ K$

*Engelhardt,A.G. and Phelps,A.V., Tech.Rept.20, Physics Dept., Westinghouse Research Labs., Pittsburgh 35, Pa.

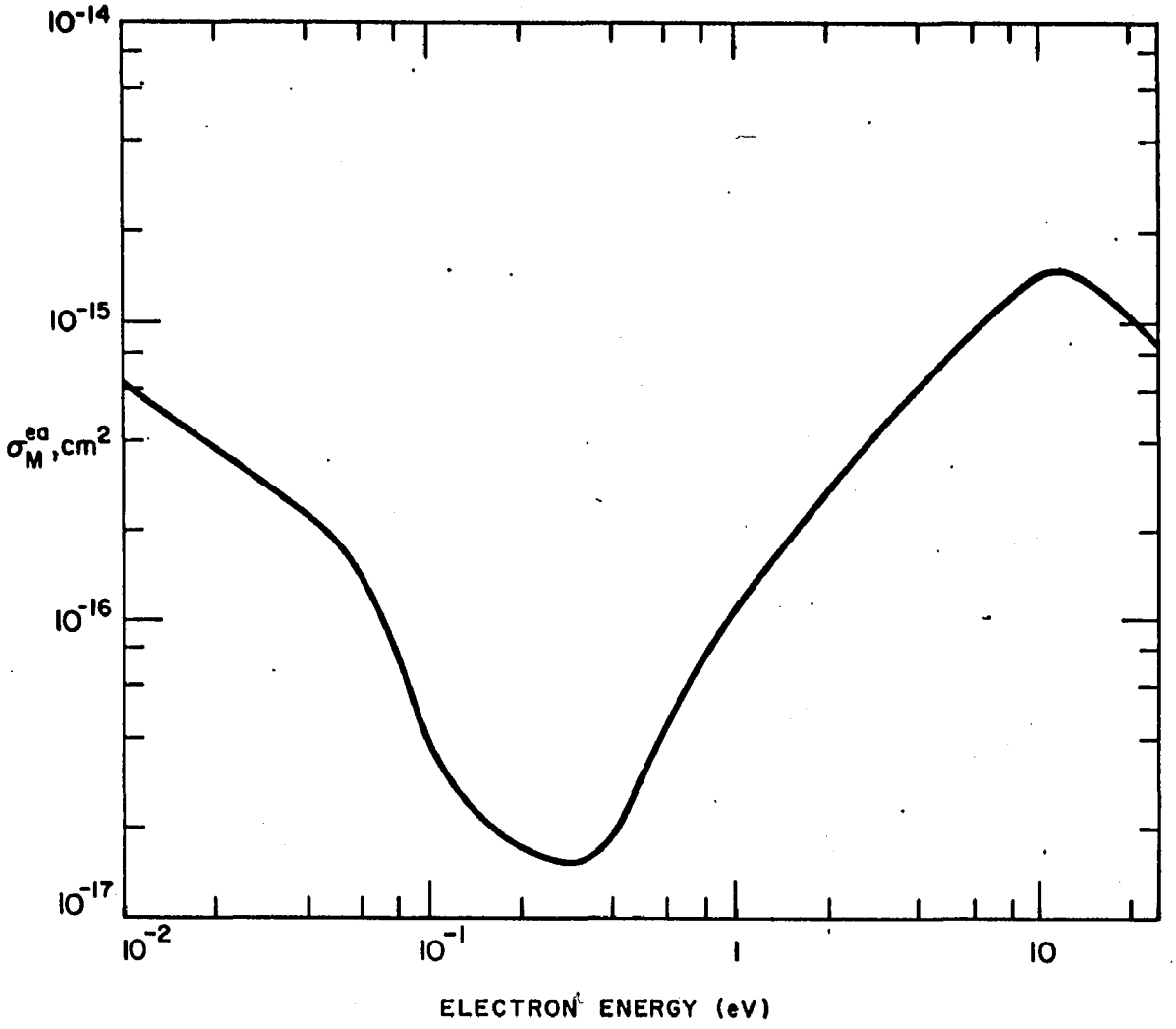

FROM ENGELHARDT, A.G. AND PHELPS, A.V., TECH. REPT. 20, PHYSICS DEPT., WESTINGHOUSE RESEARCH LABS.

A-312-S-0190

FIG. 16 MOMENTUM TRANSFER CROSS SECTION OF ELECTRON IN ARGON, DEDUCED FROM ELECTRON MOBILITY DATA

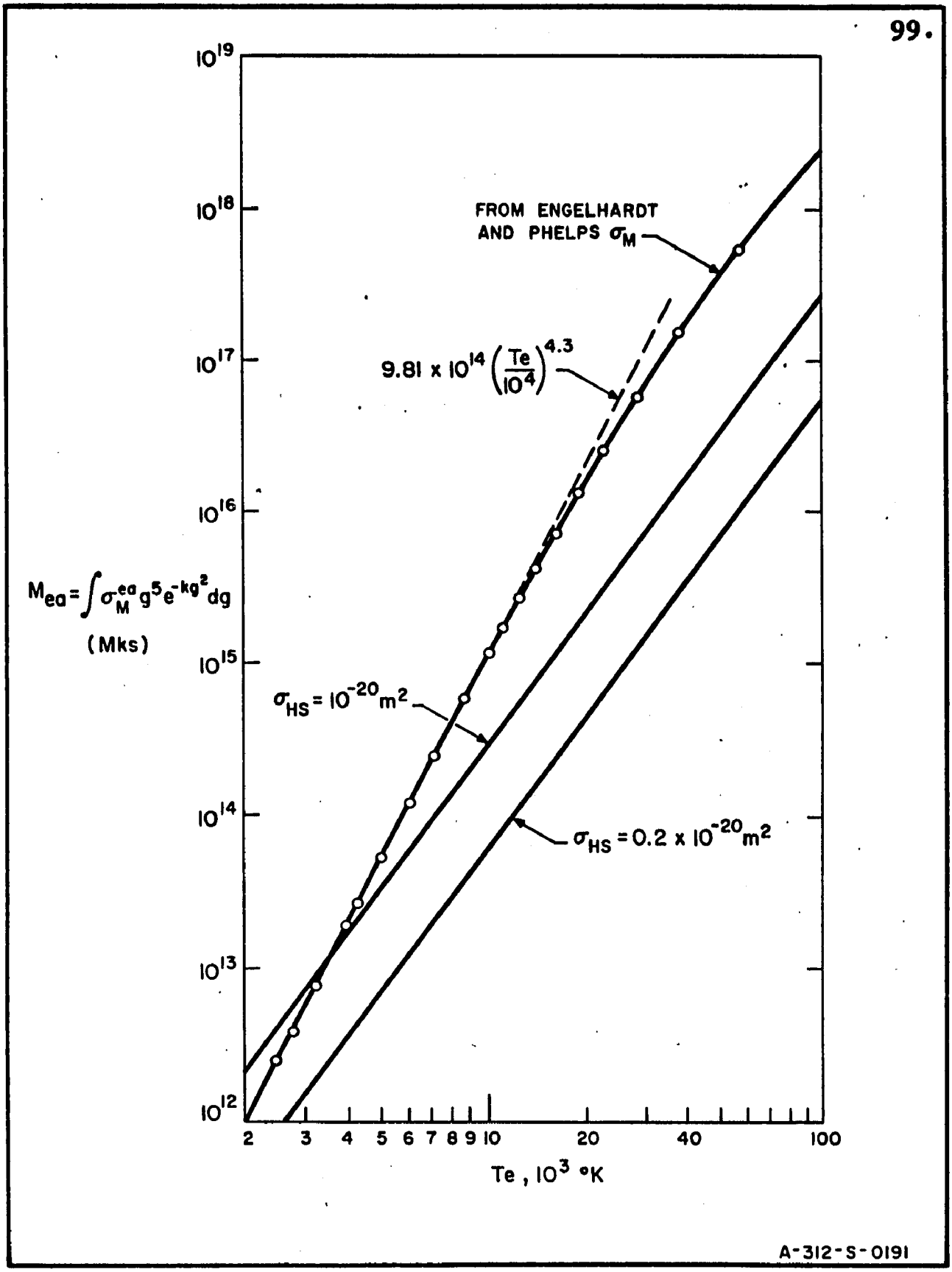

FIG. 17 VALUES OF THE COLLISION INTEGRAL FOR ELECTRONS IN ARGON

Now, using Eqs.26 and 38, the electron-atom collision frequency for argon can be expressed in closed form:

$$\nu_{ea} = 2.92\text{x}10^{-14}\ n_a(T_e/10000)^{1.8}\ \text{sec}^{-1} \qquad \text{(Eq.39)}$$

and, the electron-atom resistivity:

$$\eta_{ea} = 1.04\text{x}10^{-6}(n_a/n_e)(T_e/10000)^{1.8}\ \text{ohm-m} \qquad \text{(Eq.40)}$$

The total electrical resistivity is given by the sum of Eqs.37 and 40. The value of n_e needed is first evaluated by means of Eq.30, as plotted in Fig.18. The resistivity (plotted as conductivity to facilitate comparison with works by others) as a function of temperature at 1 atm pressure is shown in Fig.19.

There are many reported results of computations for the electrical conductivity of partially and fully ionized argon. For recent works we refer to that by Ahtye(Reference 1) and by deVoto(Reference 17) who solved the Boltzmann equation by the usual Chapman-Enskog procedure which is known to be quite tedious.

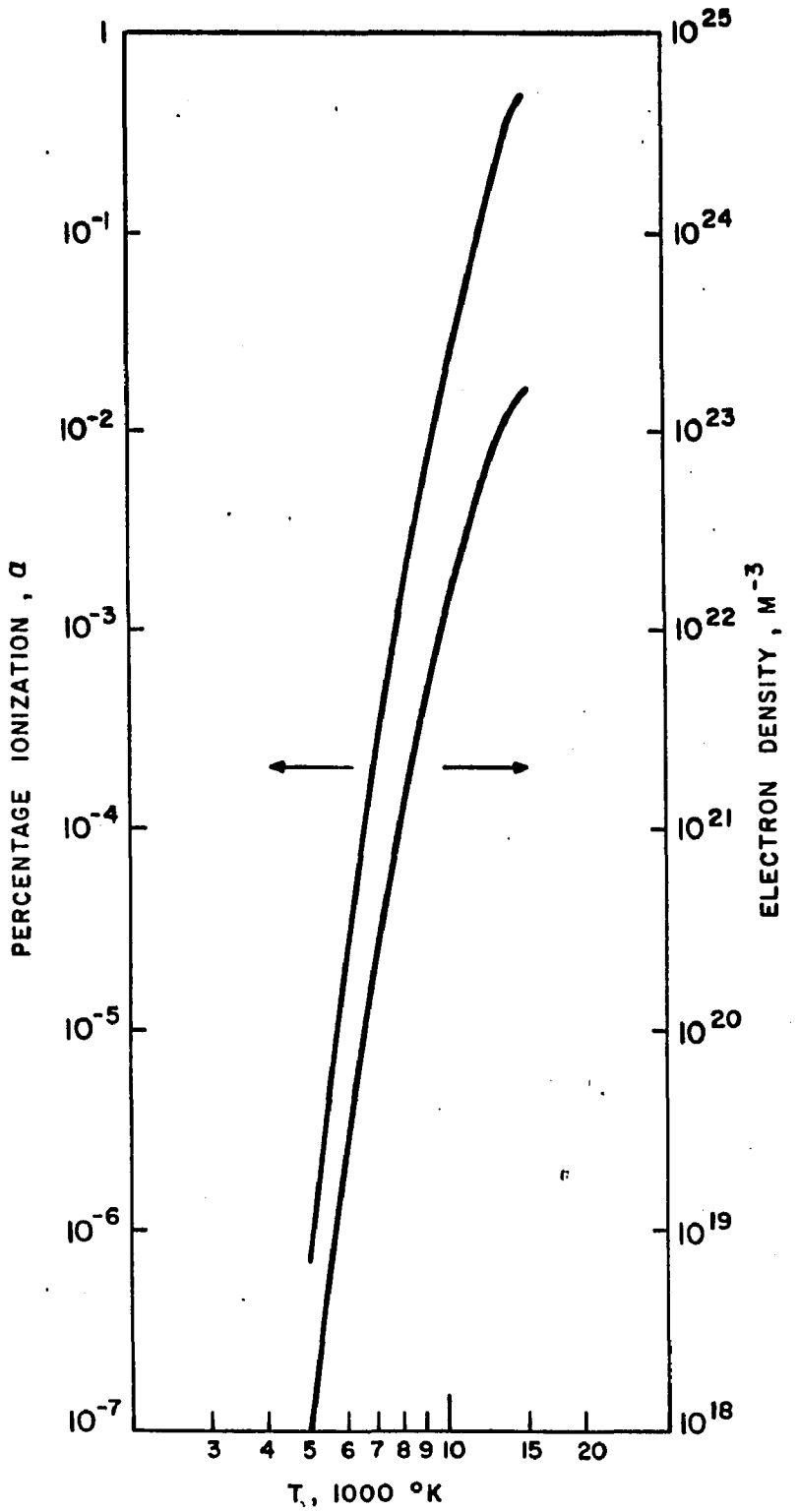

FIG. 18 ELECTRON DENSITY AND PERCENT IONIZATION OF 1 ATM. ARGON vs. TEMPERATURE

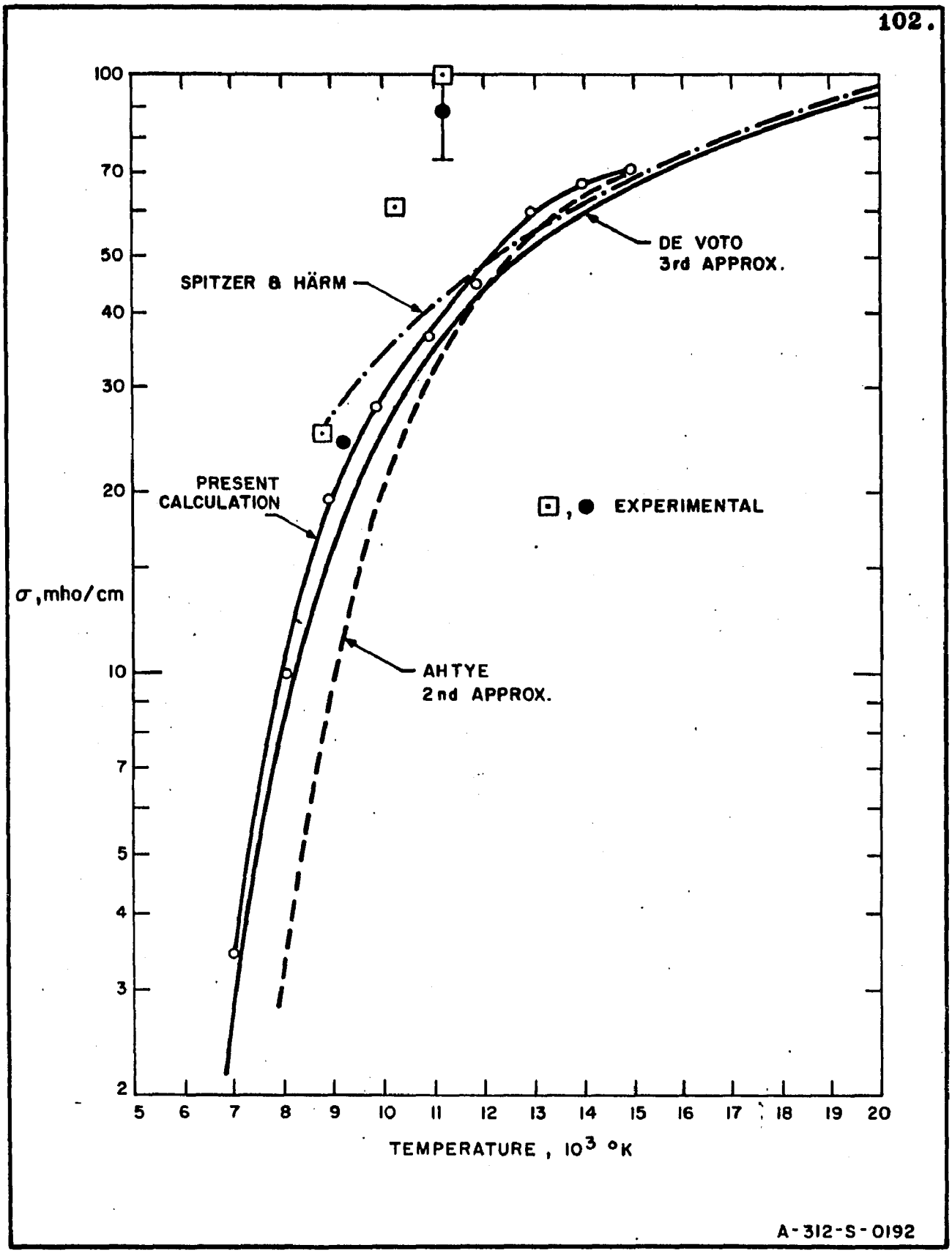

FIG. 19 ELECTRICAL CONDUCTIVITY OF 1 ATM. ARGON vs. TEMPERATURE

These results have also been plotted in Fig.19 for comparison. It is seen that below 10000°K Ahtye's results are considerably below that of deVoto's. This is not just due to the order of approximation since the 2nd approximation of deVoto is even more different from that of Ahtye. In view of the highly complex nature of their computations we refrain from commenting on the possible cause of the deviation but it is apparent that our relatively simple calculation appears to be in good agreement with that of deVoto. While this may possibly be a coincidence, still, it constitutes a desirable indication of the theoretical accuracy of the approach involving the Maxwellian distribution with superimposed drift for the electron distribution function as a starting point for computing the electrical conductivity.

DeVoto has compared his results with experimental results of Lin, Resler and Kantrowitz(Reference 36) and Pain and Smy(Reference 43,44) showing good agreement above 10000°K but very poor below. Since these results were obtained from shock-tube measurements, they are generally regarded as suspect at low temperatures where the more energetic atoms* are out of equilibrium with cool electrons.

*In shock-tubes energy is imparted from the atoms to the electrons as opposed to the situation in electric arcs.

Turning our attention to the energy equation, Eq.27, the first term on the left is clearly the change in the electron kinetic energy as the electrons traverse a temperature gradient. The second term represents the fluid-mechanical volume work done by the electrons. The third and fourth terms give the energy yielded by volume recombination. These are balanced on the right by the kinetic energy transfer due to differences of temperatures of the different components. The last term:

$$\sum_s m_e n_e \nu_{es} U_e^2 = \sum_s \frac{m_e n_e}{e^2 n_e^2} \nu_{es} J^2$$

$$= J^2 \eta$$

is immediately recognized to be the Joule heating.*

Thus, excepting radiative transfer, Eq.27 accounts for the different energy sources and sinks. Also, the left hand side is independent of any original assumption about the electron distribution function f_e.

If the plasma is homogeneous and there is no recombination then the Joule heating is exactly balanced by heat transfer due to temperature differences. This

*Or, $J(E+E_p)$ if a pressure gradient is present.

demands:

$$\sum_s \nu_{es}\left[3k(T_e-T_s) - m_s U_e^2\right] = 0$$

Or,

$$\frac{\sum_s \nu_{es} 3k(T_e - T_s)}{\sum_s \nu_{es}\, m_s} = U_e^2$$

$$= J^2/e^2 n_e^2 \qquad \text{(Eq.41)}$$

and if the heavy particles have the same masses and temperature, this gives:

$$J = n_e e\sqrt{3k(T_e-T_s)/m_s} \qquad \text{(Eq.42)}$$

which is the compatibility relation first used apparently by Vlasov(Reference 64) and by Kerrebrock(Reference 32)* for the two-temperature model of electrical conductivity.

*With δ in place of the factor 3.

It is important to note that Eq.42 is independent of the collision frequencies and therefore also of the collision cross sections. This is a consequence of the cancellation of ν_{es} in the numerator and denominator of Eq.41 which, in turn, stems from the fact that the kinetic calculations give the same collision frequency for energy transfer and momentum transfer.

We write down for future reference the two-temperature energy transfer rates between the electrons and atoms, p_{ea}, and between the electrons and ions, p_{ei}. These are obtained from the term involving (T_e-T_s) in the right hand side of Eq.26.

In general:

$$p_{es} = 2n_e \nu_{es}(m_e/m_s)\tfrac{3}{2}k(T_e-T_s)$$

and in particular:

$$p_{ea} = 1.65\times10^{-41} n_e n_a (T_e/10^4)^{1.8}(T_e-T_a) \quad \text{(mks)} \qquad \text{(Eq.43)}$$

$$p_{ei} = 2.03\times10^{-33} n_e^2 \ln\Lambda (T_e-T_i)/T_e^{3/2} \quad \text{(mks)} \qquad \text{(Eq.44)}$$

Chapter 4

EXPERIMENTAL TECHNIQUES

The FTA generator used was one of proven reliability. Details of its construction are indicated in Fig.4. The anode material used for our investigation was porous graphite(National Carbon Co., either NC50 or NC60 grade) which is a material that works consistently in the FTA scheme. The pore size distribution of NC60 graphite has a bimodal distribution with broad peaks at 15 and 33 microns. The permeability to gas flow is high and flow rates of any practical magnitude up to 200 gm/min-cm^2 could be achieved with less than about 100 psig source pressure.

The arc is sustained by a Lincoln Electric Co. SAE 300 arc welding a.c. motor-generator. With this power supply, currents as high as 250 amp can be obtained. For conveniently long arc gap, e.g. 3 cm(to facilitate diagnostic studies) the maximum current is about 200 amp.

Although not part of the present study, it should be pointed out that the physical processes occurring in the FTA anode sheath are not fully understood. Since the function of the anode, aside from collecting electrons, is to provide near it (i.e. the sheath) a source

of positive ion production essential for the neutrality of the arc column, it is intriguing that, depending on the amount of fluid transpiration, the surface temperature(determined by optical pyrometer) ranged from about 3000°C down to less than 1000°C. At such low temperatures, thermal ionization seems unlikely to provide the requisite ion production. Yet, sheath ionization due to electron impact is not obvious in view of the small sheath voltage drop observed.

From an intuitive point of view, one would expect the working fluid flow rate to exert a profound influence on the arc terminal characteristics(i.e. arc voltage versus arc current). Although marked changes are observed at very low flow rates(approx. 0 to 6 gm/min-cm^2),* the arc characteristics are quite insensitive to flow in the working range of interest to us. Figure 20 shows the V-I characteristics for three values of argon flow rate. Evidently a more than doubling of flow rate resulted in only 2 v increase in terminal voltage while in outward appearance there were very definite changes in the arc, e.g. a widening of the dark space. For instance, at high flow rate the dark(semi-luminous) space extended as much as 1 cm away from the anode while at low flow rate the distance might be only 1 or 2 mm.

*See Reference 50.

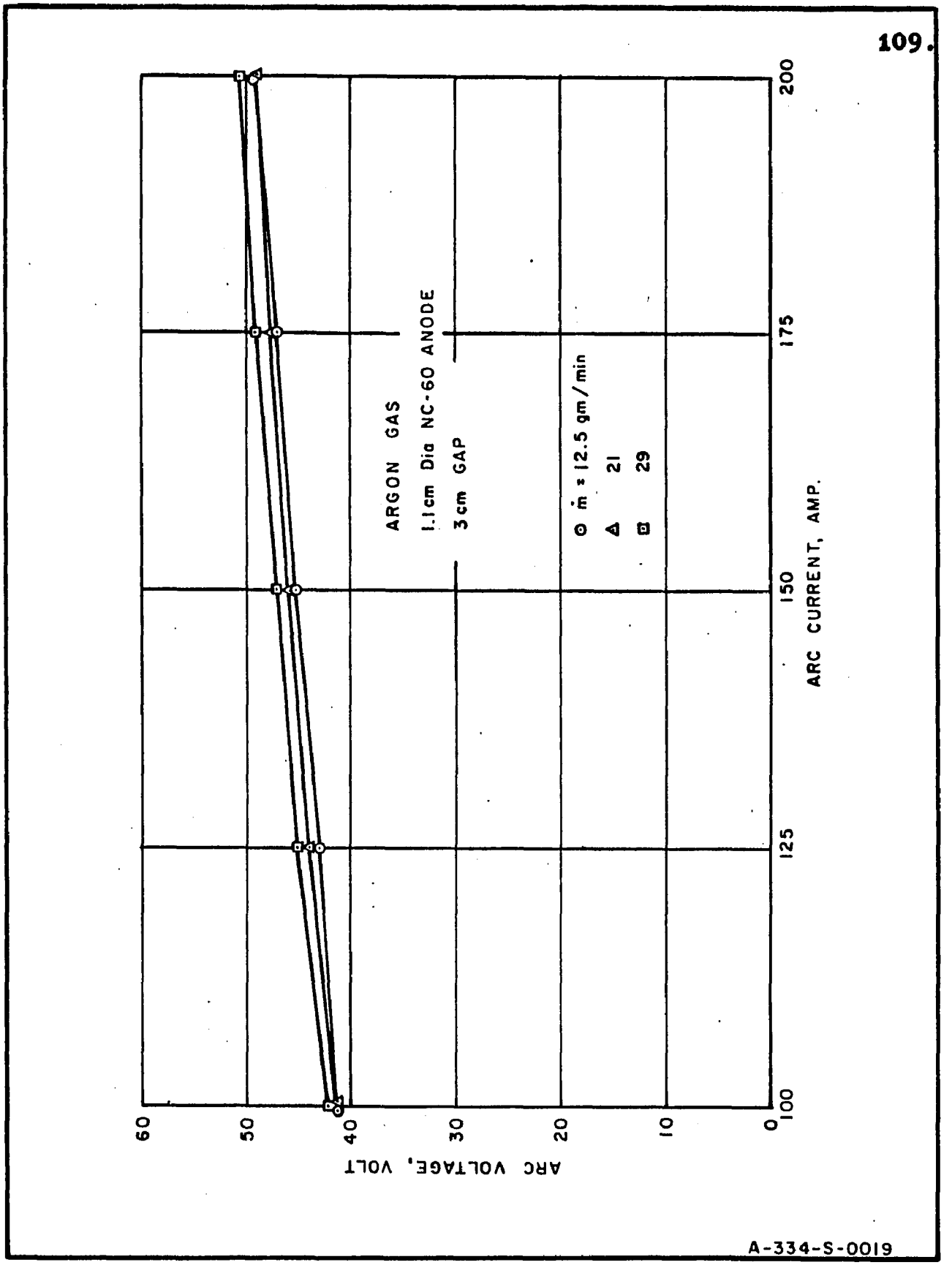

FIG. 20 ARC VOLTAGE vs. ARC CURRENT

At high flow rate, simple energy conservation alone could tell us that the neutral gas temperature would be thousands of degrees below that of the electrons. From this we might gather that not only must the electron temperature be high in order to explain the very substantial electrical conductivity but that the electron gas must be energetically only slightly coupled to the neutrals in order to explain the apparent relative immunity of the arc to blowing.

The above conjectures were examined during a comprehensive program of diagnostics involving the following measurements:

Calorimetry
Arc column current density distribution
Potential distribution
Gas temperature distribution
Electron density and temperature
High-speed photographic observation

4.1 Calorimetry

This experiment is intended to provide background information on the energy dissipated in the electrodes. From a measurement of the electrode dissipation and a knowledge of the total power input, the arc column

dissipation can be estimated.

The technique is the conventional one of monitoring the coolant(water) flow rates and temperature rises in the cooling circuit of the electrode structures. In this case, the flows are measured by elapsed time and volumetric displacement. Water temperatures are obtained by means of flow through Tee sections fitted with Chromel-Alumel thermocouples and using a Rubicon potentiometer for thermal emf readout. Anode surface temperatures are measured by a Leeds & Northrup optical pyrometer.

The results of two series of runs are summarized in Tables 4 and 5. The interpretation of results will be facilitated by referring to Fig.4 which contains a sketch of the areas of relevance and definition of some parameters. The anode dissipation, P_A, is taken to be the sum of P_{A1}(primarily from conduction across the back contact surface), and P_g, the power transferred to the gas. Since the contact bushing and the peripheral cooling jacket are both at relatively low temperatures, and the boron nitride insulation in between relatively thick, the perpheral cooling circuit and the back cooling circuit are approximately isolated from one another. This is a good indication that the anode back is cool compared with the average temperature of the

TABLE 4

SUMMARY OF FLUID TRANSPIRATION ARC CALORIMETRY

Anode Flow = 23 gm/min (Argon)
Cathode Flow = ~5 gm/min (Argon)

Anode Material : NC-50
Cathode Material: Tungsten

V,VOLT	I,amp	P_T,watt	g_A,cm	P_{A_1}	P_{A_2}	$P_{A_1}+P_{A_2}$	P_G	P_A	P_K	V_A,VOLT	T_A,°C	C_A,%	η_A,%	V_S,VOLT
36	100	3600	2	412	79	491	236	727	201	7.3	2230	55	81	2.8
38	125	4750	2	583	119	702	373	1075	270	8.6	2280	85	80	4.1
40	150	6000	2	787	167	954	430	1384	332	9.2	2370	95	79	4.7
43	175	7520	2	953	179	1155	466	1621	550	9.3	2430	100	78	4.8
45	100	4500	3	416	72	488	219	707	252	7.1	2280	50	84	2.6
48	125	6010	3	571	95	666	345	1011	342	8.1	2250	80	83	3.6
50	150	7500	3	727	143	870	400	1270	423	8.5	2315	90	83	4.0
51	175	8920	3	916	179	1095	440	1535	455	8.8	2410	95	83	4.3
54	100	5400	4	430	72	502	170	672	242	6.7	2220	40	86	2.3
54	125	6750	4	560	95	655	285	940	293	7.5	2280	65	86	3.0
54	150	8400	4	715	143	858	377	1235	333	8.2	2310	85	86	3.7

TABLE 5

SUMMARY OF FLUID TRANSPIRATION ARC CALORIMETRY

Anode Flow = 41 gm/min (Argon)
Cathode Flow = ~5 gm/min (Argon)

Anode Material : NC-50
Cathode Material: Tungsten

V, VOLT	I, amp	P_T, watt	g_A, cm	P_{A1}	P_{A2}	$P_{A1}+P_{A2}$	P_G	P_A	P_K	V_A, VOLT	T_A, °C	C_A, %	η_A, %	V_S, VOLT
35	100	3500	2	725	60	785	231	1016	238	10.2	2250	30	71	5.7
36.5	125	4560	2	571	119	690	452	1142	378	9.1	2220	60	75	4.6
37	150	5550	2	726	167	893	643	1536	450	10.2	2210	85	76	5.7
41	175	7180	2	892	167	1059	804	1863	607	10.7	2350	100	77	6.2
43	100	4300	3	428	119	547	382	929	252	9.3	2230	50	82	4.8
44	125	5500	3	560	119	679	456	1135	342	9.1	2220	60	82	4.6
45	150	6750	3	715	167	882	629	1511	441	10.1	2300	80	80	5.6
46	175	8050	3	905	214	1119	757	1876	414	10.7	2330	95	81	6.2
56	125	7000	4	512	95	607	553	1160	378	9.4	2310	70	86	4.9

curved surface. This is in qualitative agreement with previous one-dimensional transpiration cooling analysis (Reference 52) and is a remarkable demonstration of the effectiveness of the fluid transpiration scheme, considering the mere 0.125 in. thickness of the anode available for internal heat transfer.

In Tables 4 and 5, the arc gap, g_a, is defined as the axial distance between anode and cathode tip with the latter set approximately 0.5 cm below the lower edge of the arc column. This arrangement, made possible by the special cathode, removes the cathode far enough from the main discharge to make it reasonable to regard P_k as the true cathode dissipation, rather than to have to include heat transfer back from the arc jet.

The efficiency given in the tables takes into account only losses in the electrodes, radiative power being regarded as useful. It appears that the efficiencies of the runs are naturally separated into groups, each having more or less the same value, by the arc gap parameter.

In anticipation of probe measurements of the temperature of the effluent anode gas, the power transferred from the anode to the transpiring gas, P_g, is approximated by the following relation

$$P_g = c_p \dot{m} T_A C_A/100 \quad \text{watt}$$

where T_A is the anode temperature, C_A the (apparent) coverage of the anode face by the arc termination. The volt equivalence of anode power is then obtained by using the relation

$$V_A = (P_{A1} + P_{A2} + P_g)/I \ .$$

The anode sheath voltage is approximated by

$$V_s = V_A - 4.5 \quad \text{volt}$$

in which 4.5 ev is taken to be the anode work function. We note that V_s appears in the neighborhood of 4 to 5 v. (last column, Tables 4 and 5).

4.2 Arc Column Current Density Distribution

The current density, J, is crucial to an interpretation of arc energy and momentum transfer phenomena; however, it is in general not easy to measure. A direct means of measuring J does not exist and it can only be deduced from the spatial distribution of self magnetic field. The basis of its determination can be traced to the following Maxwell equation:

$$\nabla \times \vec{B} = \mu_o \vec{J}$$

in the limit of zero displacement current.

Thus, in a cylindrical coordinate system,

$$\vec{J} = \mu_o^{-1}\left\{\frac{1}{r}\frac{\partial B_z}{\partial \theta} - \frac{\partial B_r}{\partial z}, \frac{\partial B_r}{\partial z} - \frac{\partial B_z}{\partial r}, \frac{1}{r}\frac{\partial}{\partial r}(rB_\theta) - \frac{1}{r}\frac{\partial B_r}{\partial \theta}\right\}$$

or, when there is rotational symmetry in $\vec{J}$,

$$\vec{J} = \left\{0, \quad 0, \quad J_z\right\}$$

$$= \mu_o^{-1}\left\{0, \quad 0, \quad \frac{\partial B_\theta}{\partial r} + \frac{B_\theta}{r}\right\} \qquad \text{(Eq.45)}$$

The local J is therefore derivable from the local B and

its spatial derivatives. For arc currents in the range of several hundred amps the local B is quite small, e.g. 100 gauss, or 0.01 weber/m^2, and considerable difficulty in measurement is to be expected. This is particularly so when the probe dimension must be kept small to avoid undue perturbation of the arc column.

There are four principal methods of measuring magnetic field:

(a) magnetic resonance(electron, ion or nuclear)

(b) magnetoresistivity

(c) magnetic induction

(d) Hall effect

Method (a) can be eliminated because of the elaborate arrangement required. Method (b) can be miniaturized but is basically useful for high B only because of low sensitivity and high temperature coefficient. For example, Bismuth has $\triangle R/R_0 \approx 0.1$ at 0^oC, 2000 gauss, dropping to about 0.005 at 100^oC.

Method (c) is, of course, commonly used. For time-varying B field, Faraday's law insures induced voltage for a stationary coil. For stationary field, induction must be obtained by relative motion of the coil probe with respect to the B field. Three configurations, viz.

Linear motion transverse probe

Rotating probe

Current transformer(linear motion)

have been explored in considerable detail and found to be impractical in our case.

The last (d) method turned out to be the most efficacious largely due to the availability of the Hall element made of semiconducting Indium Arsenide (InAs) which possesses very high Hall coefficient, reasonable temperature coefficient, and small size.*

Even with commercially available Hall elements (see Fig.21a) probes of acceptable size(see Fig.21b) could be made. Typical probe outputs in the arc are shown in Fig.22 and they indicate the clean quality of the traces which are repeatable.

Figure 23 shows the circuit for the gaussmeter. The high-speed probe transport mechanism and its associated controls are shown in Figs.24 and 25. The same transport is used for all the other probings to be described subsequently.

*Preliminary results on the Hall probe determination of arc plasma current density have been published by the author(Reference 60).

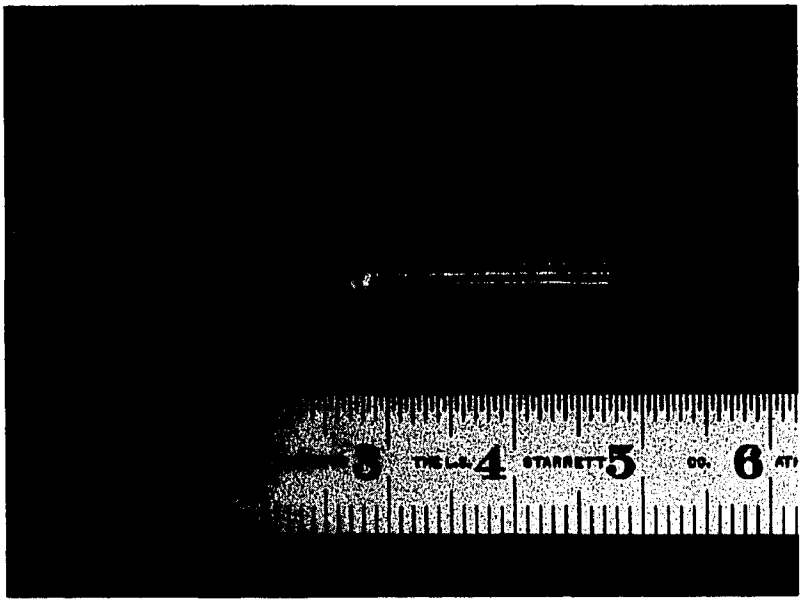

(a) Hall Element

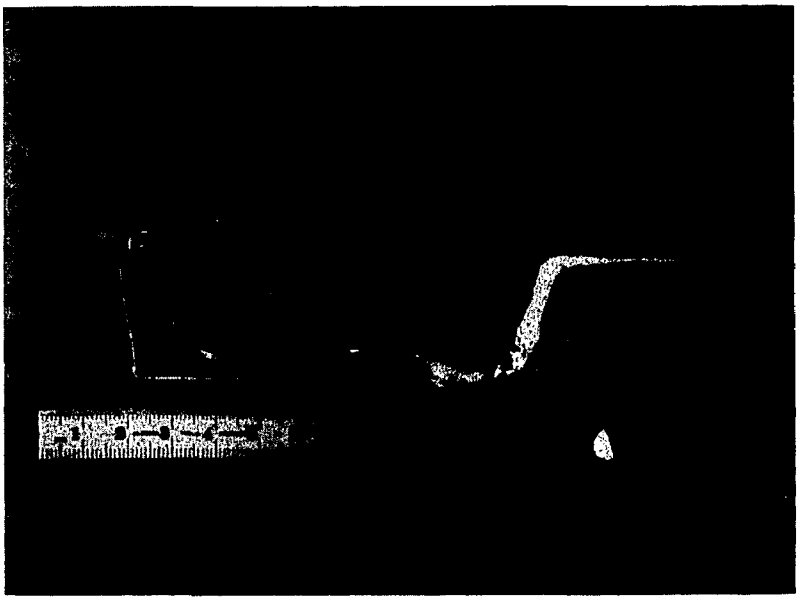

(b) Probe Assembly

Fig.21 Hall-effect Magnetic Probe

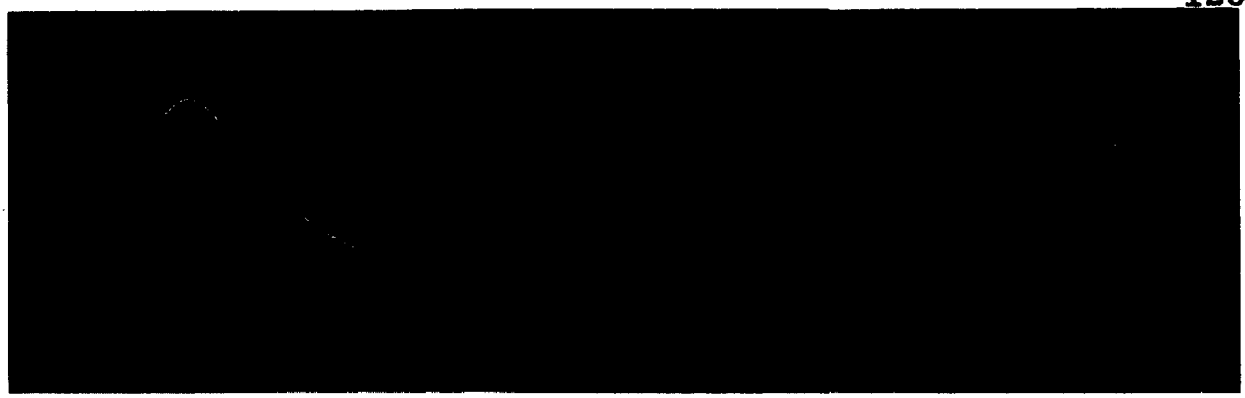

z = 0.7 cm
I = 150 amp

z = 1.0 cm
I = 150 amp

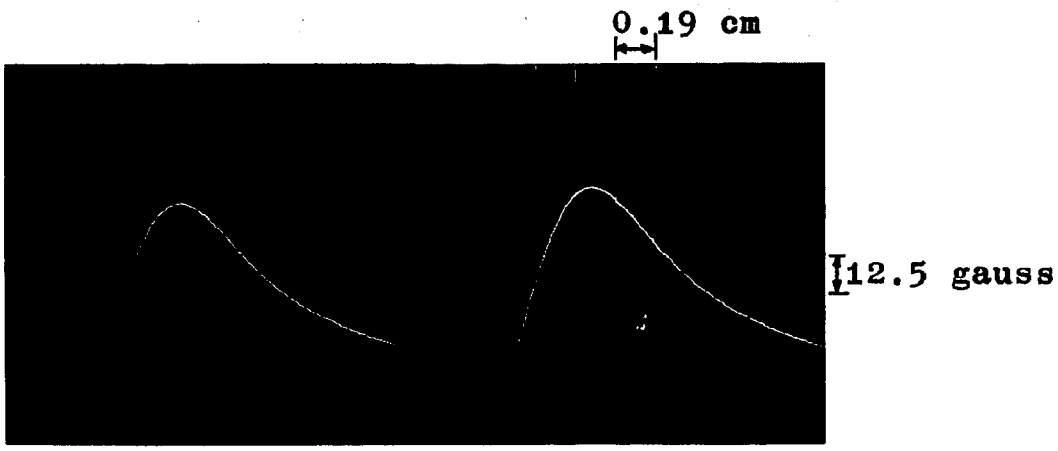

z = 1.0 cm
I = 125 amp

z = 0.7 cm
I = 125 amp

Fig.22 Records of Hall Probe Output

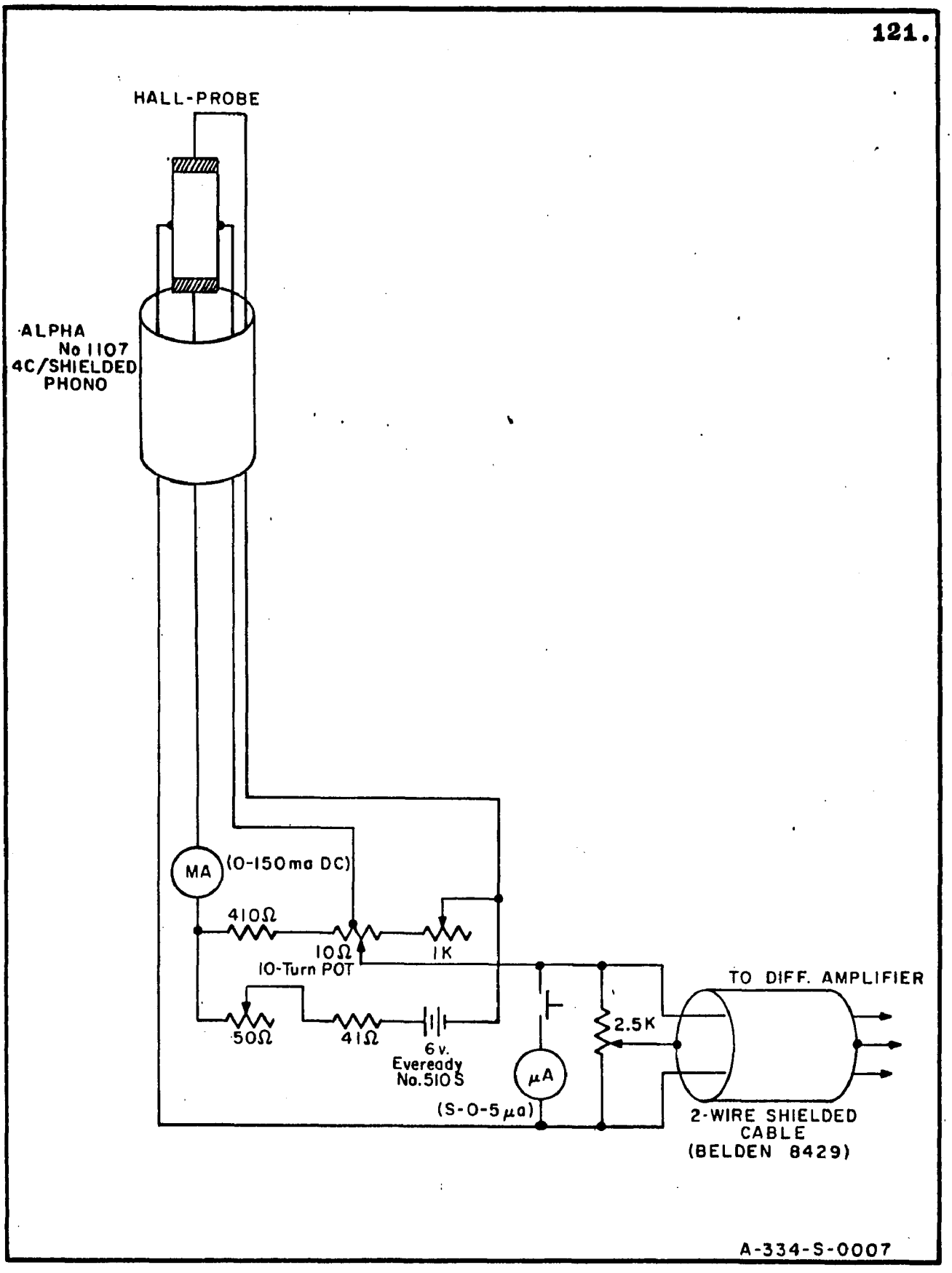

FIG. 23 D. C. GAUSSMETER CIRCUIT

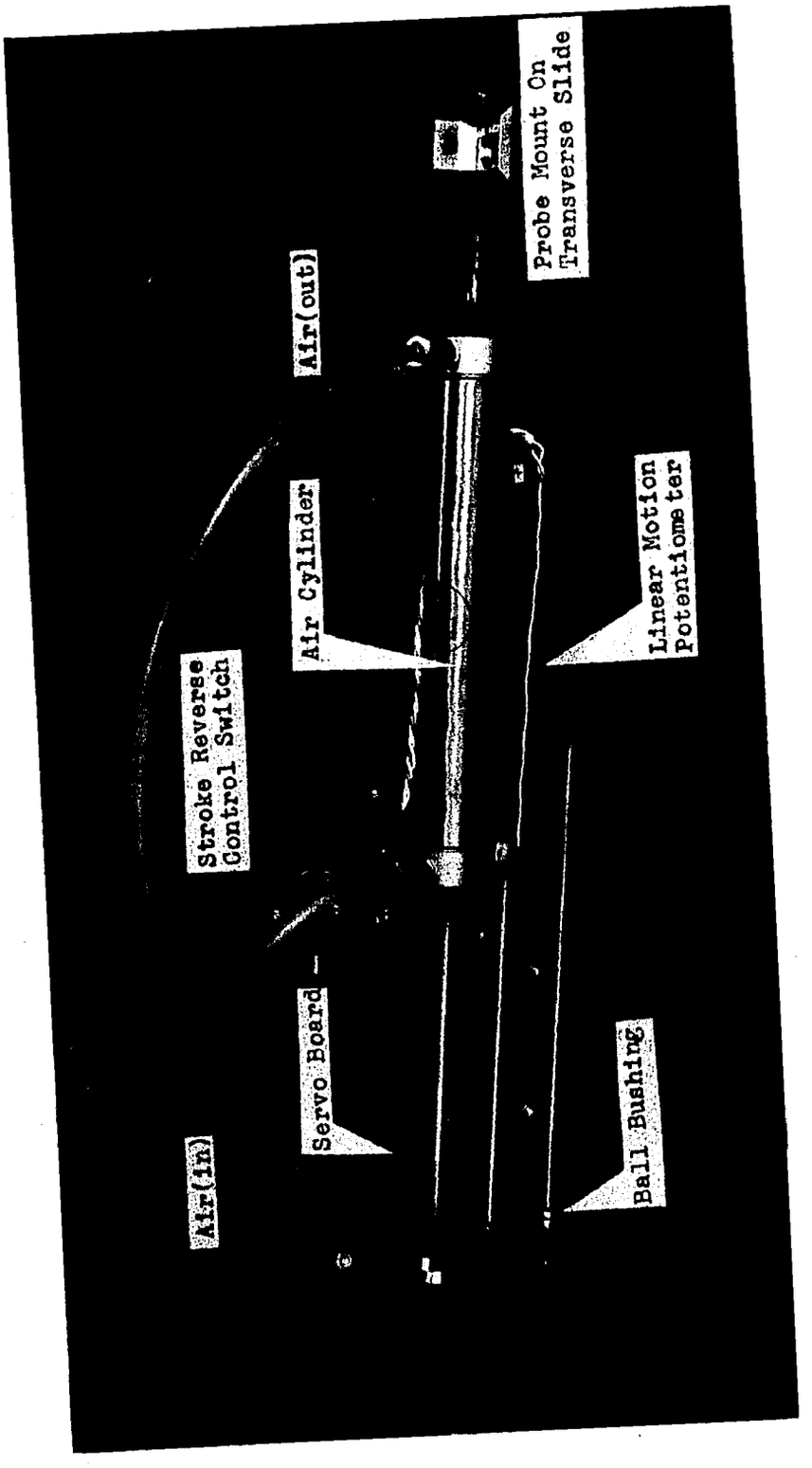

Fig.24 Assembly Photograph of the Pneumatic Probe Transport

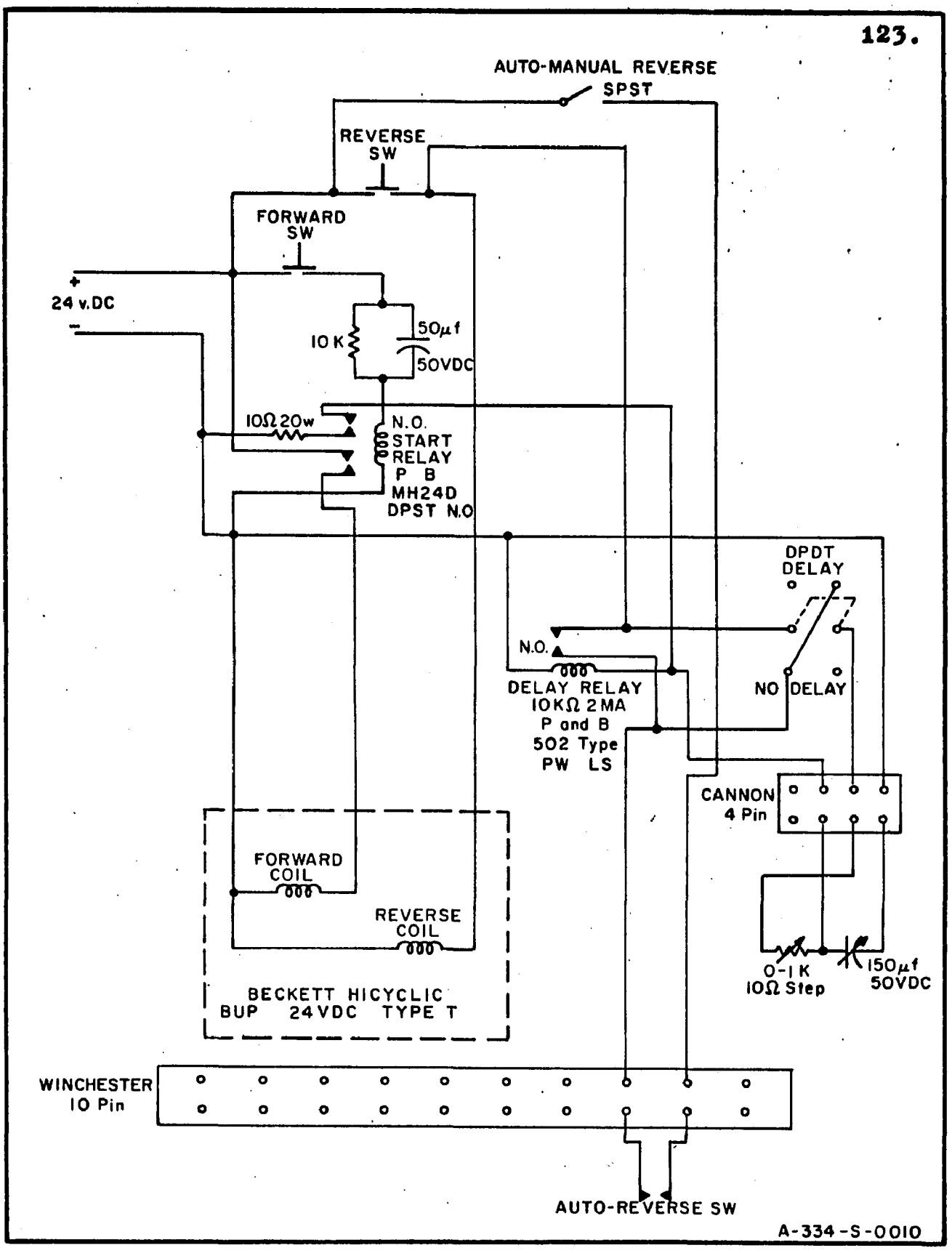

FIG. 25 ELECTRICAL CIRCUIT FOR PNEUMATIC PROBE MECHANISM

4.3 Potential Distribution

While in ordinary conductors or in electrolytes electric potential mapping is a straight-forward matter, in plasma such is not the case. Langmuir and Mott-Smith (Reference 35) reported back in 1924 the theory and procedure for obtaining the potential, temperature and charge density in a plasma with charged particle mean free path,

$$\text{mfp} \gg \text{sheath thickness} \approx \text{probe dimension.}$$

This was the beginning of what is now generally called the Langmuir probe. The essential features of the method are: (see Reference 37)

(1) A variable voltage applied between the electrostatic probe and a reference electrode, both immersed in the plasma, gives rise to a current-voltage relation.

(2) At large negative voltages the probe current saturates to a value related to the positive ion density by:

$$I_{i_{sat}} = A\, n_i (8kT/\pi m_i)^{\frac{1}{2}}$$

(3) At large positive voltages, similarly,

$$I_{e_{sat}} = A\, n_e (8kT/\pi m_e)^{\frac{1}{2}}$$

(4) At small negative potentials,

$$T = \frac{e/k}{\frac{d(\ln I_e)}{dV}}$$

(5) The knee of the positive branch is at the true plasma potential.

(6) The floating voltage V_f, referred to V_{plasma}, where $I_e = I_i$, $I = 0$, is

$$V_f \cong \frac{-kT}{2e} \ln(m_i/m_e) \qquad \text{(Eq.46)}$$

Note: V_f is <u>always</u> negative with respect to the plasma potential.

Such a scheme is simply too good to be abandoned even for work in denser plasmas in which the original key stipulation of large mfp is no longer satisfied. Not surprisingly, we have seen in recent years new treatments of the Langmuir probe problem in dense,

diffusion and mobility controlled discharge. Cohen(Reference 13), Su and Lam(Reference 56), among others, have made numerical calculations which confirmed the general features of the original scheme, with the following modifications:

(1) The plasma potential is at the inflection point of the V-I curve, rather than at the knee of the positive branch.

(2) Saturation of currents do not generally occur except for large $\frac{\text{probe radius}}{\text{Debye length}}$. The knees are not well-defined.

(3) The currents are proportional to

$$n\, v_{th} l/r_p$$

where l is the appropriate mfp, r_p the probe radius and v_{th} the thermal speed. Thus, the currents are proportional to the random current of the plasma but attenuated greatly by the very small length ratio.

Quite recently, Grey and Jacobs(Reference 25) gave experimental confirmation of a simplified interpretation of a cooled Langmuir probe. They reasoned that the probe will be surrounded by a diffusion and mobility controlled layer. But, approximately one Debye length from

the probe, electrostatic field effect dominates and, though in this layer the charged particles suffer several hundred collisions, that is not sufficient to cause departure from the collisionless case. Thus, all the original attributes of the Langmuir probe are recovered except that(not explicitely stated by the authors, but evident in their results) the currents are to be modified by the ratio $1/r_p$.

Using the circuit of Fig.26, we obtained some V-I traces by inserting a spherical platinum probe of about 0.05 mm diameter into the center of the arc column for about 50 ms duration. For the most part, our probe is therefore cool as in the case of Grey and Jacobs. Furthermore, our electron temperature(about $10000^{o}K$), electron density(about 10^{16} cm^{-3}), and ambient pressure(1 atm) are almost the same as theirs. Hence, their reasoning should apply in our case.

Figure 27 gives the outputs of probings at distances of 1, 3, 5, and 7 mm from the anode. It is seen that most of the traces fall on the negative regime because the very high electron saturation currents were beyond the capacity of the signal generator driving the probe. Since the signal generator was set at 1000 Hz the multiple traces indicate low frequency fluctuation of column properties. The floating voltage(I = 0)

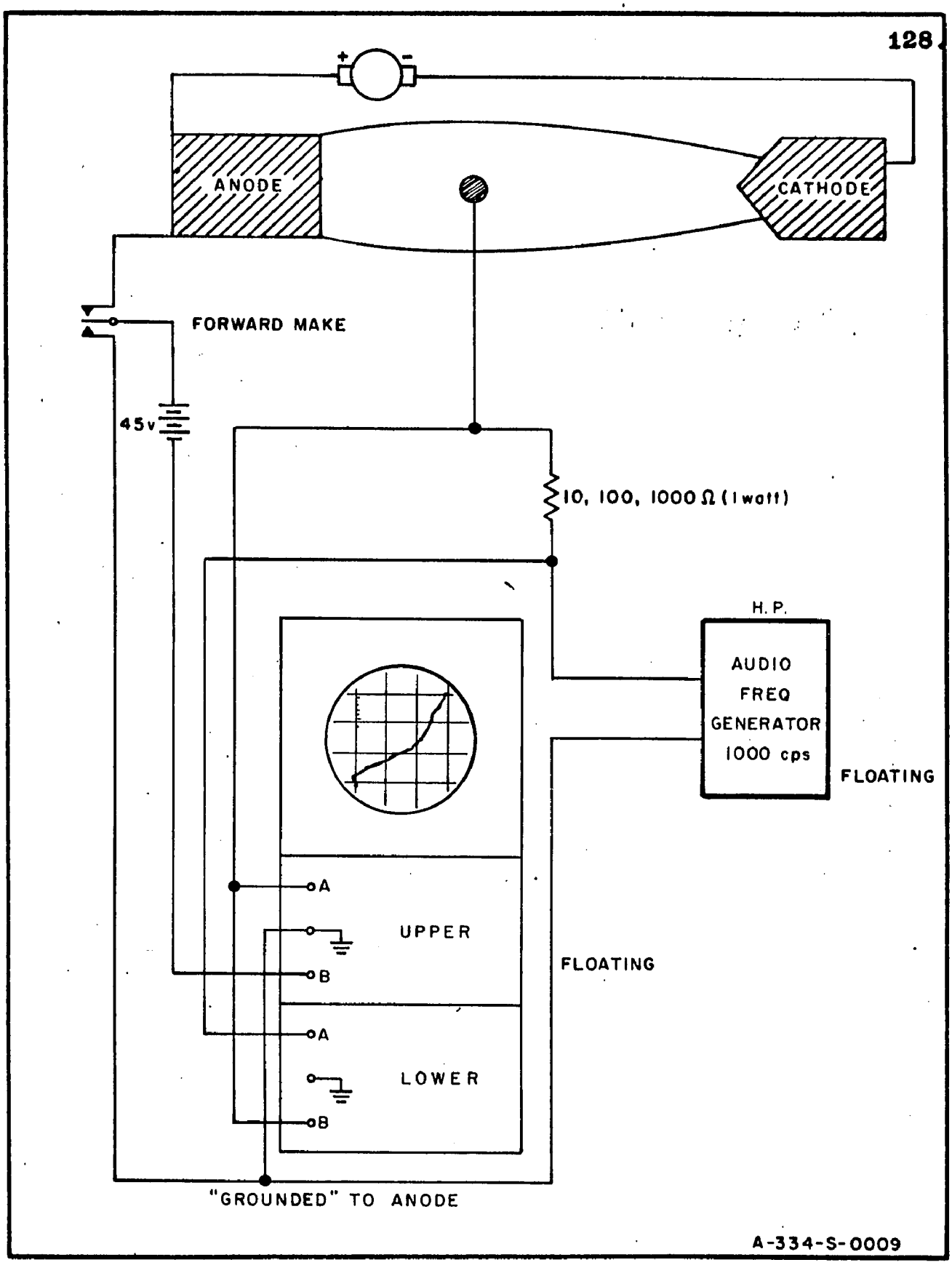

FIG. 26 LANGMUIR PROBE CIRCUIT

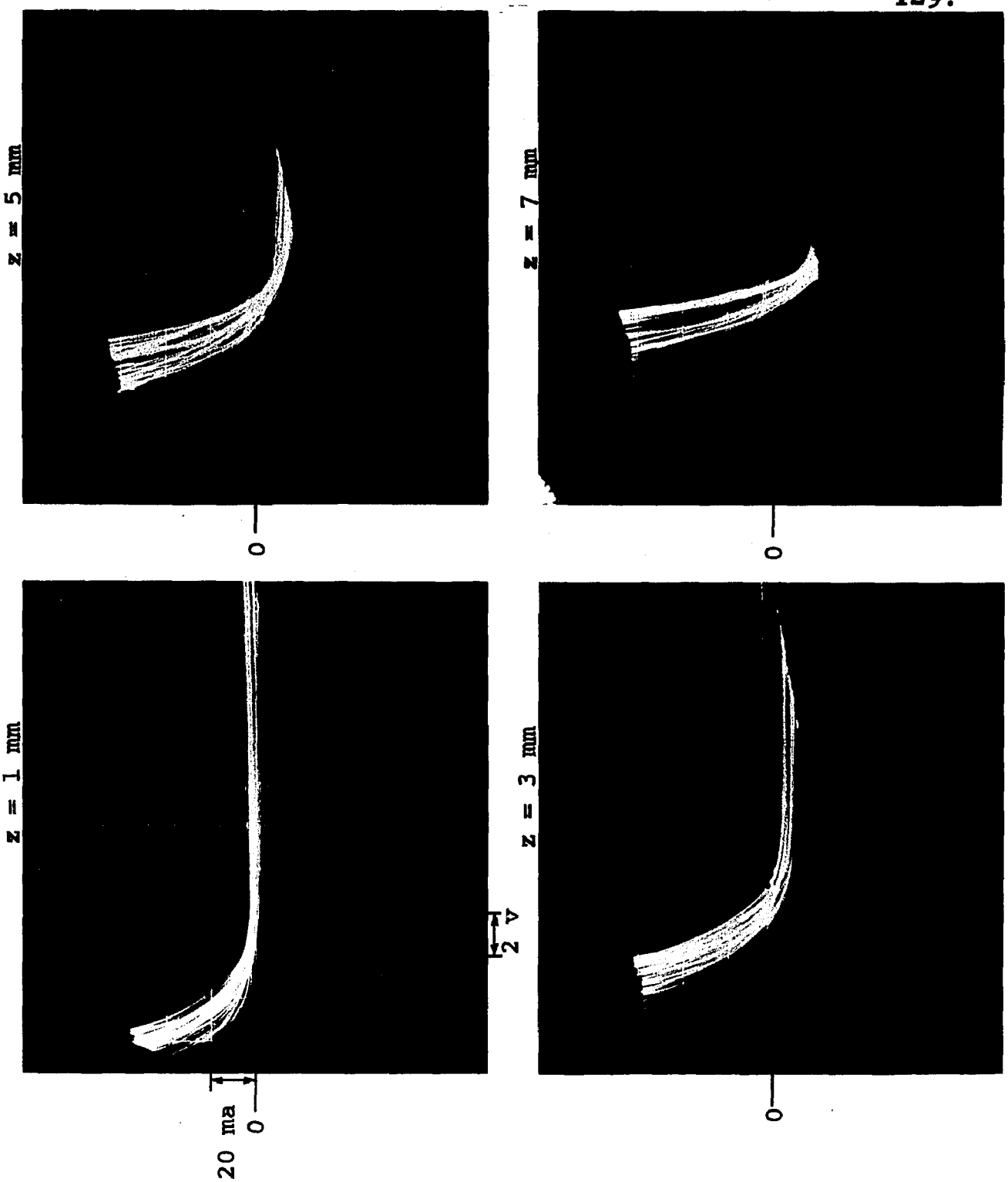

Fig.27 Records of Langmuir Probe Output

fluctuates by 1 to 2 v and the ion saturation current fluctuates by as much as a factor of 2.

In spite of the fluctuations, the average potential and charge density should still be useful since they enter the model equations in a mostly linear fashion. From some of the better curves the electron temperatures were extracted. The indicated temperatures were about 11000°K - in fair agreement with spectroscopic data. This would suggest that the fluctuations were primarily caused by density and potential variations.

Since Fig.27 does not yield sufficient information on either the saturation electron current or the inflection point, we rely on the floating potential to give the plasma potential. According to Eq.46 the floating potential is depressed by about 4 v from the plasma potential. This is proportional to the temperature (slowly varying) and therefore does not critically affect the final results. This seems well borne out in Grey and Jacob's experiments. In our case, based on the sheath voltage taken from calorimetry data, the depression should be about 6 v.

Profiles of the floating potential were obtained by rapid radial traverses of a spherical probe across the column at various axial stations. The probe output

was connected to the input amplifier of a Tektronix 502A oscilloscope(10^6 ohm input impedance), thus insuring essentially floating condition. The traverse position was monitored by the output of a conductive plastic film linear motion potentiometer. Typical results are shown in Fig.28. These permit the determination of the axial electric field, E.

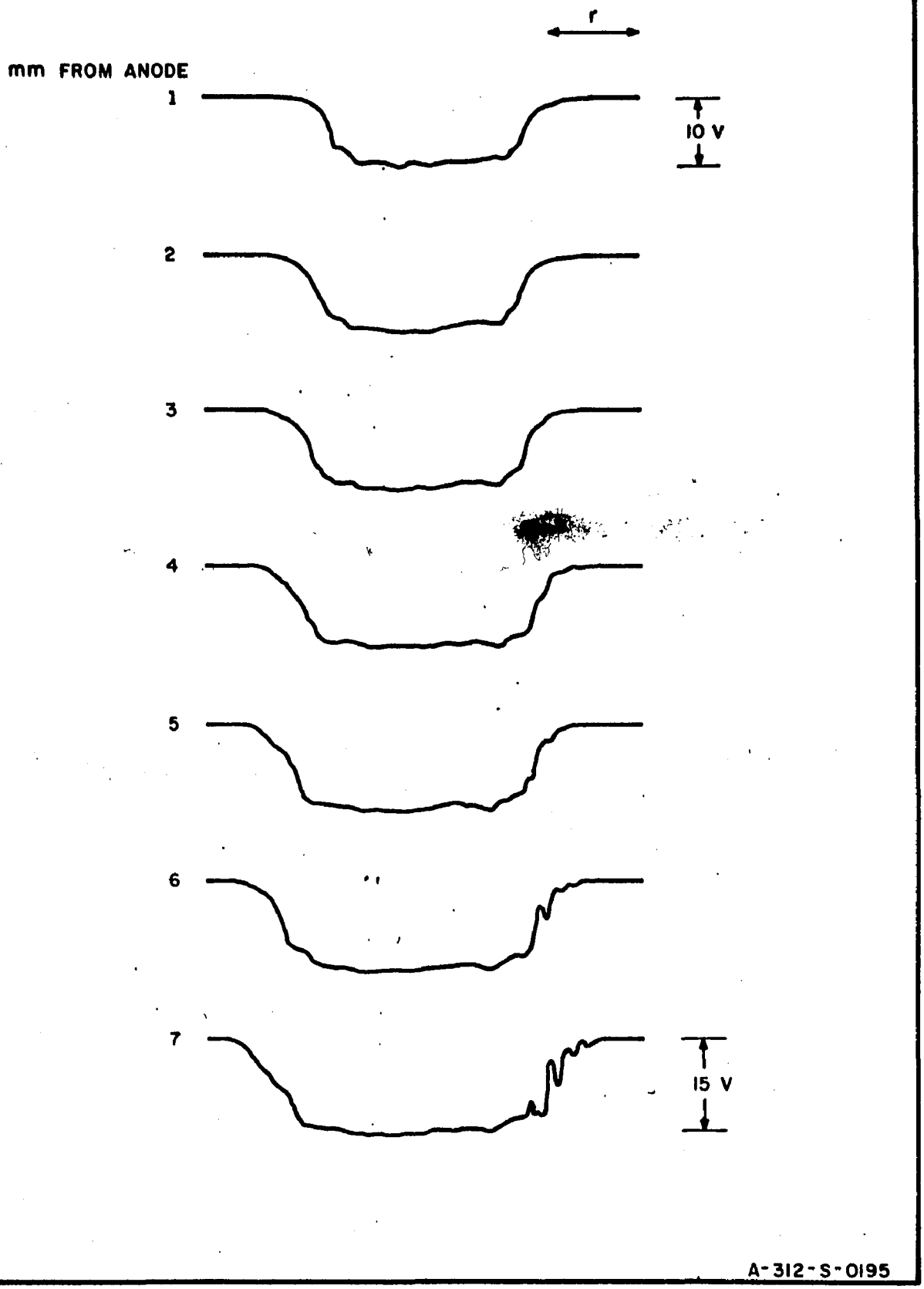

FIG. 28 ARC FLOATING POTENTIAL DISTRIBUTIONS

4.4 Gas Temperature Distribution*

In the section touching upon nonequilibrium considerations we tentatively concluded that the electron velocity distribution should be Maxwellian and similarly for the heavy particles, but with a lower temperature. Furthermore, in the calculation for charged particle density, the various electronic excitation temperatures of the atomic and ionic bound states have been identified with the electron temperature. Even if the excitation temperatures were not exactly equal to the electron temperature they may deviate even more from the translational temperature of the heavy particles. This possibility deprives us of one of the most valuable means of determining the heavy particle temperature - i.e. the spectrometric measurement of either the absolute or relative intensities of spectral lines.**

Insertion of a temperature sensor probe(i.e. a thermometer) into the arc and then reading the steady state

---

*The material discussed in this section and in Appendix D is contained in a separate paper submitted to the Journal of the Electrochemical Society, in Nov.,1966, for publication.

**On the other hand, line and continuum radiation originating from the higher states should provide information on the electron temperature. The continuum, in particular, will be utilized because of available published data on its intensity as function of T_e(see Section 4.5)

temperature is clearly out of the question because even the heavy particle temperature in the coolest region of the column, i.e. near the anode surface, is beyond the temperature limits of all existing temperature sensing materials including thermocouples, resistance thermometers, thermistors, etc.

The application of a highly internally-cooled, gas enthalpy sampling probe and calorimeter system has been developed to a reasonably reliable state, notably by Grey and his coworkers(Reference 24), wherein the temperatures of arc plasma jets have been successfully probed. Such cooled probes, however, because of the need for coolant and gas sampling passages, are quite complicated in construction and limited in the extent to which they can be miniaturized. In a private communication,* it has been brought to the attention of this author that the insertion of such a highly cooled probe into a current-carrying plasma column results in rather gross distortion of the arc column and erroneous probe readings. As a result of this and the complicated auxiliary equipment involved, the sampling probe also seems to be impractical for the conduction column.

*Messrs E.Soehngen, Director, and P.Schreiber of the Thermo-Mechanics Lab., Aerospace Research Laboratories, Wright-Patterson AFB, Ohio.

In a previous study(Reference 61) as well as more recent work with new experimental findings(Reference 62), the measurement of extremely high gas temperature by a transient thermocouple probe has been investigated by the author in some detail. In Reference 61 it was shown that certain published works(References 48, 59) pertaining to what at first glance appear to be quite different techniques of transient probings were, in fact, completely equivalent to what the author called the single-insertion, single-probe, heat flux ratio technique. In Reference 62 the efficacy of the ratio technique was shown to be limited to the temperature domain below approximately twice the maximum allowable probe temperature. At the same time, the feasibility of an absolute flux technique was shown to hold promise up to 9000°K or even higher temperatures. The interested reader is referred to Appendix D for a short account of the basic considerations pertaining to the use of the transient probe.

For the present purpose, where radiation and conduction losses can be shown to be quite negligible, the heat transfer to an unshielded spherical probe is:

$$T_g = R_f M \frac{dT_p}{dt} + T_p \qquad \text{(Eq.47)}$$

where $R_f = 1/A_p h$ is the boundary layer thermal resistance.

A_p = probe sufrace area

h = surface heat transfer coefficient

M = (probe mass X heat capacity), thermal mass

In heat transfer literature h is often correlated in experiments through the Nusselt number:

$$Nu = hl/\lambda$$

We have found the correlation compiled in a recent book by Kutateladze and Borishanskii(Reference 34) to be satisfactory:

$$Nu = 2 + 0.35Pr^{0.36}Re^{0.58} + 0.03Pr^{0.33}Re^{0.54} \qquad \text{(Eq.48)}$$

where $Pr = \mu c_p/\lambda$ is the Prandtl number

μ = viscosity

$Re = \dot{m}l/\mu$ is the Reynolds number.

Using Eq.48 and the values of gas transport properties(Amdur and Mason, Reference 3) at the film temperature

$$T_f = \tfrac{1}{2}(T_g + T_p)$$

a series of calibration curves for argon has been computed. For $\dot{m}$ = 0.2 and 0.35 gm/cm^{2}sec, the two flow rates of especial interest, the curves are shown in Fig.29 and Fig. 30. As will be shown later, these apparently work satisfactorily up to 9000^{o}K, beyond which a correction is necessary.

The need for corrections at higher gas temperatures is manifested by the fact that the indicated gas temperatures from probe measurements become higher than that of the electrons, as obtained from continuum intensity measurements. This is clearly impossible not only by the nature of the arc discharge but also because this results in violation of energy conservation. It turned out that the transport properties of Reference 3 were computed without the contribution of charged species. Results computed by Ahtye(Reference 1) show that at about 8000^{o}K ionization effects are prominent and cause greatly enhanced values for λ , in particular. The use of $T_f = \frac{1}{2}(T_p + T_p)$ thus may fail to properly correlate heat transfer through the boundary layer because of the large variation in transport properties along the temperature gradient. A simple procedure for correcting the calibration curves was then arrived at specifically to take into account the outer boundary layer where the aforementioned ionization effects take place.

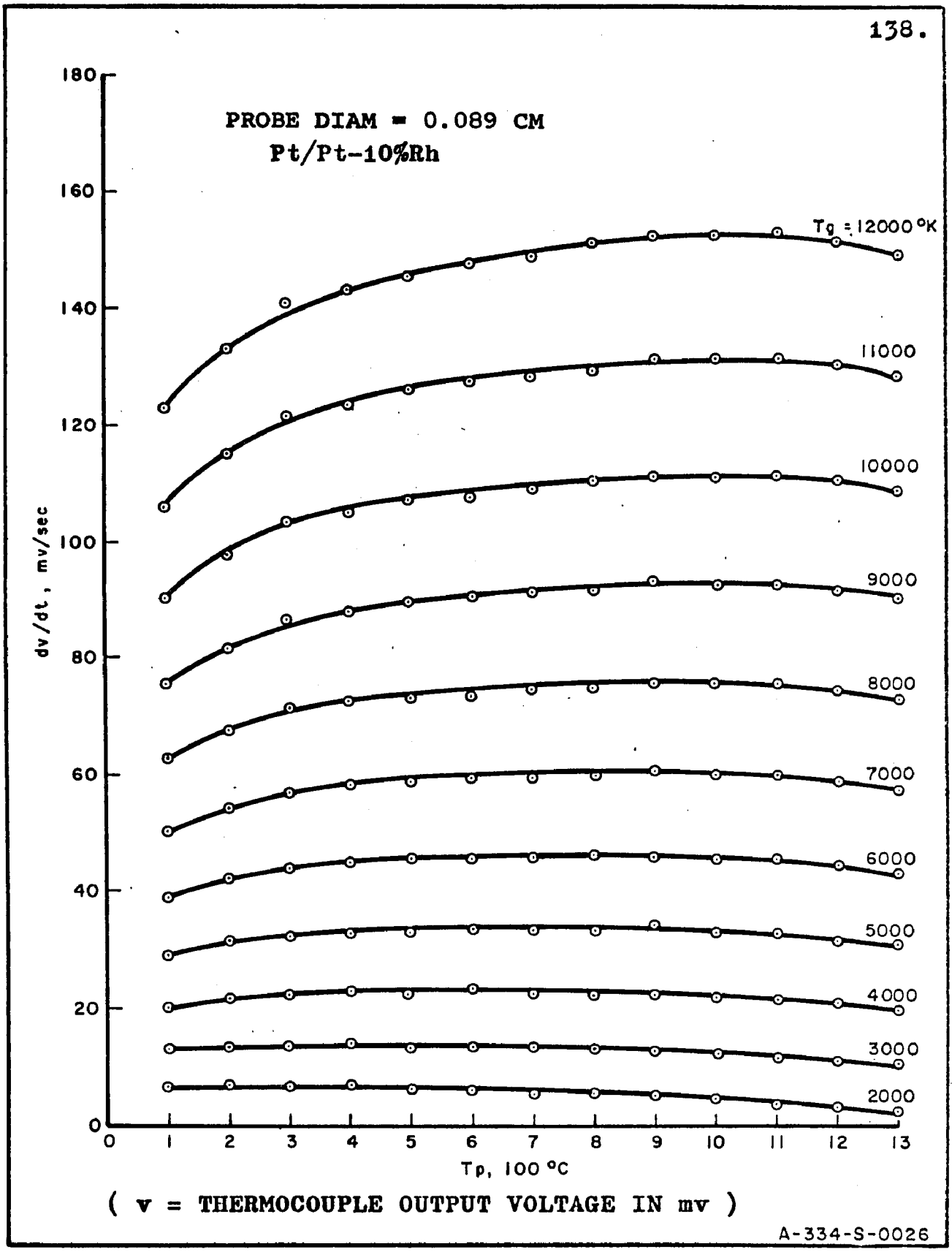

FIG. 29 CALIBRATION CURVE FOR $\dot{m}$ = 0.2 gm / sec.

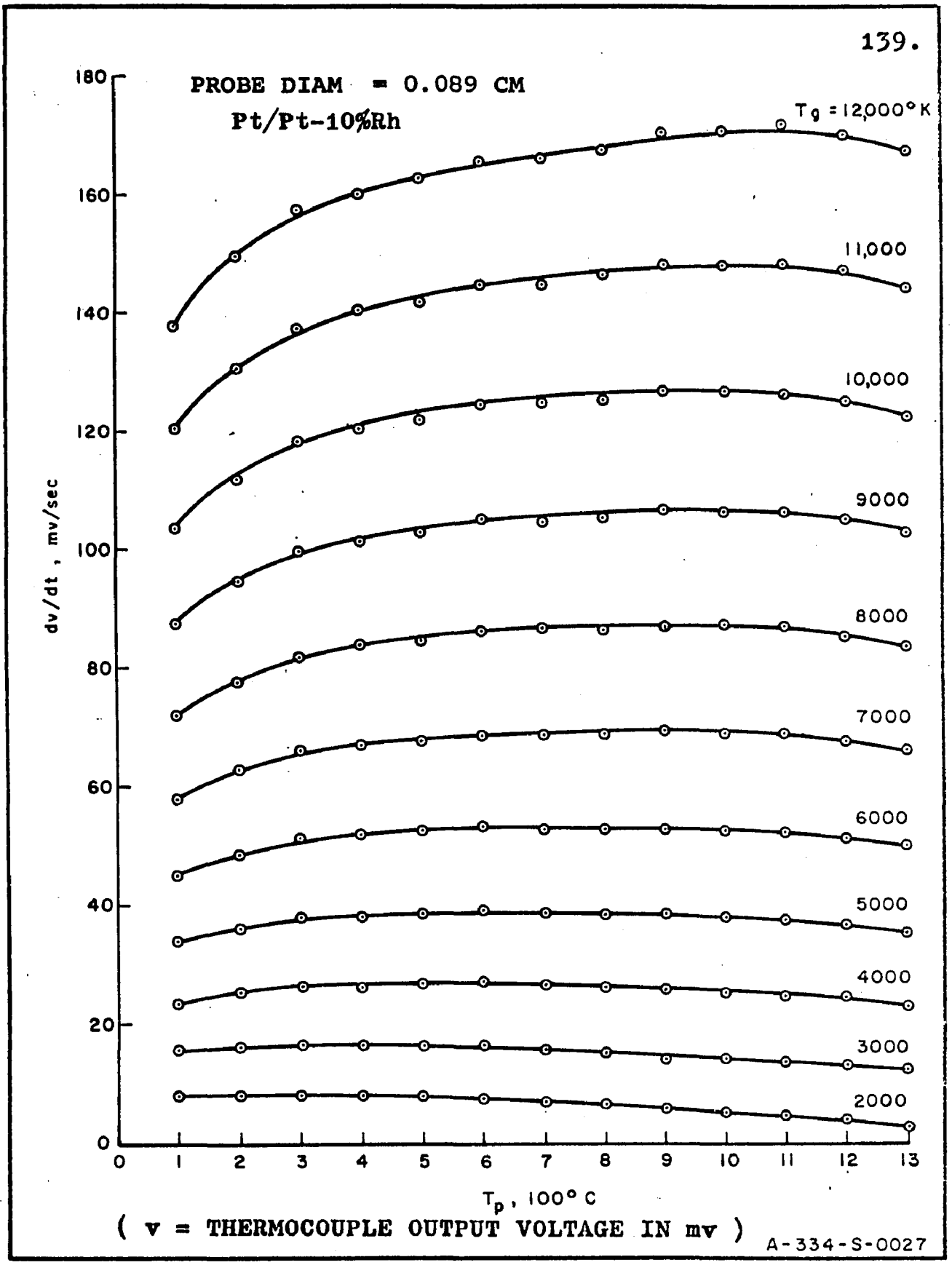

FIG. 30 CALIBRATION CURVE FOR $\dot{m}$ = 0.35 gm/sec

We first noted that for argon at high temperature the Prandtl number becomes small, e.g. $\sim$0.4. Therefore according to boundary layer theories(see Pai, Reference 42, pp.42, 170) the velocity boundary layer and the thermal boundary layer are no longer similar. Since

$$\frac{\delta_u}{\delta_T} \sim (Pr)^{\frac{1}{2}}$$

where δ_u and δ_T are the velocity and thermal boundary layer thickness, respectively, we see that the thermal layer should extend considerably beyond the velocity layer. That is, the velocity layer should exist in the cooler(wall) portion of the thermal layer and the high temperature portion of the thermal layer exists more or less in a potential flow field.

The potential motion of fluid around a sphere is given by Prandtl and Tietjens(Reference 47, p.151) whose figure indicates that near the sphere surface the streamlines are nearly parallel to the surface except in the forward and rear stagnation zones. Since ourside the velocity(viscous) layer the energy equation becomes simply

$$\nabla \cdot \lambda \nabla T = \vec{m} \cdot \nabla (c_p T) \qquad \text{(Eq.49)}$$

where the left hand side gives the conduction heat transfer and the right hand side the convection heat transfer. Now, referring to Fig.31, we see that the forward stagnation zone(FS) receives convection heat while the rear stagnation zone(RS) loses* convection heat by virtue of the fact that $-\nabla T$ is directed radially away from the sphere. Around the remaining surface of revolution(N), due to the orthogonality of $\vec{m}$ and ∇T, heat convection vanishes. Since (N) is likely to be more extensive than (FS) and (RS) together, and, the heat convection to the latter tends to cancel out, in a rough approximation, for purposes of estimating effects of λ variation in the outer thermal layer, we may simply use the conduction equation

$$\nabla \cdot \lambda \nabla T = 0$$

which, in a spherically symmetric temperature field is:

$$\frac{d}{dr}\left(r^2 \lambda \frac{dT}{dr}\right) = 0$$

*It is known from practice that the rear stagnation zone is usually turbulent or possesses secondary flows and heat is not necessarily convected away. This is, in fact, one major difficulty of treating flow around spheres.

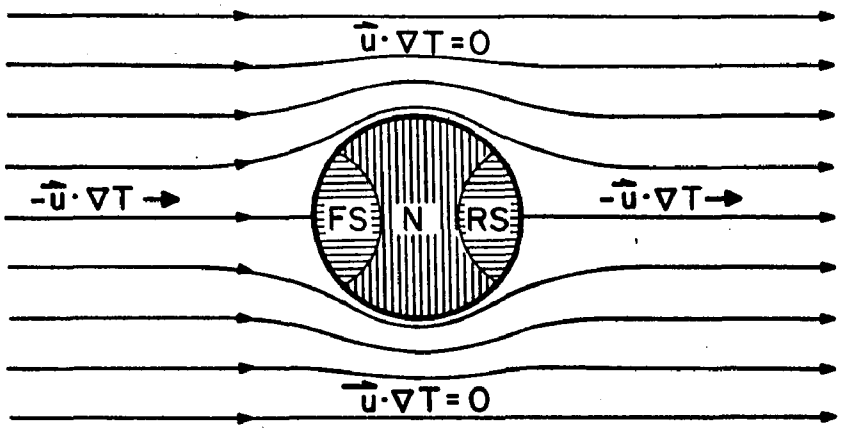

A-334-S-0034

FIG. 31 SCHEMATIC DIAGRAM OF FLOW FIELD AROUND A SPHERE ILLUSTRATING CORRECTIVE HEAT TRANSFER IN VARIOUS ZONES

Now, referring to Fig.32 which is a sketch of the velocity and temperature distributions, we suppose at $T_{cr} = T(r_{cr})$, λ starts to increase significantly; then, for the same total heat Q transferred to the sphere, the free stream temperature must be lowered by an amount δT_g from T_g if the latter is obtained assuming $\lambda = \lambda_{cr}$ = constant. It is easy to show that for the solid curve(λ = constant):

$$Q = 4\pi r \lambda_{cr}(T_g - T)$$

and for the broken curve($\lambda = \lambda(T)$, ϕ = heat potential)

$$Q = 4\pi r\left[\phi(T_g-\delta T_g)-\phi(T_{cr})\right] .$$

Equating the two equations and recalling that,

$$\lambda_{cr} = \left.\frac{d\phi}{dT}\right|_{T_{cr}}$$

we have,

$$\left.\frac{d\phi}{dT}\right|_{T_{cr}}(T_g-T_{cr}) = \phi(T_g-\delta T_g) - \phi(T_{cr}) \qquad \text{(Eq.50)}$$

which allows the determination of δT_g in a simple geometrical fashion from a plot of ϕ vs. T. This is

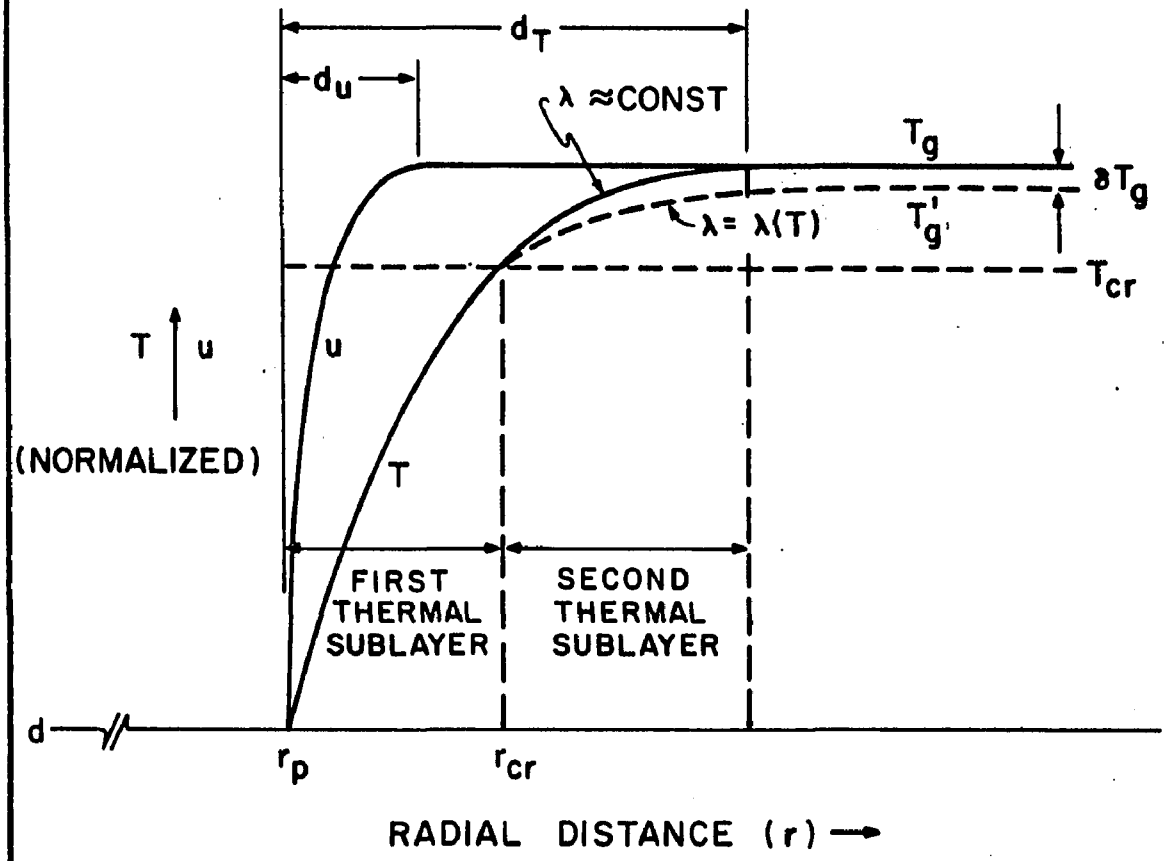

A-334-S-0032

FIG. 32 SKETCH OF VELOCITY AND THERMAL BOUNDARY LAYER PROFILES SHOWING INFLUENCE OF VARIABLE λ

demonstrated in Fig.33. The critical temperature T_{cr} is taken to be 9000°K because experimental checks indicated that up to that temperature the use of Eq.48 in conjunction with $T_f = \frac{1}{2}(T_g+T_p)$ appears to be quite adequate. We see, for example, a correction $\delta T_g = 900°K$ must be subtracted from the calibration curves at 12000°K.

Application of this simple correctional scheme will be shown and discussed later.

For probing of the arc column a three-element spherical thermocouple probe of Pt-10%Rh/Pt/Pt such as shown in Fig.34 was used. The differential output of the probe enables the use of high common-mode rejection differential amplifier(Reference 61, 62) to discriminate against stray signals in the arc column.

Two typical probe output traces are shown in Figs. 35 and 36. The slight fluctuation of probe output near the anode(Fig.35) as compared with the smooth curve away from the anode(Fig.36) is due to actual difference in arc column conditions, not to stray signals.

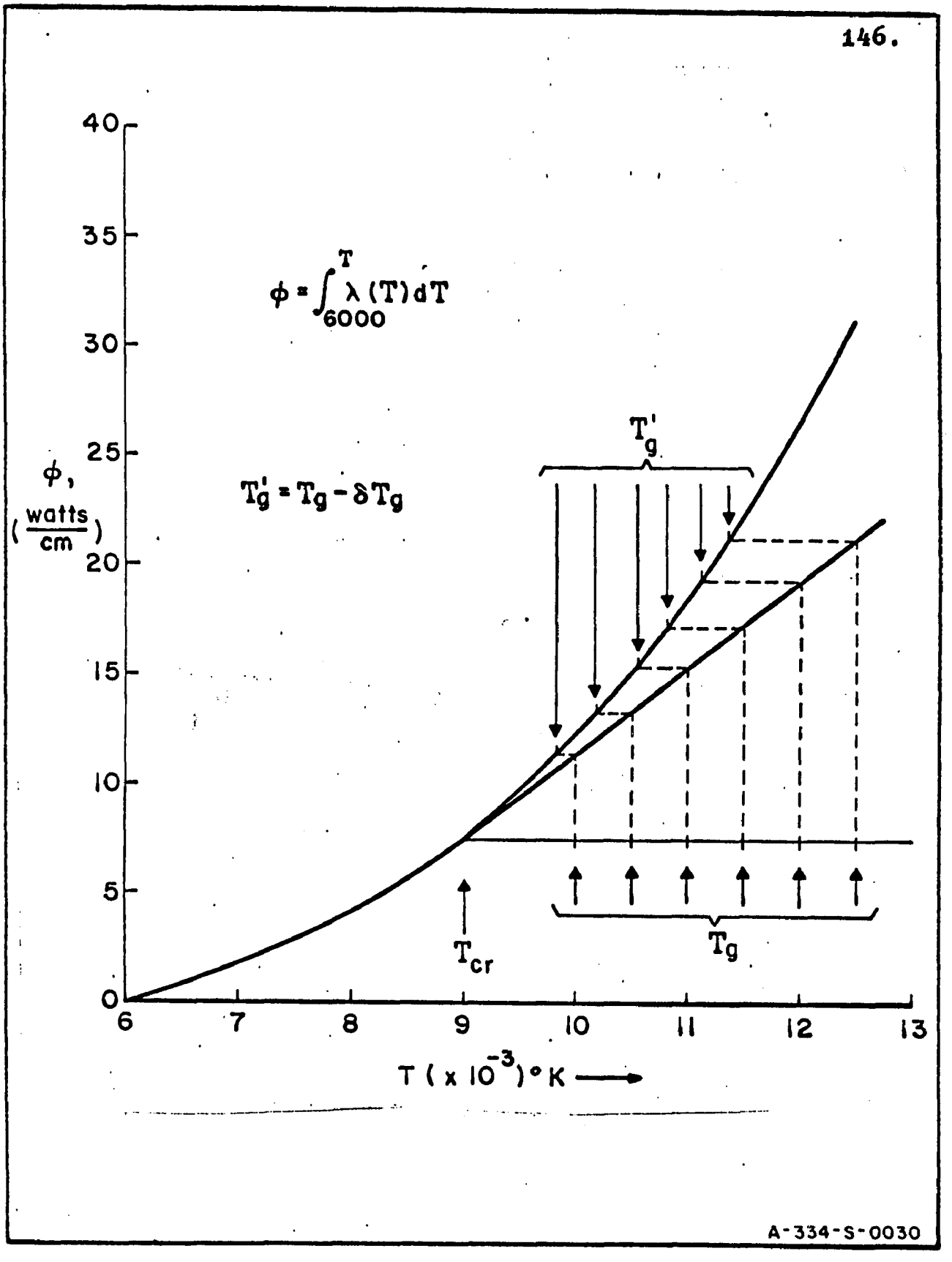

FIG. 33 TEMPERATURE CORRECTION IN ARGON FOR $T_g > 9000^\circ K$

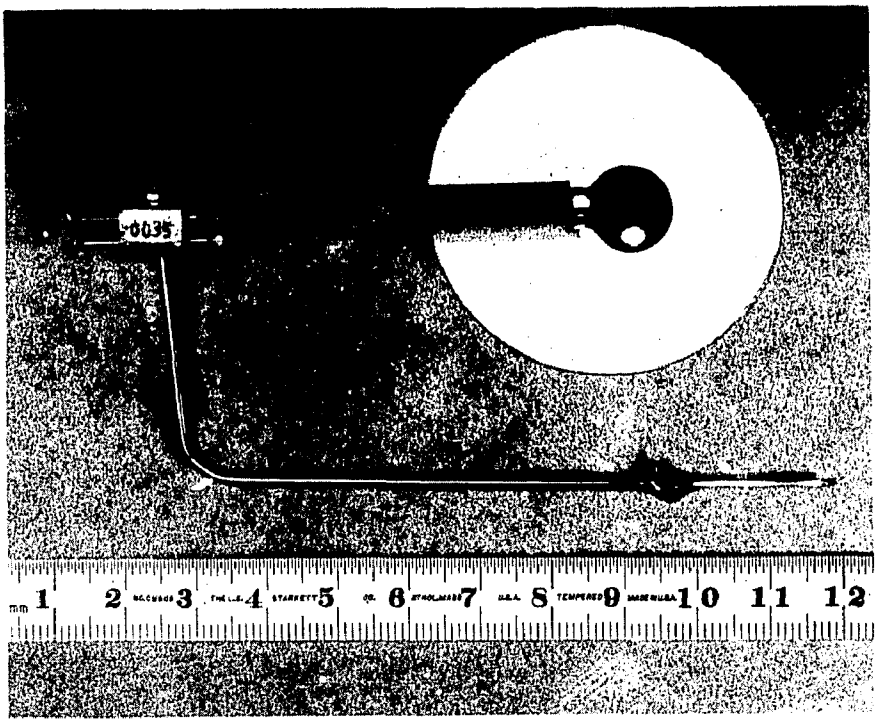

Fig.34 Photograph of a Typical Thermocouple Probe Assembly

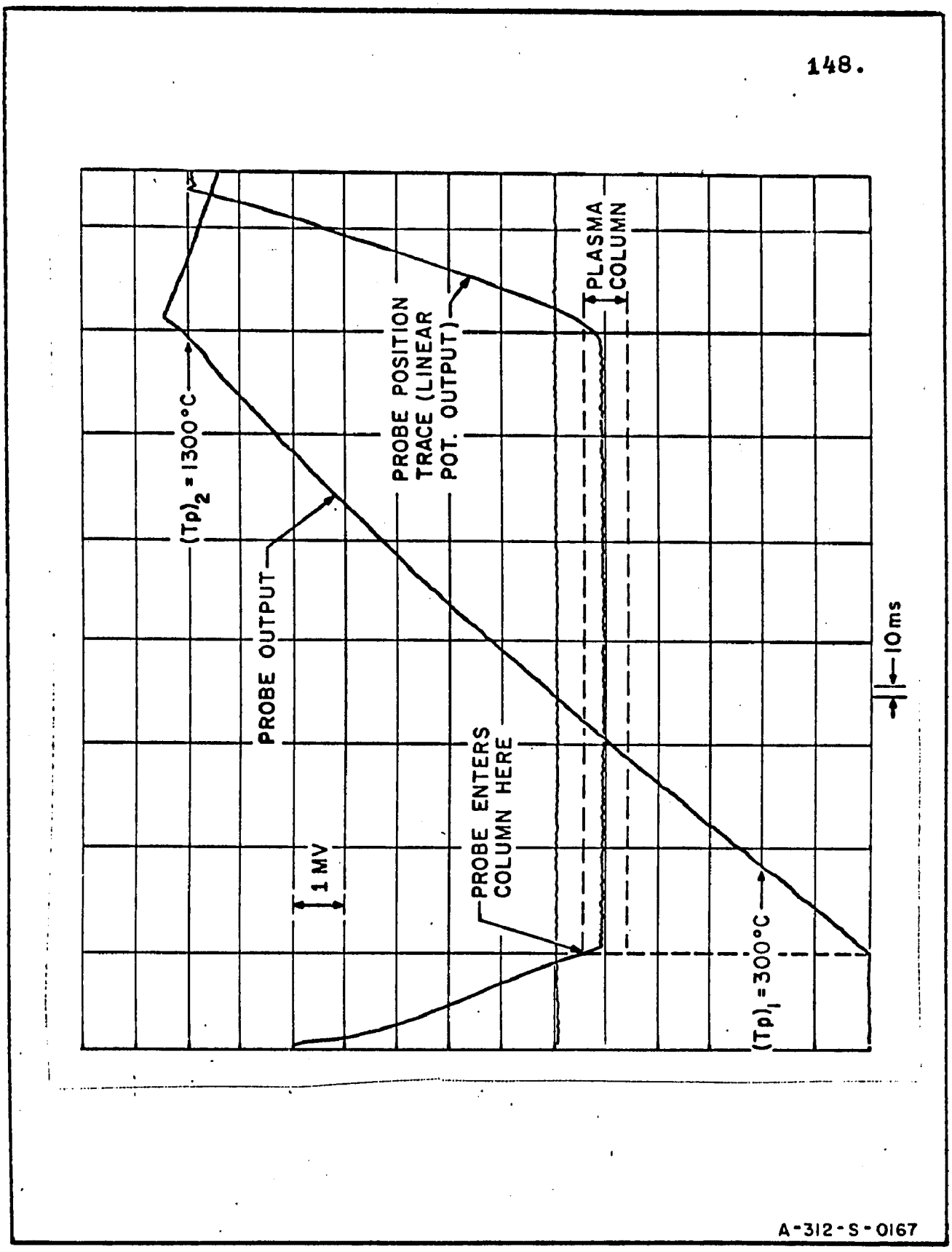

FIG. 35 PROBE OUTPUT vs. TIME , ON AXIS 1.5 mm FROM ANODE

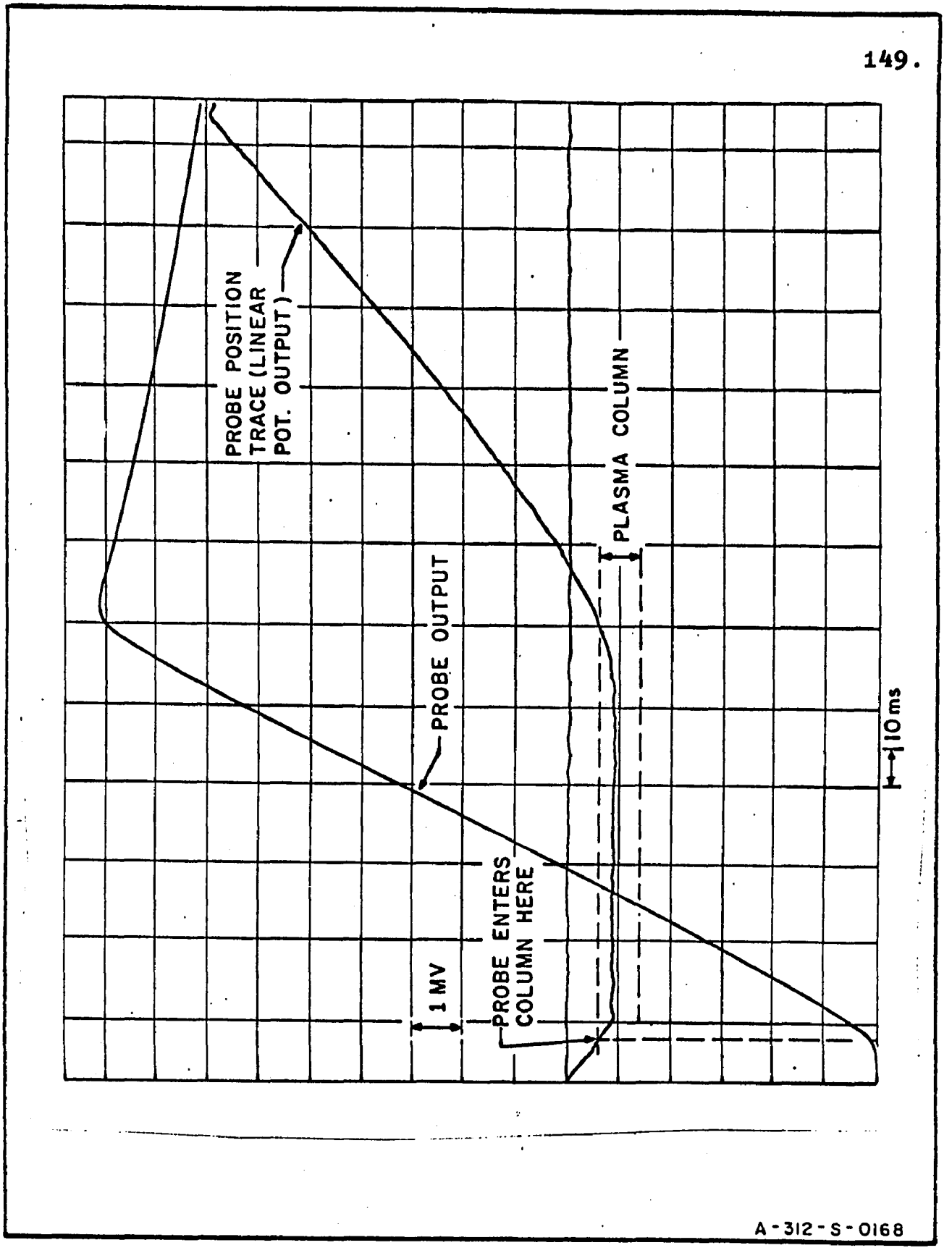

FIG. 36 PROBE OUTPUT vs. TIME , ON AXIS 10.5 mm FROM ANODE

4.5 Electron Density and Temperature

It is well known that as the temperature of a gas is increased the thermal radiation emitted increases rapidly. When the gas becomes appreciably ionized it is, in fact, a rich source of not only line but also continuum radiation. The emission thus can be utilized to determine the temperature of the gas(see Griem, Reference 26) as long as a state of local thermal equilibrium exists.

In a nonequilibrium plasma, the excited state populations may not be uniquely related to one temperature and it is questionable which line emission will be indicative of which temperature. The continuum emission, primarily due to the electron-ion free-free and free-bound transitions, is indicative of the electron temperature and the electron density - as long as the electrons posses a Maxwellian distribution(Chen, Reference 12). The theoretical basis for this was first provided by Kramers(Reference 33) and by Unsöld(Reference 63), for hydrogenic ions. They showed that the continuum emission intensity was given by:

$$I_\nu = C \frac{n_e^2}{T_e^{\frac{1}{2}}} (1 - e^{- h\nu/kT_e}) \qquad \text{(Eq.51)}$$

where C depends on some atomic constant. For argon, the "constant" C has not yet been computed but in many experiments it was found to vary only slightly with wavelength, and, the $n_e^2/T_e^{\frac{1}{2}}$ variation was amply confirmed. In particular, Morris, Bach and Yos(Reference 39) have measured I_ν for argon in the 2500-6500 Å region as a function of temperature in a wall-stabilized (equilibrium) arc. Their data will be accepted as a calibration for spectrometrically determining n_e and T_e.

First, in order to select a suitable wavelength region which is reasonably free of line emission, we converted an Ealing 26-380 spectrometer into one capable of recording the arc spectra. The arrangement is shown in Fig.37. Wavelength recording is obtained by means of a 25-turn potentiometer directly attached to a shaft of the spectrometer wavelength leadscrew. Intensity readout is obtained by means of a EG&G SD-100 silicon photodiode. Connections to a low-noise amplifier and a EAI 1130 X-Y recorder completes the scheme.

In use, a cross section of the arc column can be focused on the frontslit of the spectrometer by the use of an achromat lens and the lens can be traversed in the two traverse directions. A linear motion poten-

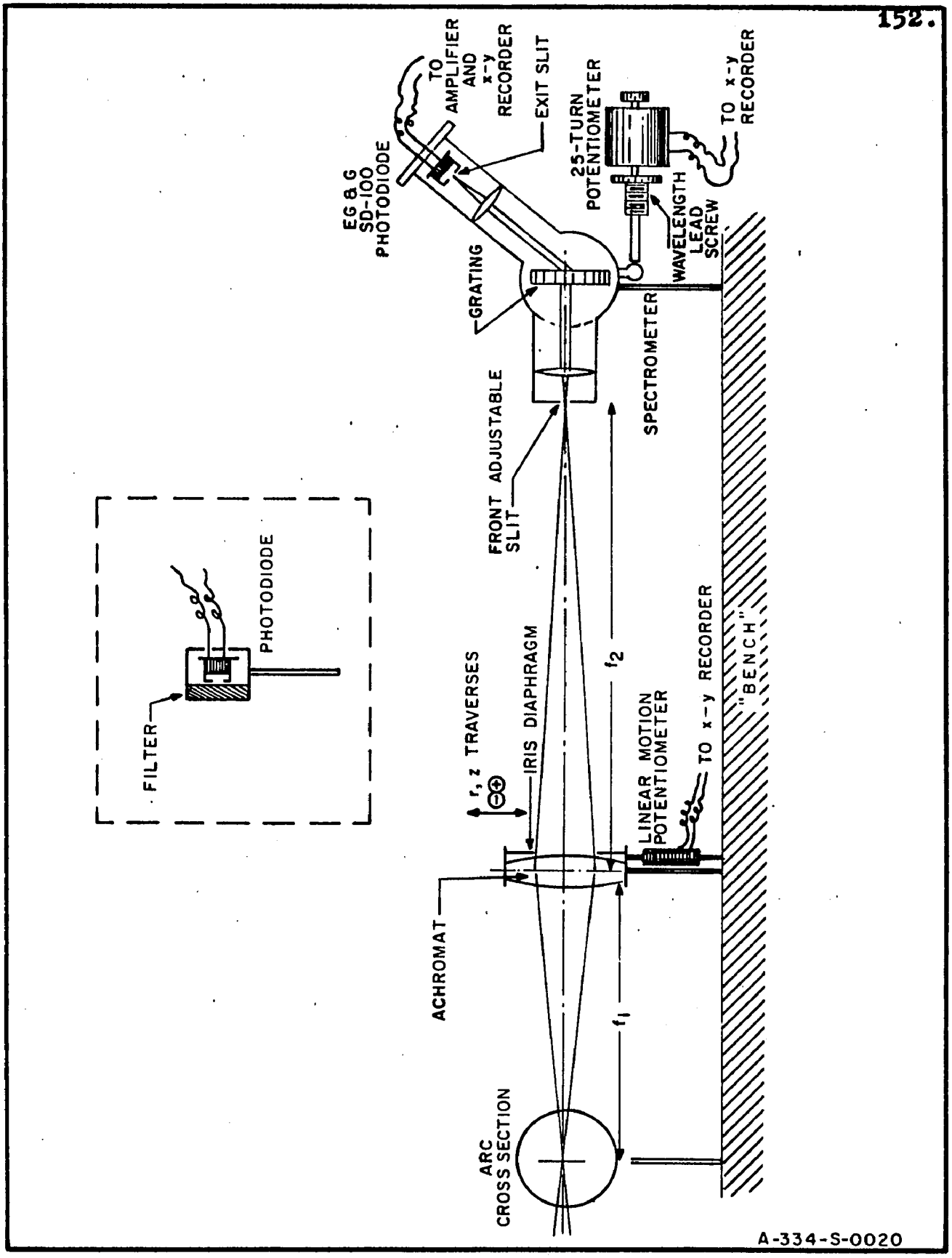

FIG. 37 ARRANGEMENTS FOR SPECTRAL INTENSITY MEASUREMENTS

tiometer attached to the lens enables the chordal scan of the column intensity to be recorded also.

A typical spectrum of the column may be seen in Fig.38 and most of the significant argon lines can be identified. Quite observable continuum emission is evident which, in fact, predominates in the short wavelengths. The continuum around 5000 Å was chosen for more detailed scans.

For ease of measurement, an interference filter (Baird Atomic Type B-10) having about 60 Å bandwidth was used in conjunction with a RCA 7326 photomultiplier tube*, as shown in Fig.39, for higher sensitivity. Spectral calibration of the entire system was made using a NBS certified tungsten ribbon lamp as a source.

To convert the chordal intensity distribution to a radial distribution an Abel inversion must be performed. This is done simply by numerical method(Nestor and Olsen, Reference 41). For rapid checks, a simplified 8-point scheme has been computed by us as illustrated, together with the inversion matrix, in Fig.40. A separate 50-point computer program has also been set up and used.

Figures 41 and 42 show results of chordal scans and the inverted radial distribution, for two axial stations in the arc column.

*Photomultiplier instrumentation designed by C.Stojanoff.

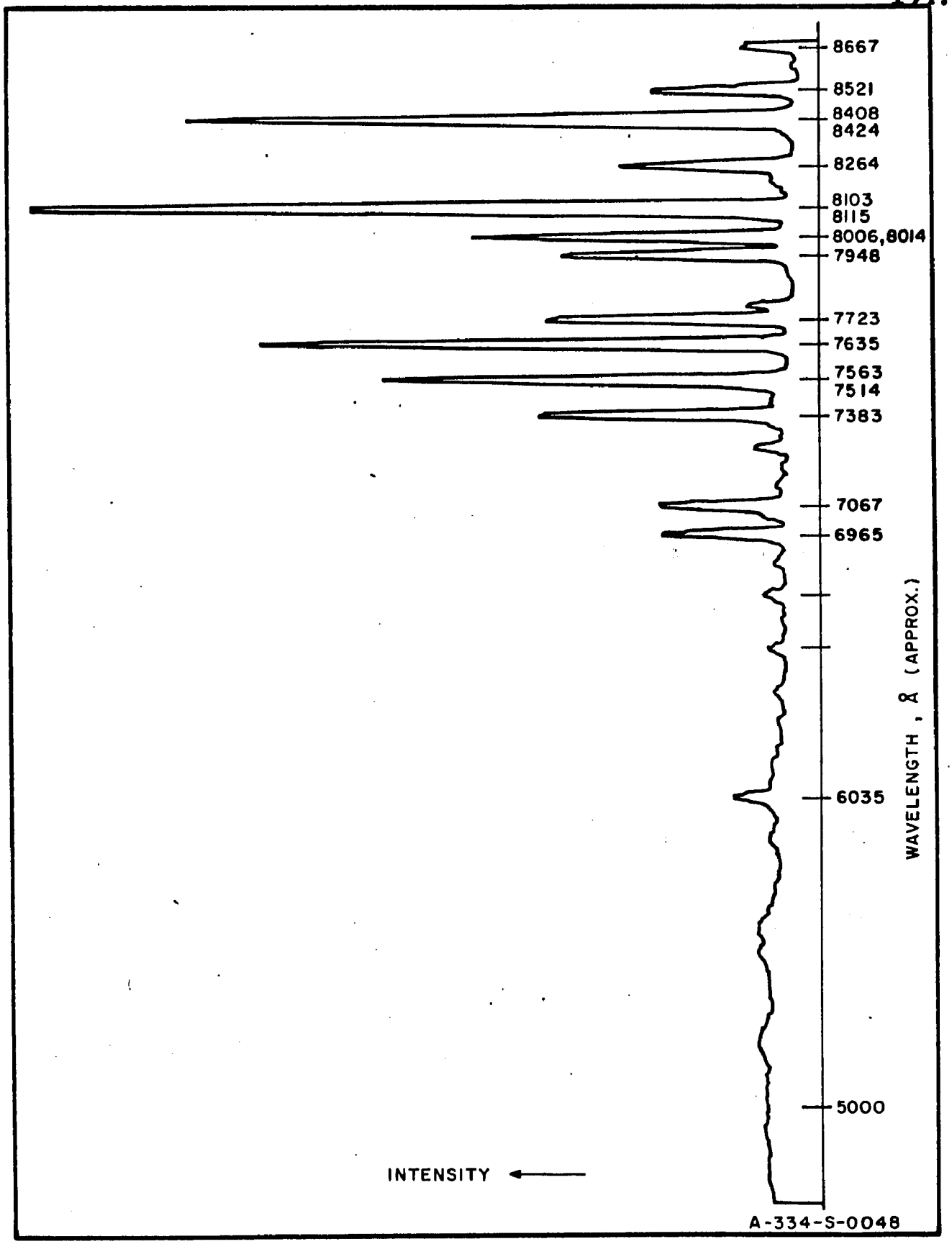

FIG. 38 TYPICAL SPECTRA OF AN 1 ATM. ARGON ARC COLUMN

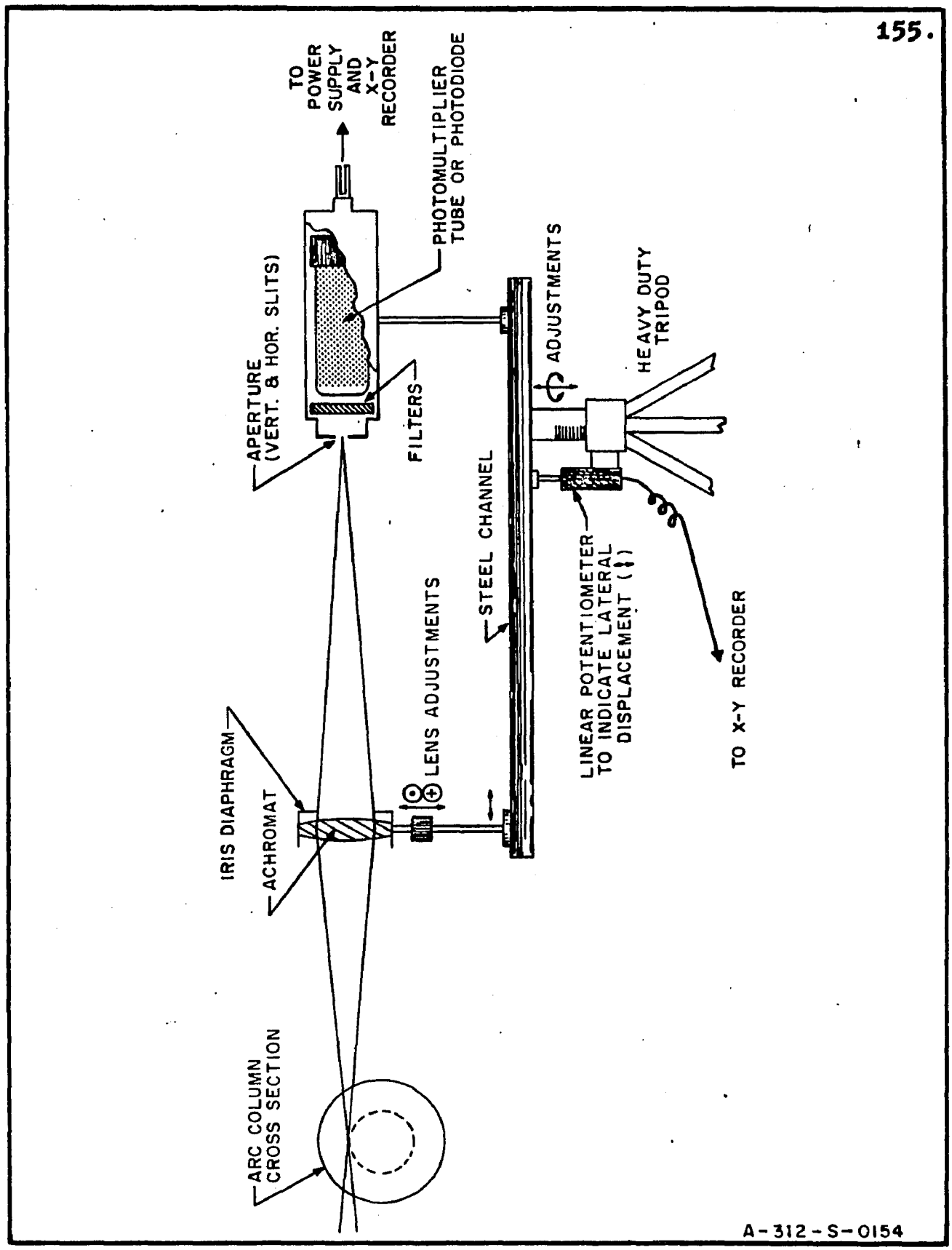

FIG. 39 OPTICAL SCHEME FOR SPECTRAL INTENSITY MEASUREMENTS

8x8 ABEL INVERSION COEFFICIENTS

Kmn		m 1	2	3	4	5	6	7	8
n	1	.203							
	2	.170	.188						
	3	.119	.157	.173					
	4	.100	.108	.146	.156				
	5	.081	.094	.106	.124	.135			
	6	.080	.083	.088	.096	.114	.112		
	7	.080	.080	.080	.083	.085	.100	.082	
	8	.080	.080	.080	.080	.080	.080	.088	.031

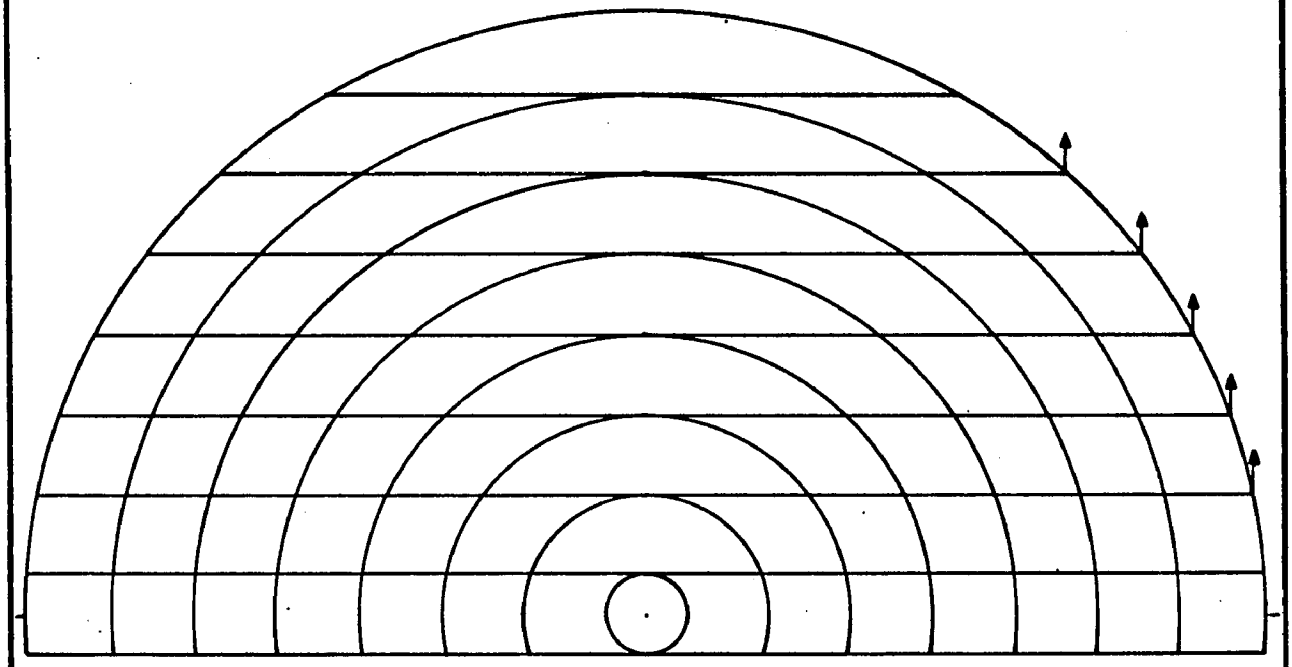

A-334-S-0023

FIG. 40 A 8x8 ABEL INVERSION SCHEME

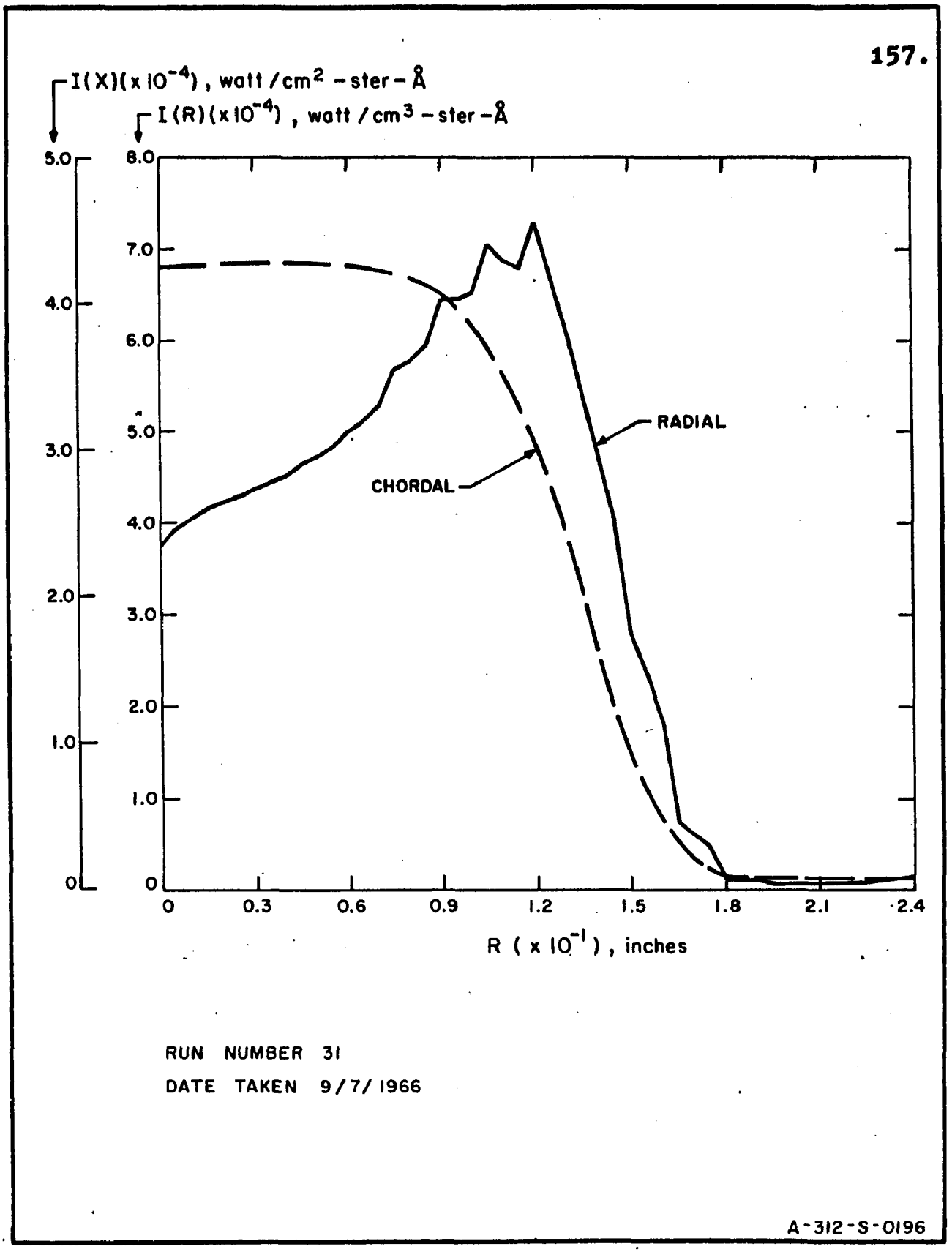

FIG. 41 CHORDAL AND RADIAL INTENSITY DISTRIBUTION OF 5000 Å CONTINUUM , 2.75 mm FROM ANODE

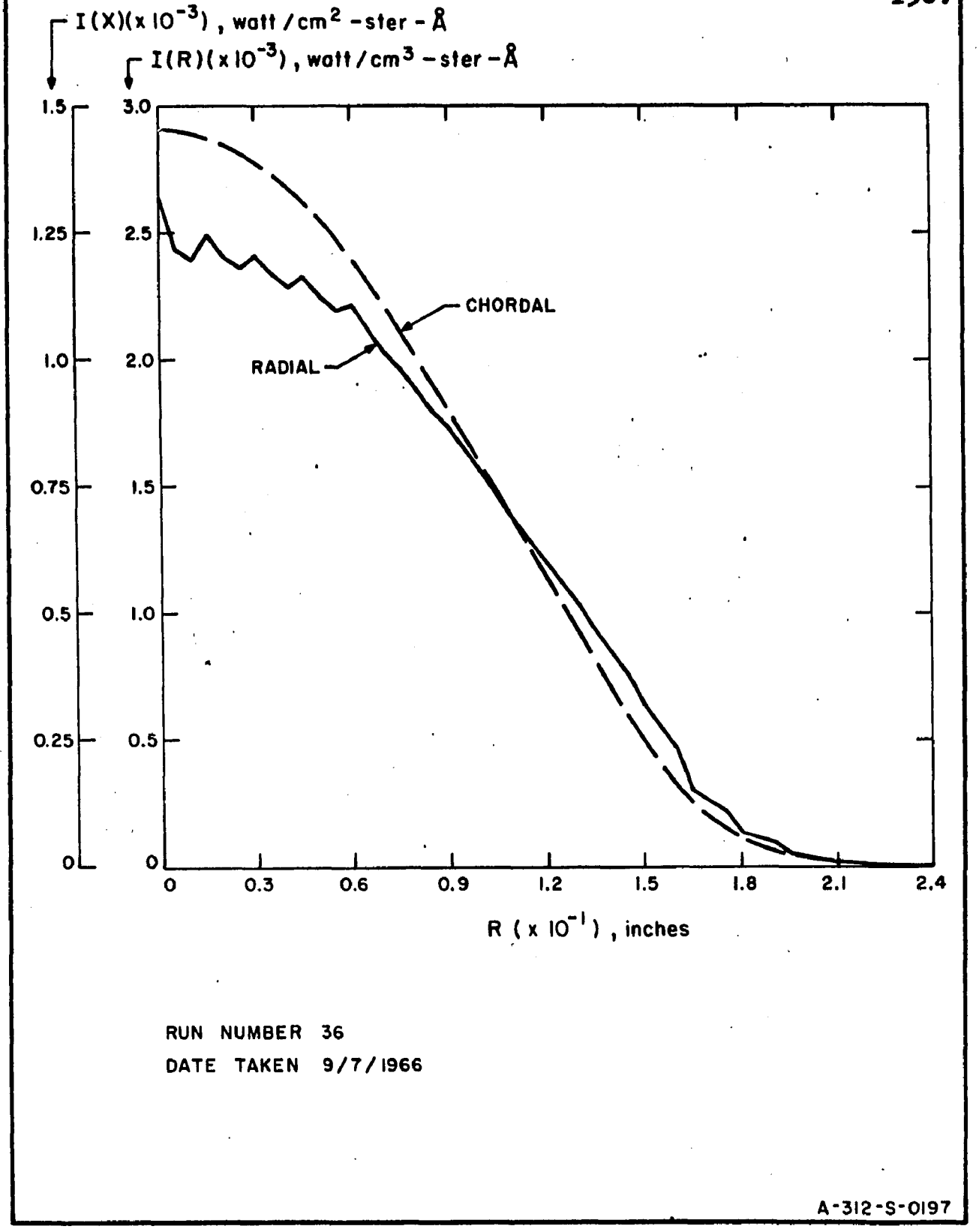

FIG. 42 CHORDAL AND RADIAL INTENSITY DISTRIBUTION OF 5000Å CONTINUUM, 9 mm FROM ANODE

The calibration curve is shown in Fig.43 and is derived from data of Morris, Bach and Yos,* as stated earlier. Note that the off-axis peak of Fig.41, which may be real or due to experimental errors, would account for an increase of only 300°K from the axis temperature and therefore is not very significant.

---

*With revision kindly supplied by P.Schreiber of ARL.

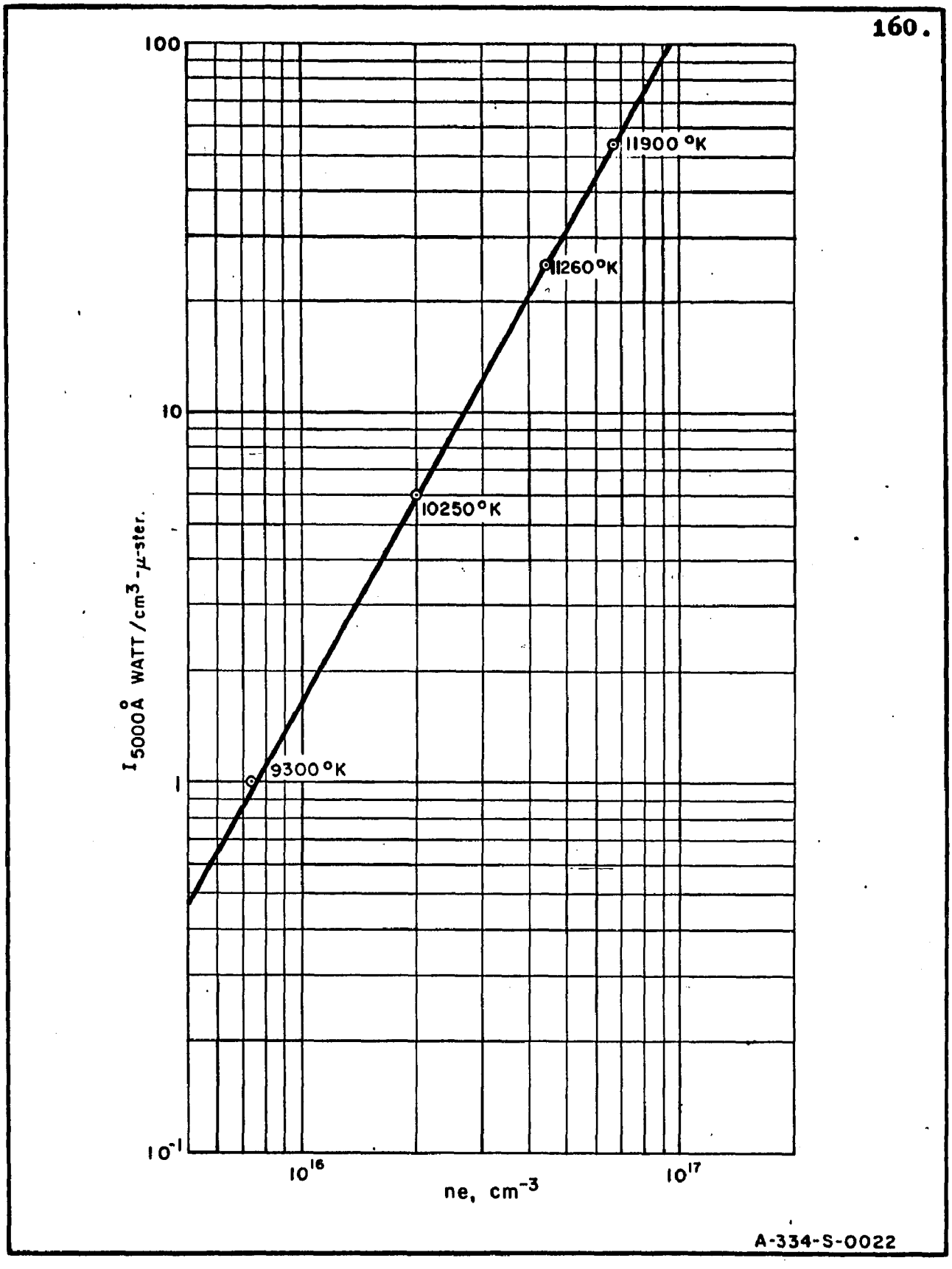

FIG. 43 CALIBRATION DATA FOR THE 5000 Å CONTINUUM OF ARGON
(From Reference 39, with revision)

4.6 High-Speed Photographic Observation

A Dynafax Model 350 camera capable of taking 200 frames at speeds up to 35000 fps, with exposure time as short as 5 microsec. per frame, was used to observe any fluctuating features in the arc that might escape visual detection. Some typical frames are reproduced in Fig.44, 45, 46, and 47.

A slower 8 mm Fastax camera(up to 18000 fps) but with 100 ft.film capacity was used to record more extended events, such as the arc column being traversed by a probe as reproduced in Fig.48 and Fig.49.

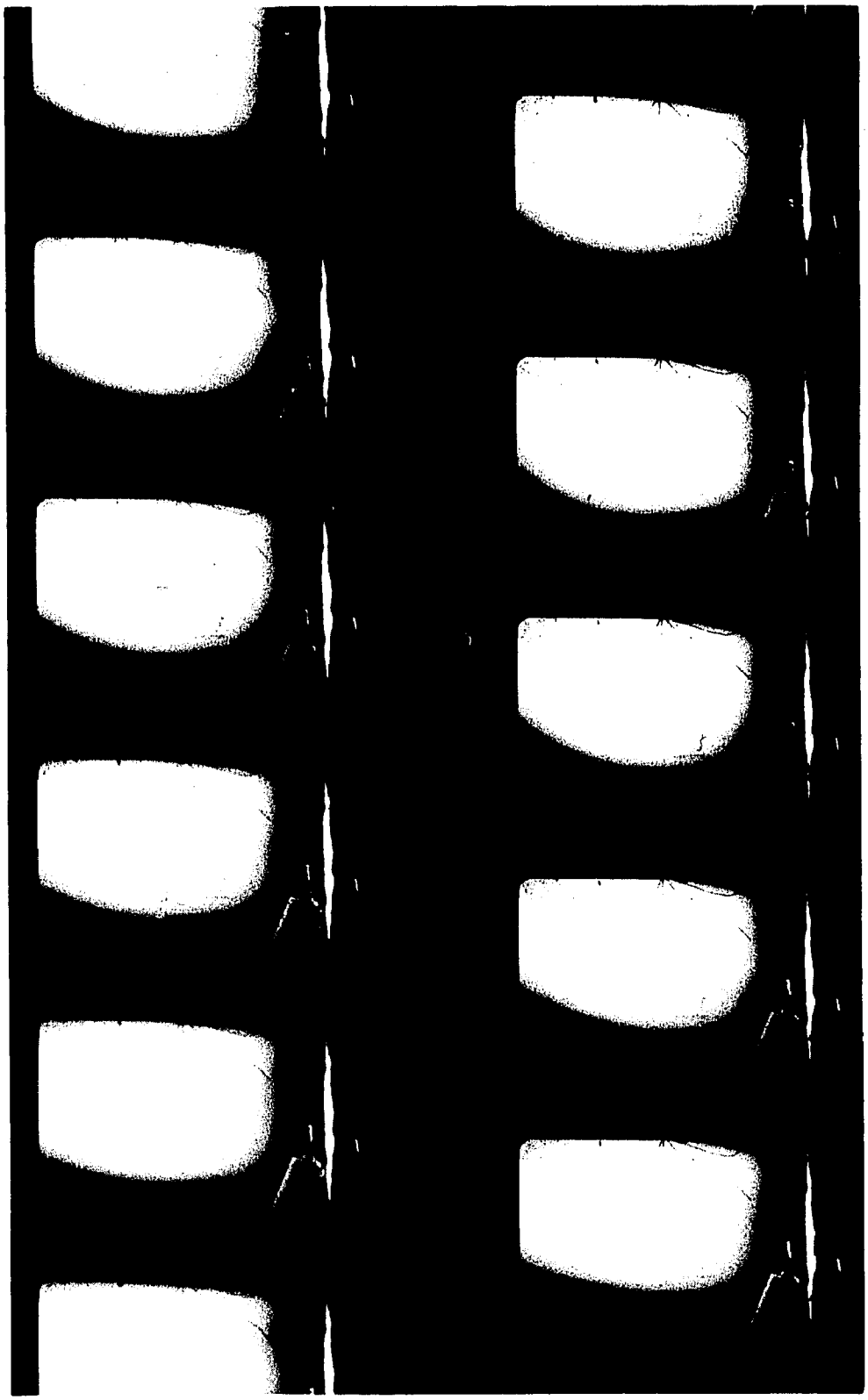

Fig.44 Dynafax Pictures of a 150 Amp Argon Arc
$\dot{m}$ = 0.2 gm/sec, 5000 fps.

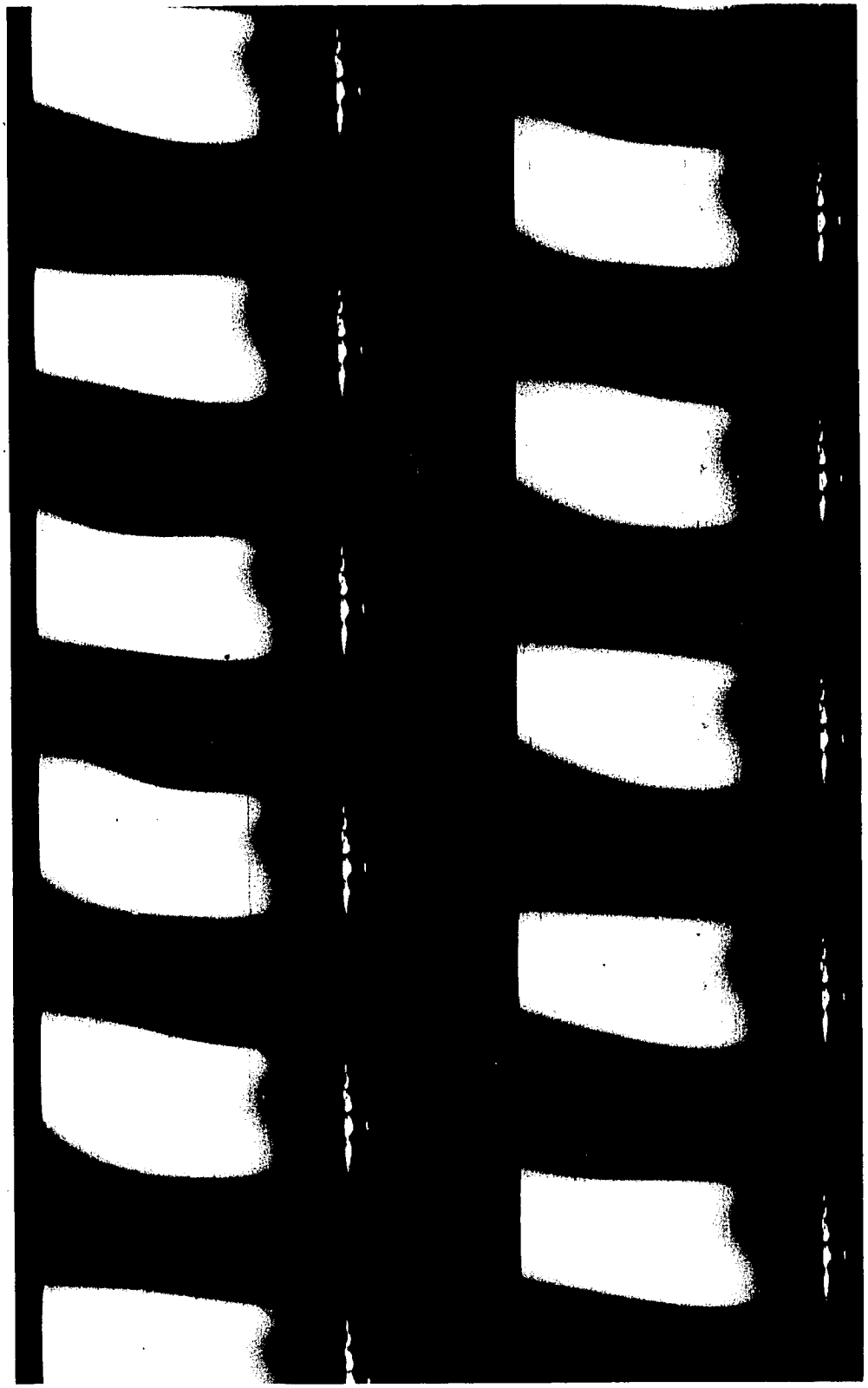

Fig.45 Dynafax Pictures of a 150 Amp Argon Arc
$\dot{m}$ = 0.35 gm/sec, 5000 fps.

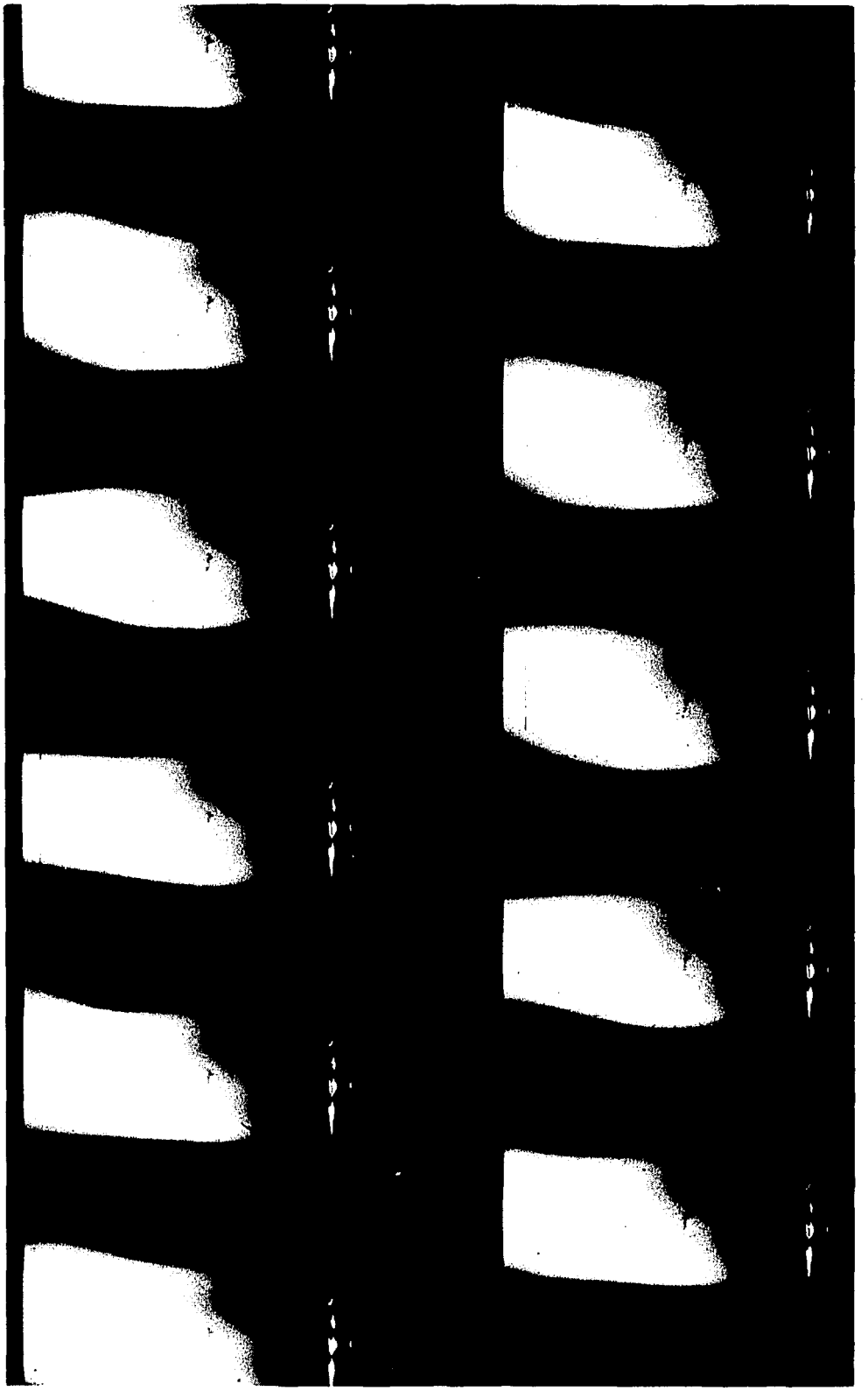

Fig.46 Dynafax Pictures of a 150 Amp Argon Arc $\dot{m}$ = 0.5 gm/sec, 5000 fps.

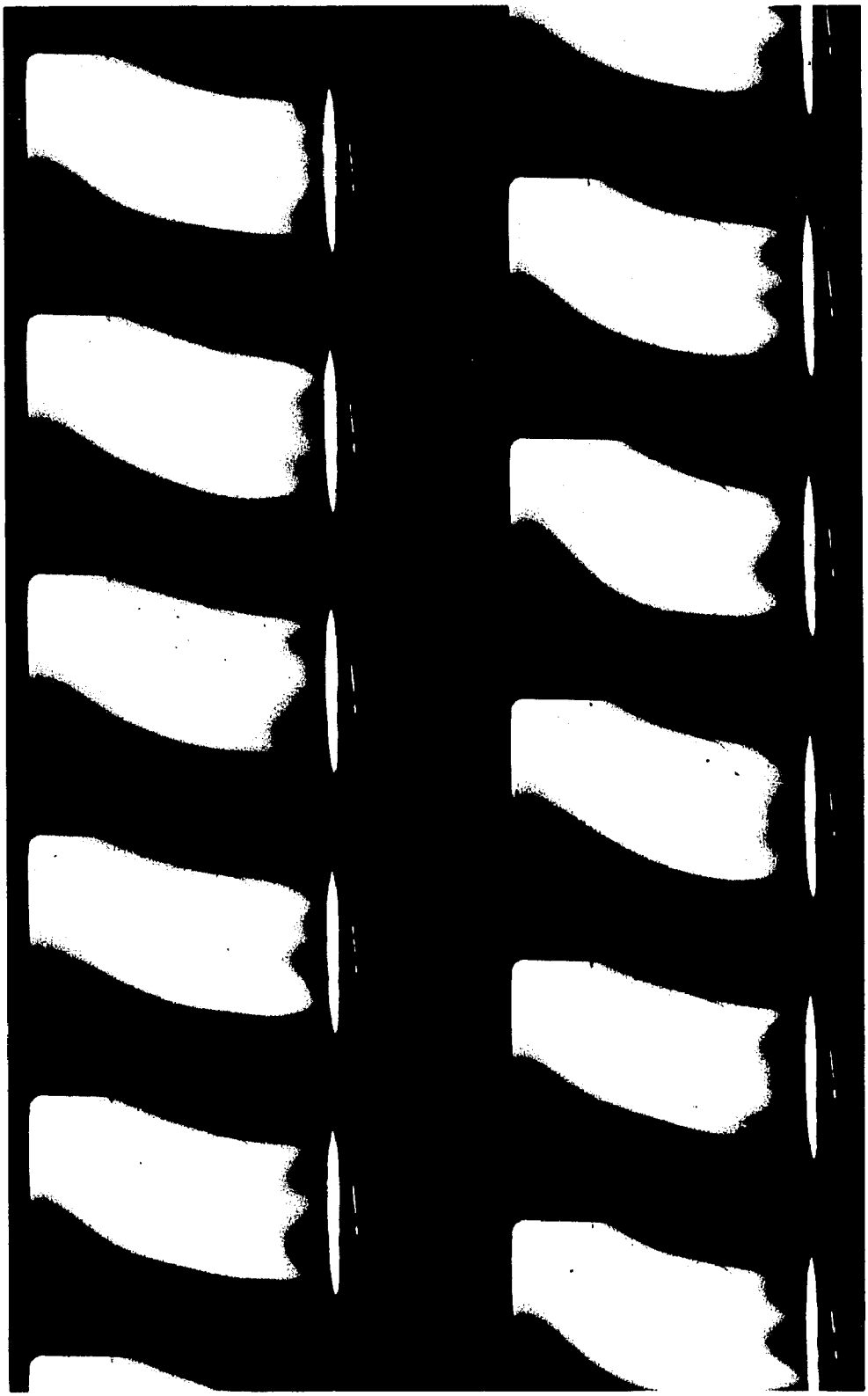

Fig.47 Dynafax Pictures of a 200 Amp Argon Arc
$\dot{m}$ = 0.2 gm/sec, 5000 fps @ 15 μsec/frame.

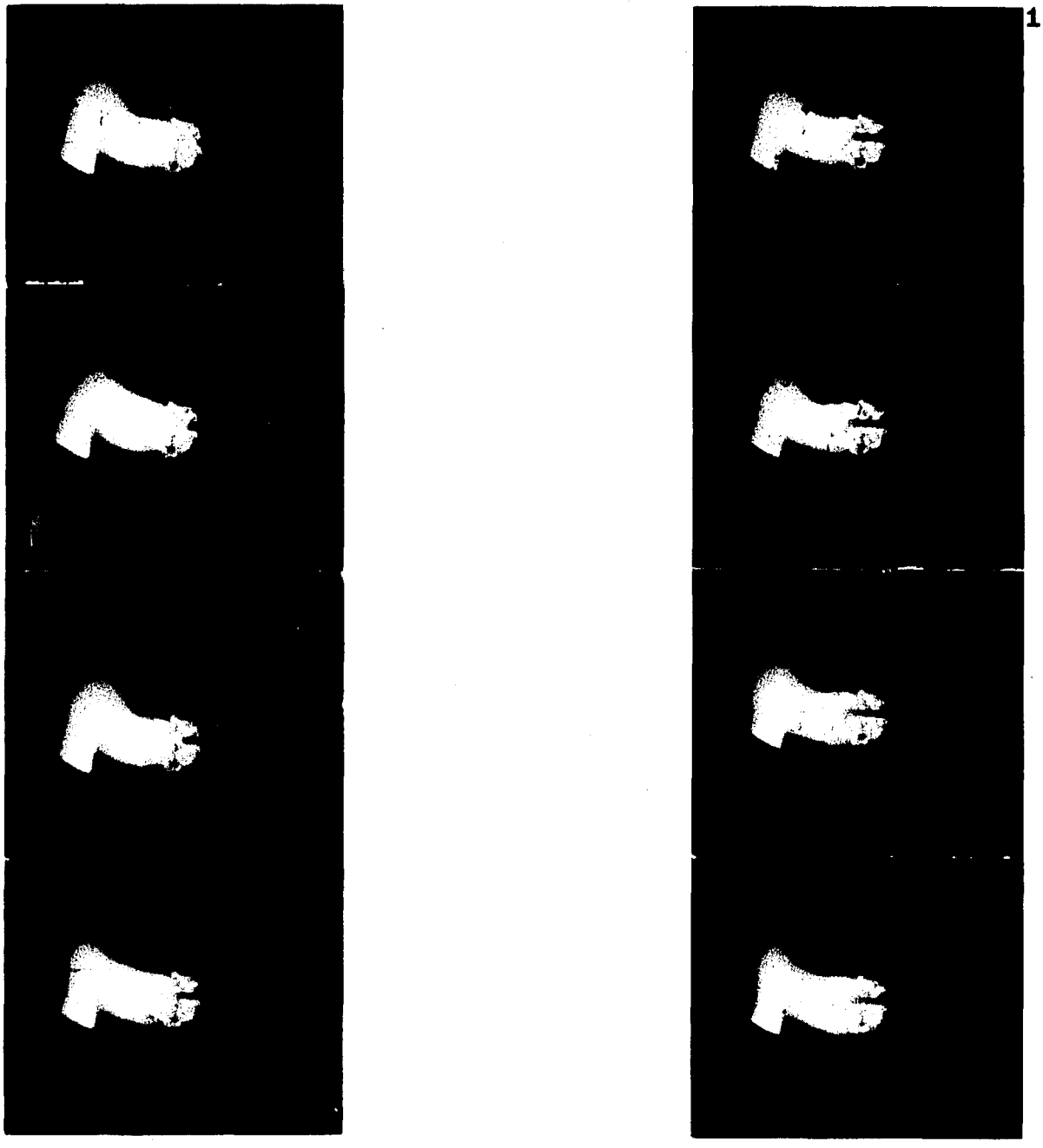

Fig.48 Fastax Pictures of a 150 Amp Argon Arc Being Traversed by a Hall Probe Tip, 10000 fps.

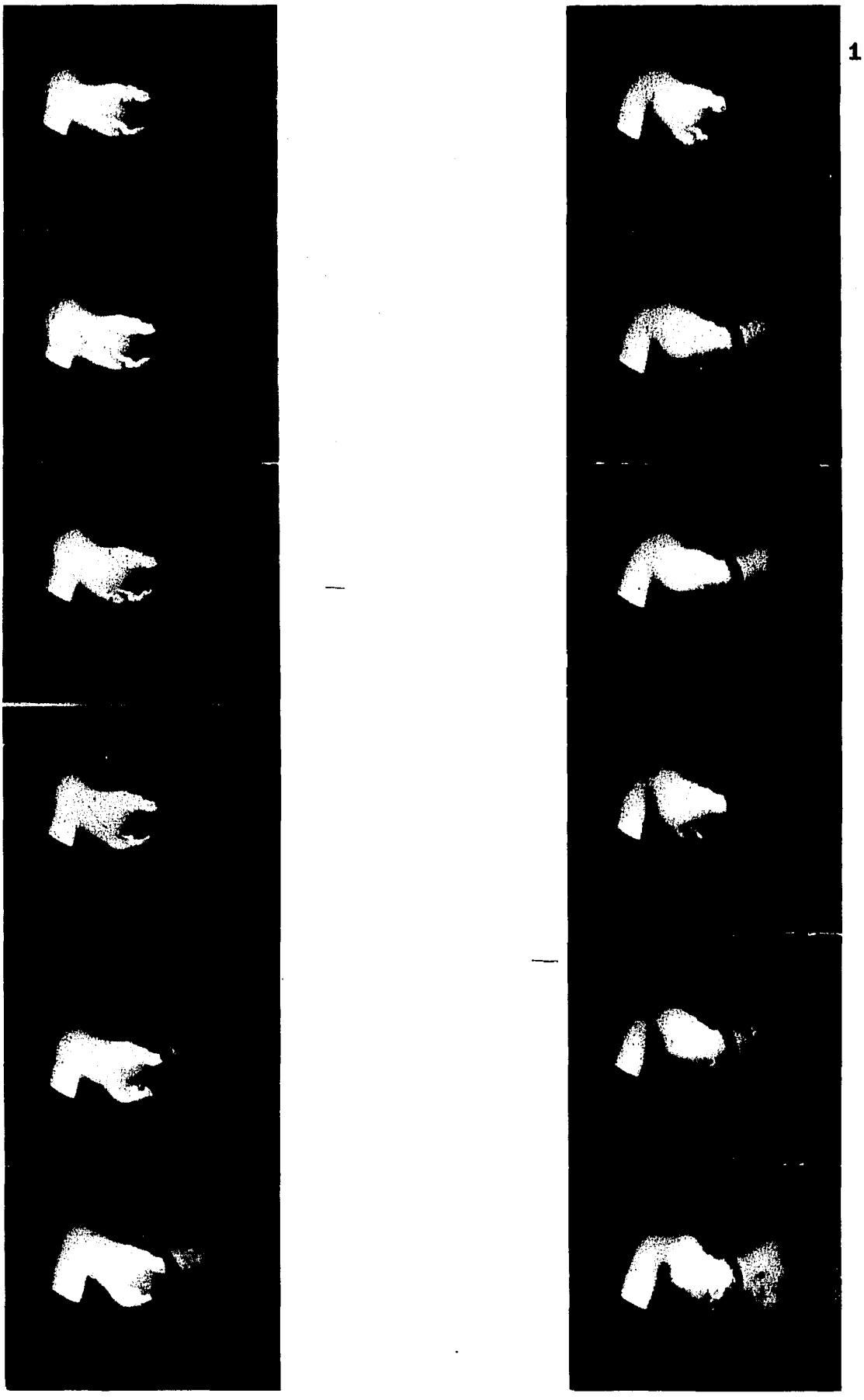

Fig.49 Fastax Pictures of a 150 Amp Argon Arc Being Traversed by the Bulky Probe Stem, 10000 fps.

Chapter 5

EXPERIMENATAL RESULTS

It was possible to operate the fluid transpiration arc over a considerable range of externally controllable parameters - i.e. arc gap, arc current, gas flow. A complete diagnostics program covering each set of parameters generally requires a very substantial investment in time and risks, given the unpredictability of hazards of local probings of the arc column, the lengthy spectrometric measurements, and, the high cost of its associated data reduction. As a result, in our investigation, many individual diagnostic measurements(e.g. thermocouple probe) were carried out over a wide range of parameter variations in an effort to check the validity and to understand the behavior of the arc to that particular type of probing.

Out of these individual measurements two complete sets of data have been assembled for the following arc conditions:

Arc gap = 3 cm

Arc current = 150 amp

Anode diameter = 1.1 cm

Anode material = NC60 porous graphite

$\dot{m}$ = 0.2 gm/cm^{2}sec (Case I)

$\dot{m}$ = 0.35 gm/cm^{2}sec (Case II)

The bases for the choice of these conditions are as follows:

After numerous runs it was our experience that the length of arc gap, beyond about 2 cm, had little or no bearing on the nonequilibrium portion of the positive column. The 3 cm gap was considered ample to allow probe and spectrometric measurements, even though with the power supply available more than 6 cm arc gap had been achieved. In the latter case the extra arc column was found to be nearly fully developed and therefore was of no use in the present study.

The arc current of 150 amp was chosen on the basis of anode coverage and column size. Although currents from 60 to 250 amps had been achieved, it was found that in the 60 to 150 amp range the column size merely increased with current without exhibiting marked changes in its other aspects. Fastax motion picture recordings showed that for the lower currents the column diameter in relation to the Hall probe(the least miniaturized of the probes) was such that as the probe entered the column very noticeable displacement of the discharge resulted. For a 150 amp column, the perturbation by Hall probe is negligible as shown in the sequence of Fastax pictures reproduced in Fig.48. We see that the entrance of the slender probe tip(where the sensor is located) causes

no visible change in the arc. In a later sequence of the same probing event, Fig.49, the much bulkier portion of the probe stem enters into the column. One can clearly see the resulting abnormal bulging of the column at first and the deflection of the column completely to a position above the probe finally. Notice also the hairpin bend in the mixing zone as a result of probe perturbation upstream. For lower current arcs even the slender probe tip could cause such perturbation.*

Above 150 amp the extent of the anode dark space decreased and became invisible to the naked eye. Figure 47, reproduced from the Dynafax pictures of a 200 amp arc, shows that, in reality, the nonequilibrium zone is punctured by a number of smaller bright columns undergoing rapid motion. This we surmise to be due to possible anode surface phenomena since above 175 amp the anode surface was completely covered and the column could not further extend its coverage when the current was again increased. Also, as will be discussed later, at 200 amp the electron temperature near the anode was higher and this favors the formation of a filamentary structure rather than a homogeneous nonequilibrium column.

The choice of $\dot{m}$ was guided by the general observation that at very low flow the nonequilibrium zone was

*The significant data are taken only during immersion of the slender probe tip,which, at 150 amp, causes no noticeable disturbance.

too small to be conducive to insertion of probes and spectrometric measurements. At very high flows, on the other hand, streaky structures can be seen to issue forth from the anode - possibly indicating gross thermal and electrical inhomogeneities on the anode due to the massive blowing. The qualitative change of the dark space with $\dot{m}$ is demonstrated in the Dynafax pictures reproduced in Figs.44, 45, 46 for $\dot{m}$ = 0.2, 0.35, 0.48, respectively. Note the diffuse nature of the dark space for $\dot{m}$ = 0.2 and, incidentally, the apparent lack of perturbation by the presence of a bulky potential probe (the 1/16 in diameter insulator as compared with 1/32 in for most other probes). In Fig.45($\dot{m}$ = 0.35) the dark space is considerably extended but still not marred by excessive streaks. In Fig.46($\dot{m}$ = 0.48) streaks become much more noticeable and the dark space is much distorted.

Some Hall probe results are shown in Figs.50, 51, 52, and 53. Also shown are the current density reduced according to Eq.45 by numerical and graphical means. In all the cases the total current integrated from the current density distribution deviates not more than $\pm$10% from the total arc current measured with a $\pm$5% current shunt and millivoltmeter. This degree of accord tends to support the general validity of the J measure-

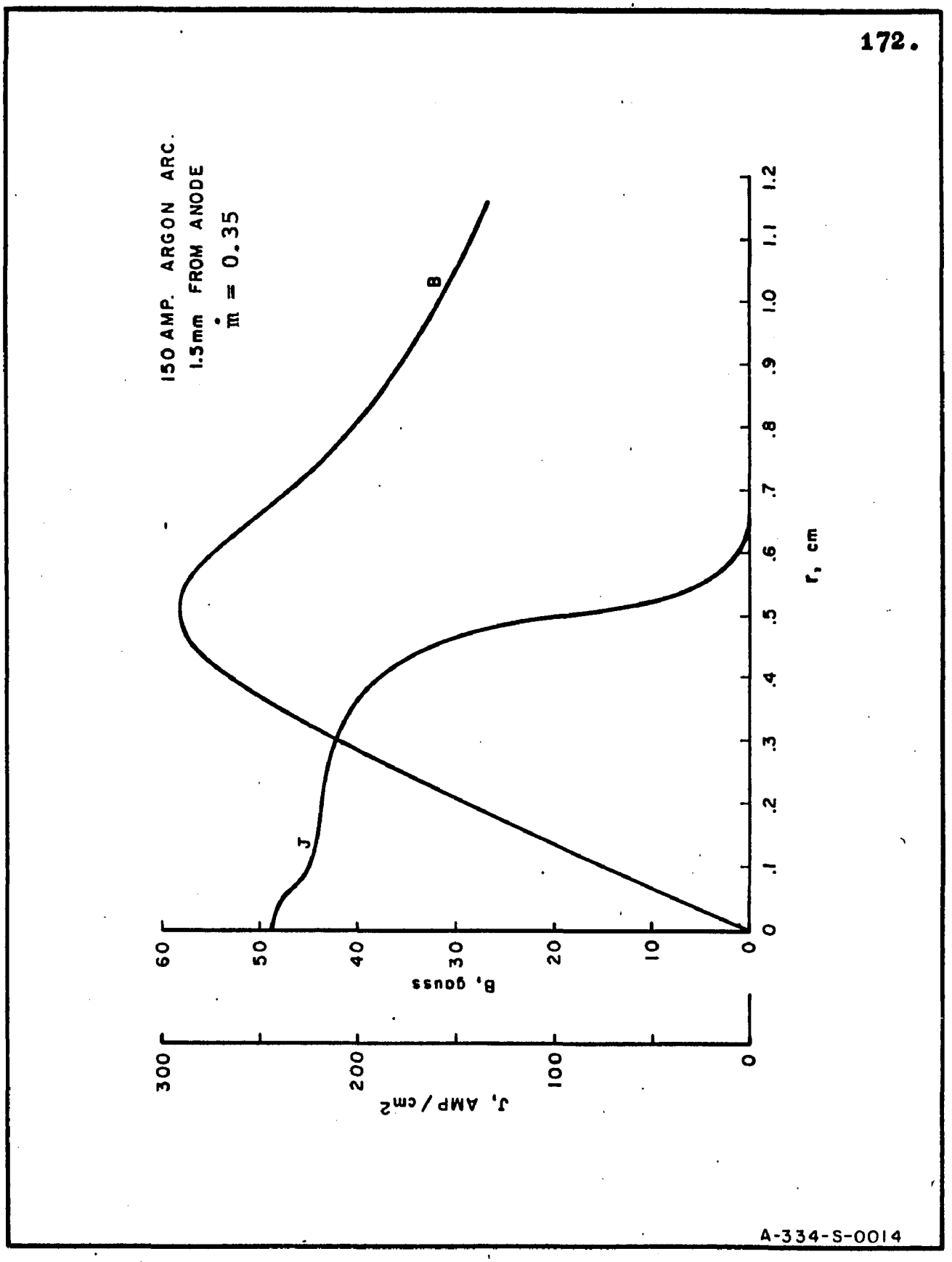

FIG. 50 RADIAL CURRENT DENSITY DISTRIBUTION AT 1.5mm. FROM ANODE

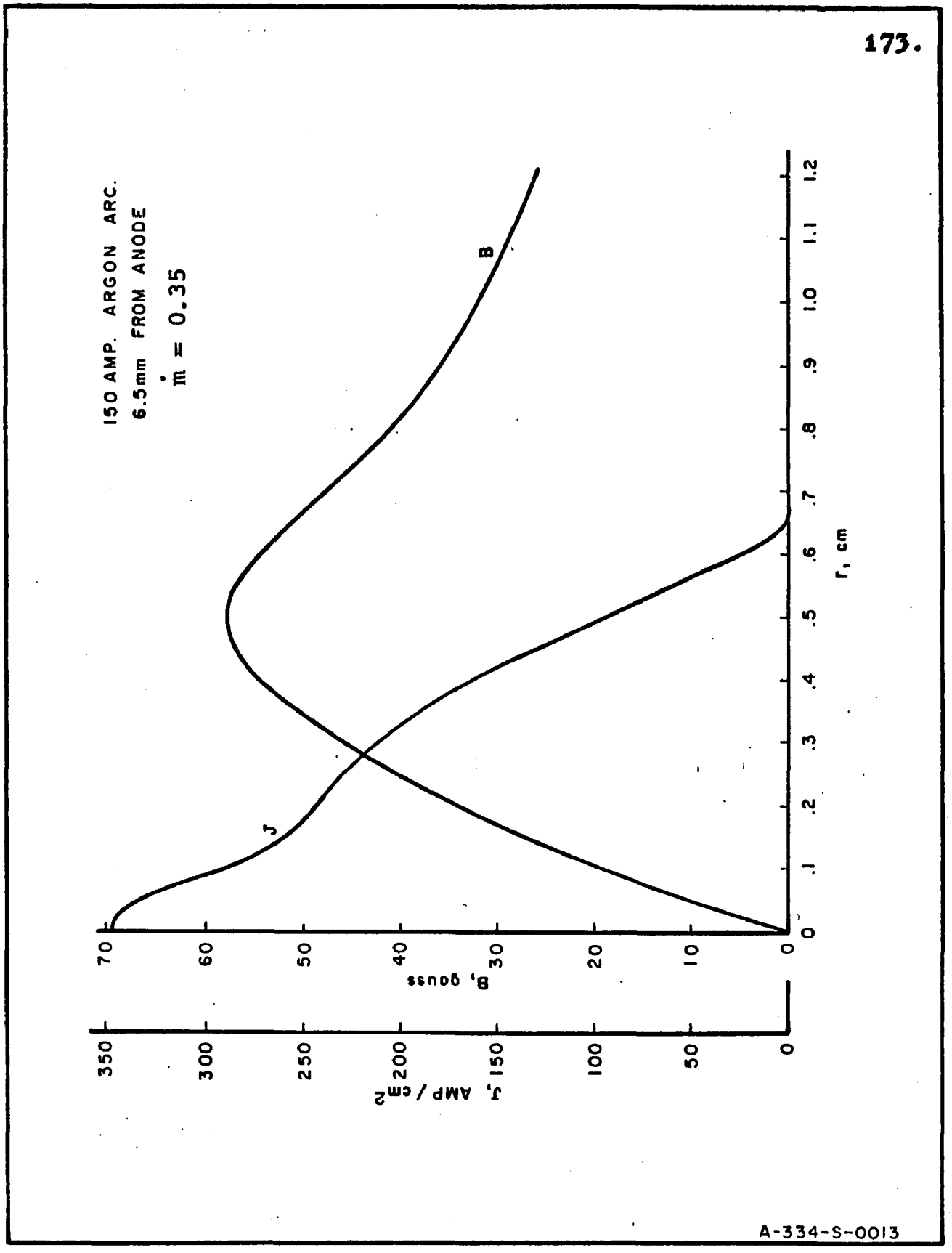

FIG. 51 RADIAL CURRENT DENSITY DISTRIBUTION AT 6.5mm. FROM ANODE

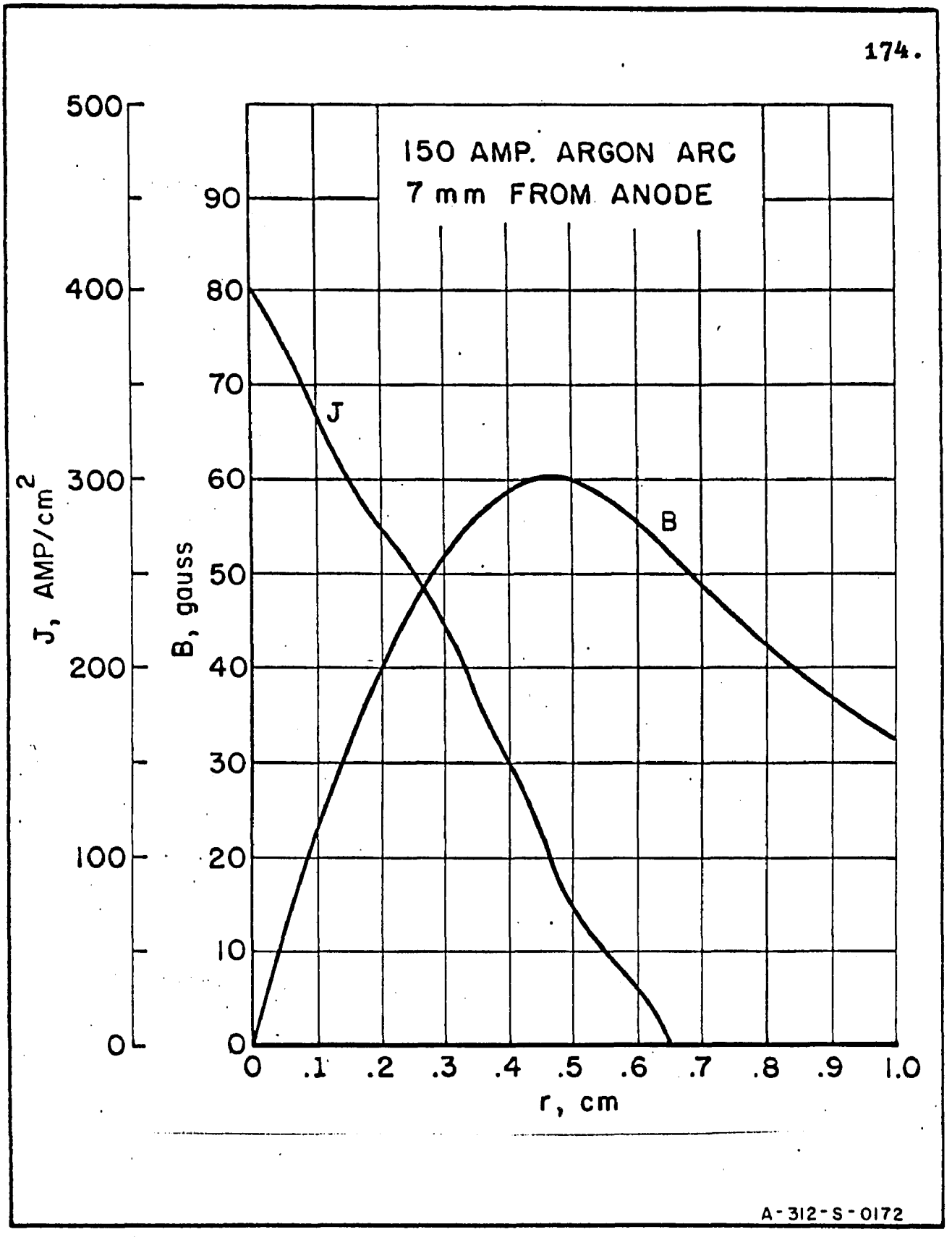

FIG. 52 RADIAL DISTRIBUTION OF MAGNETIC FIELD AND CURRENT DENSITY IN AN ARGON ARC (150 AMP., $\dot{m}$ = 0.2, 7 mm FROM ANODE)

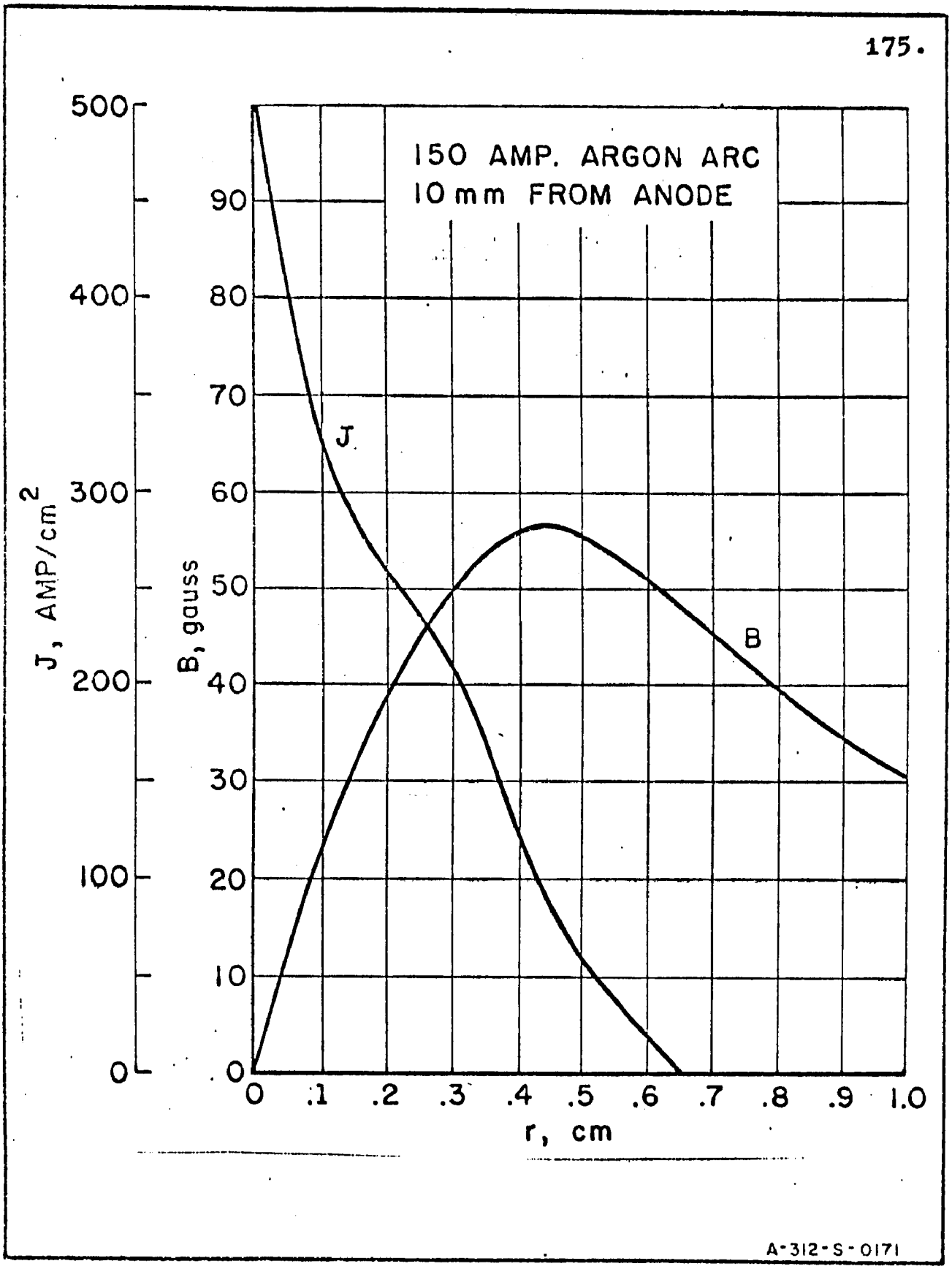

FIG. 53 RADIAL DISTRIBUTION OF MAGNETIC FIELD AND CURRENT DENSITY IN AN ARGON ARC (150 AMP., $\dot{m} = 0.2$, 10 mm FROM ANODE)

ments. It is evident that near the anode J(r) approaches a flat-top distribution quite well and therefore substantiates the claim of quasi one-dimensionality. Further away from the anode the flat top vanishes although the extraordinarily sharp peak on the axis as shown in Fig.53 is probably not real. The disappearance of a flat distribution as one moves away from the anode is, first of all, to be expected from the theoretical analysis leading to Fig.10. The Hall probe results indicated that more is involved than that. For, aside from the tendency for the hot column to attain a non-flat radial profile the charged particles also have, in addition, a tendency to converge as one goes away from the anode.

The above mentioned effect is strikingly demonstradted in Fig.54 which shows the equipotential lines replotted from a series of potential probe radial traverses at different axial positions. From this we see that the peaking of current density at the axis away from the anode can be explained by the focussing effect of the electric field(lens) distribution. Also, notice the high electric field(closely spaced equipotential lines) near the anode as versus further down stream.

The axial distribution of these axis properties

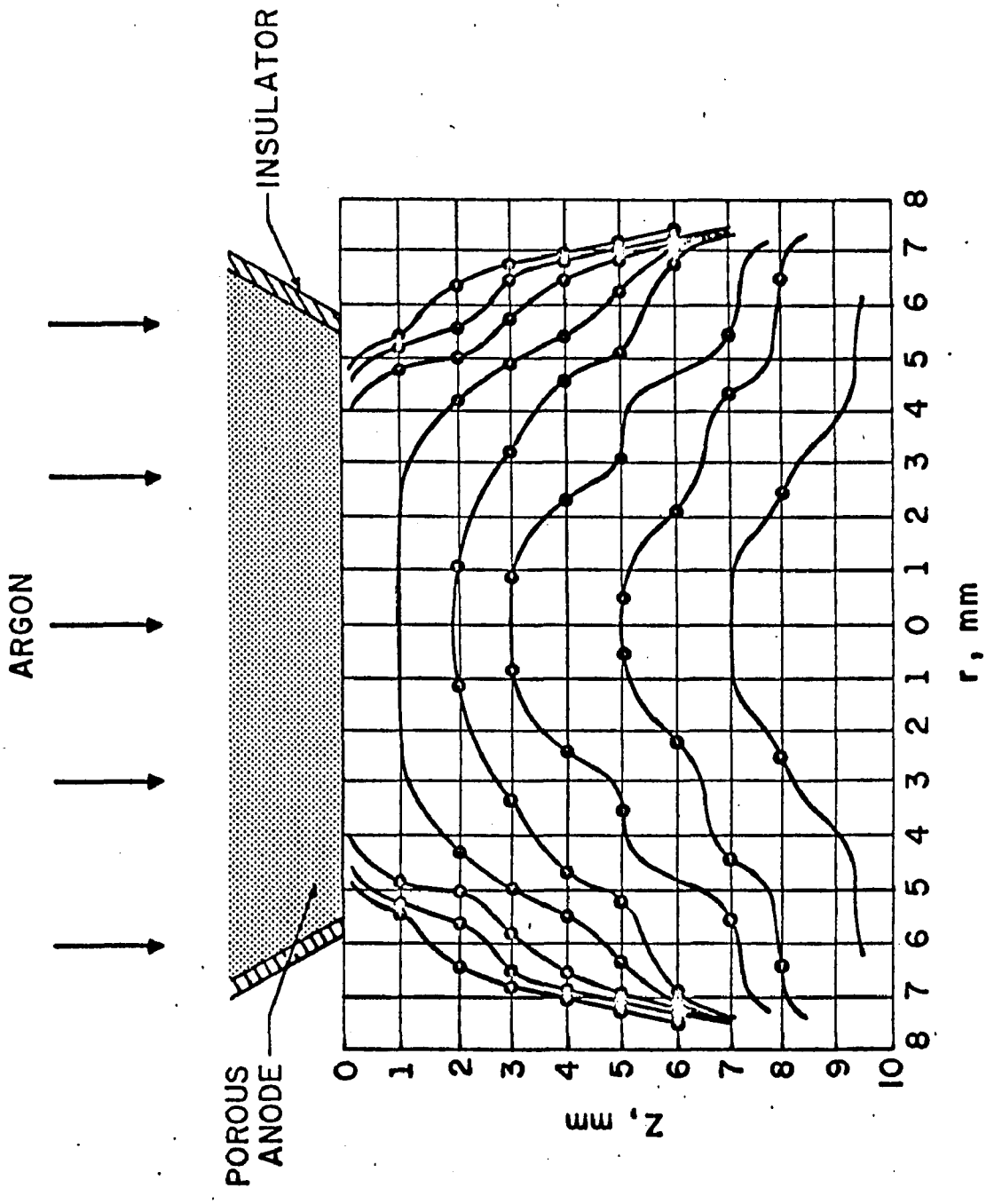

FIG. 54 EQUIPOTENTIAL PLOT OF A 150 AMP. ARGON ARC POSITIVE COLUMN

are collected in Figs.55 and 56. Also shown are the spectrometrically determined T_e and n_e and the probe determined T_g. In the case of T_g the corrections due to abrupt thermal conductivity variation as discussed earlier are also included.

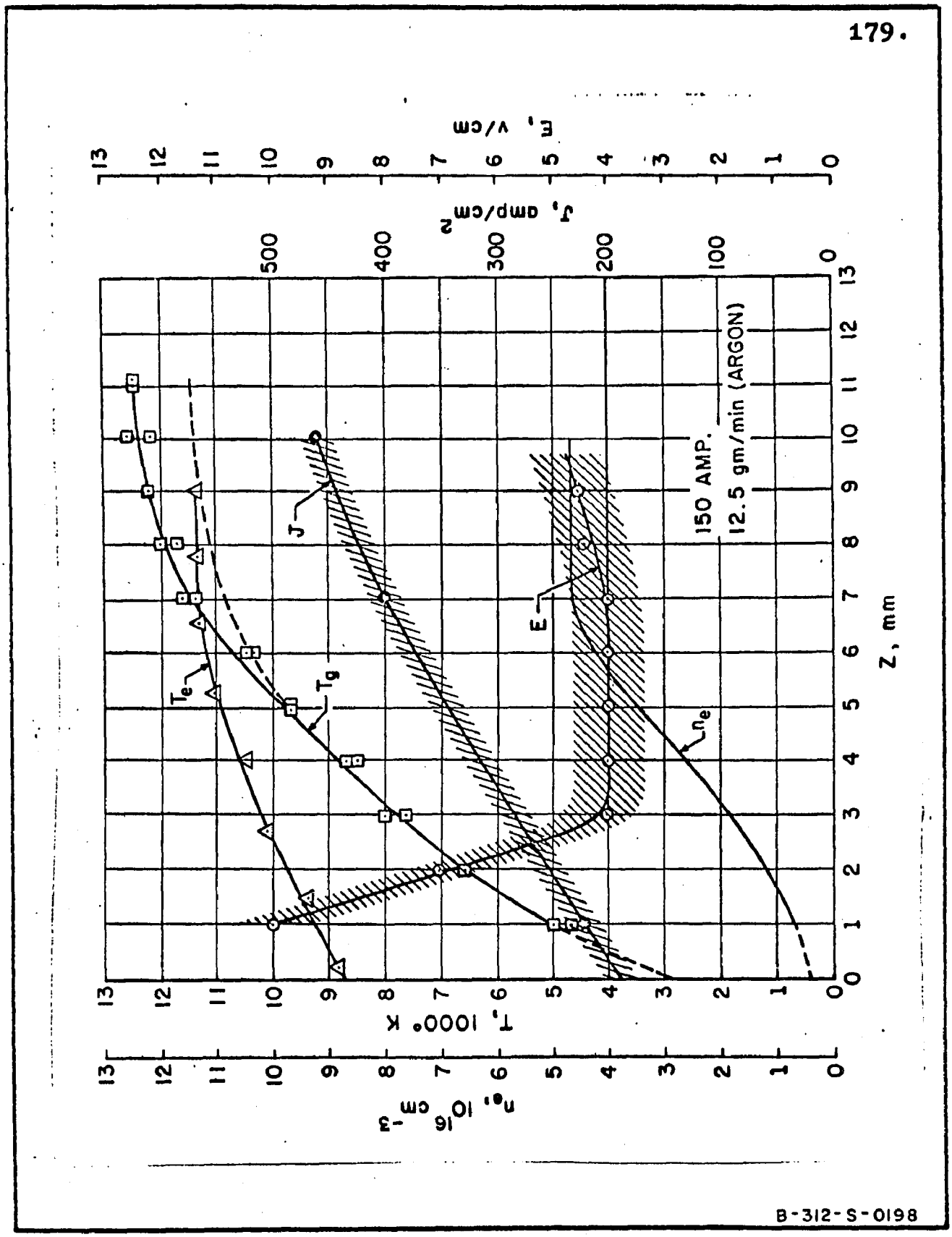

FIG. 55 AXIAL DISTRIBUTION OF ARC PROPERTIES – CASE I

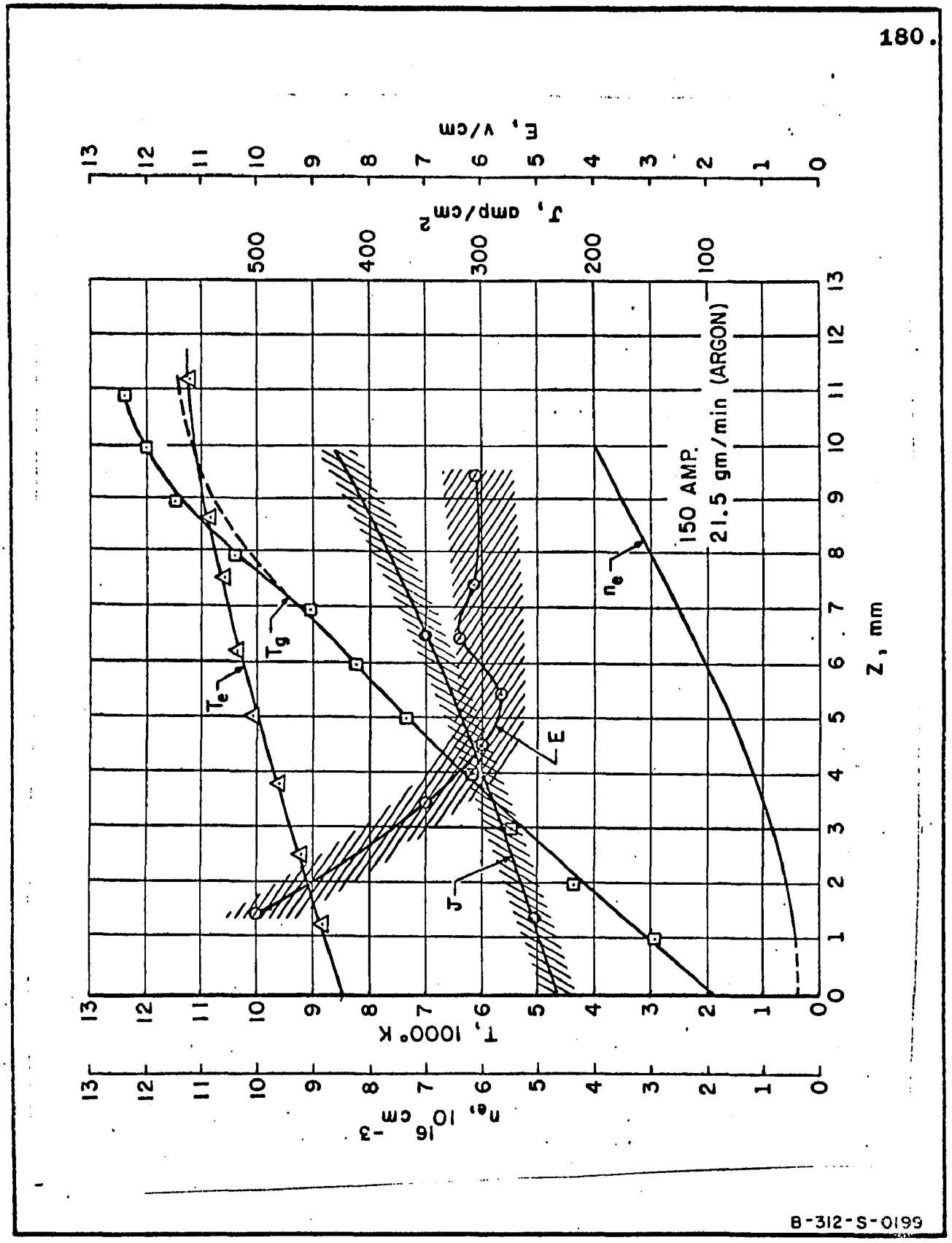

FIG. 56 AXIAL DISTRIBUTION OF ARC PROPERTIES — CASE II

Chapter 6

DISCUSSION OF EXPERIMENTAL RESULTS AND CORRELATION WITH THEORETICAL CALCULATION

The results can now be interpreted in order to answer the following specific questions:

1. How uniform and one-dimensional is the actual arc column? Is it, or part of it, describable by the proposed streamtube analysis? What is the filamentary structure sometimes observed?
2. How does the highly convectively-cooled arc column maintain its electrical conducting property? What are the magnitudes of the conductivity?
3. If there is electron-heavy particle nonequilibrium, is the two-temperature conduction "law" in evidence? In short, are the following relations valid?

a. $$\eta = \frac{\sum_s m_e \nu_{es}}{e^2 n_e}$$

with n_e given by Eq.30 - ionization equilibrium at temperature of the electrons

and,

b. The compatibility relation

$$J = n_e e\left[3k(T_e - T_s)/m_s\right]^{\frac{1}{2}} \qquad \text{(Eq.42)}$$

4. What are the dominant modes of energy transfer? Is energy balance observed? What are the observed rates of temperature relaxation?

In answer:

1. The thermocouple probe radial tranverses shown in Fig.57 indicate that the neutral gas column preserves its exit column diameter and a flat temperature distribution to a remarkably long distance, in agreement with the simple analysis of Section 3.2. Because of the manner of gas injection into the column, $\dot{m}$ should also be uniformly distributed. Since it was impractical to determine mass flow rate in an arc environment for such low flow rates(e.g., use of pitot tube requires dynamic pressure measurement as low as 0.005 psi), a flow visualization method was employed to see if the flow was convergent or divergent and to see if there might be entrainment of the surrounding gas.

A photograph of such a study is shown in Fig.58 where smoke particles have been injected outside of the arc column. First, notice the clear-cut edge of the

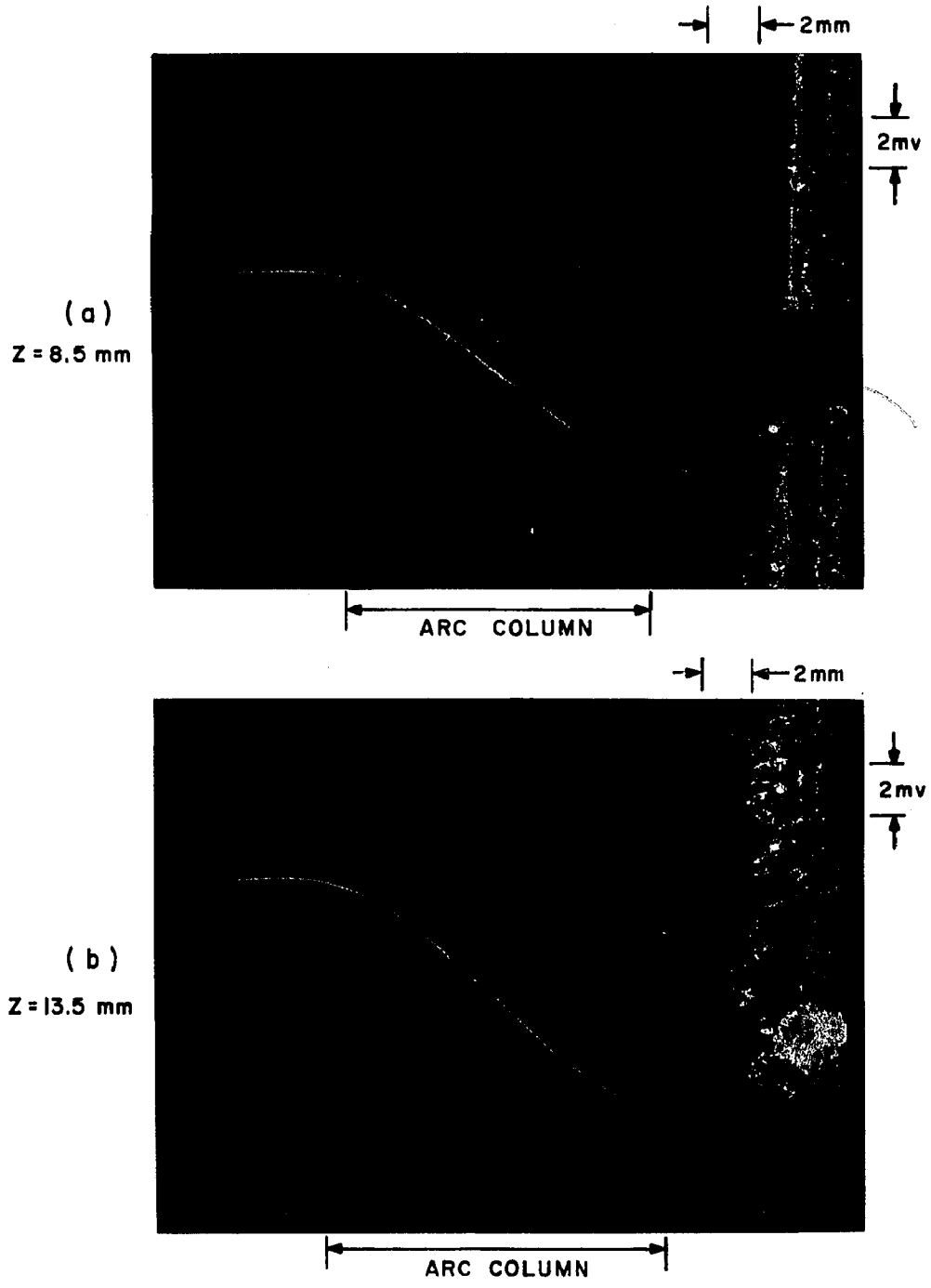

810H-312-0347
A-312-S-0163

FIG. 57 THERMOCOUPLE OUTPUTS vs. RADIAL TRAVERSE

Fig.58 Flow Field Visualization of Arc Column with Smoke Injection.

luminous column showing the arc in its first 1.5 cm to be perpendicular to the anode surface. The smoke stream just outside of the column widens slightly as it moves down stream, indicating the extent of viscous mixing layer. We feel that on the basis of such studies the zone along the arc axis up to 1.5 cm from the anode should be essentially that of a one-dimensional gas flow. Since visualizing a smoke stream is sometimes difficult under such a strong arc light(mostly from the equilibrium portion of the arc), fine powder of MgO which emits a characteristic green light has been found to be of help.

From the potential and current density probings we found the J distribution to be somewhat peaked away from the anode. Therefore, the electrons and the gas stream lines should be as sketched in Fig.59. The nonuniform nature of the J distribution is compensated by the following:

(a) J can be measured.

(b) In restricting the interpretation of data to the region near the axis, a locally one-dimensional change can still be assumed.

In the dark space the relative visual uniformity exhibited in Figs.44 and 45 indicates that the column

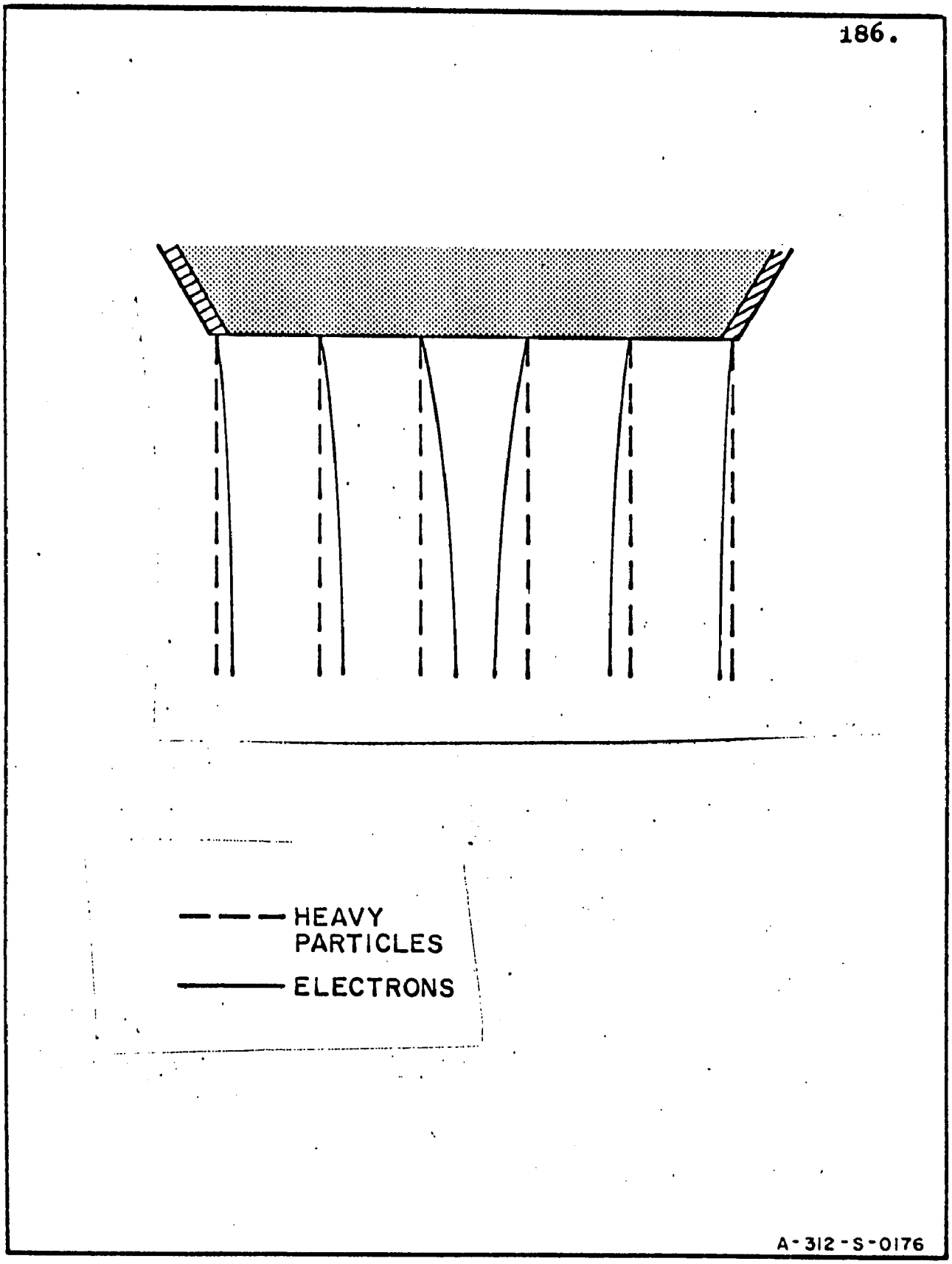

FIG. 59 SKETCH OF STREAMLINES OF AN ARC COLUMN

charge concentration is well-behaved. The streaks visible should be interpreted with the understanding that the arc light is largely due to continuum emission, and, hence varies as n_e^2. Thus, a 4 to 1 ratio in intensity is due to only a 2 to 1 ratio in n_e and a very small change in T_e. Granted that potential probe results often show fluctuations which might suggest the existence of small filaments of concentrated currents, possibly in local equilibrium with the gas. In view of Table 1, however, unless accompanied by large electric fields (Note: E was never observed to be more than 15 v/cm in any case, including those depicted in Fig.47) and by a temperature of at least 11000^{o}K(not evident), such filaments could not account for any but a tiny fraction of the total arc current. We feel confident, therefore, that the homogeneous streamtube approach of interpreting the data along the axis will be valid in these columns.

2. To one familiar with conventional "thermal" arcs, any reference to the subject most likely will evoke a vision of ultra high arc gas temperatures and intense arc luminosity. If, further, the question of local thermal equilibrium(LTE) is brought up, the statement that the arc was running at one atmosphere is generally all that is required to subdue initial doubt about LTE in such a discharge. Thus, just as the glow discharge at

low pressure has been accepted as a nonequilibrium(high T_e) and low thermal gas(low T_g) entity so the atmospheric pressure arc discharge has often been endowed with the properties of LTE and high enthalpy, as a matter of confidence. While these notions were supported by facts in most instances they are not the necessary conditions.

From a kinetic theory point of view, the requirement for any gaseous discharge is, first of all, the maintainance of a sufficient concentration of free electrons. The conductivity is then given by the general relation

$$\sigma(T_e) = n_e(T_e) \cdot \Theta(T_e)$$

where the second factor, $\Theta(T_e)$, is directly proportional to the free electron mobility and inversely proportional to the sum of collision frequencies,

$$\Theta(T_e)^{-1} \propto \nu_T = \nu_{ei} + \nu_{ea}$$

For the Coulomb part of the conductivity we see that, from Eq.37, in the first order,

$$\nu_{ei} \propto n_e T_e^{-3/2}$$

and therefore the Coulomb contribution is not sensitive to n_e,* and, increases with $T_e^{3/2}$.

The neutral contribution, however, from Eq.40, is

$$\nu_{ea} \propto n_a T_e^{3/2}$$

and this part is directly proportional to n_e/n_a but <u>decreases</u> with $T_e^{3/2}$. Thus, if n_e/n_a were arbitrarily "frozen" at a high level then σ would increase with T_e. Conversely, if n_e/n_a were frozen at a low level, σ would <u>decrease</u> with T_e. Intermediate between the two cases, σ would not be appreciably affected by T_e.

In low density discharges collisions are infrequent among the species and approximately frozen flows of electrons can in fact occur. So, in many instances, T_e may not be a particularly useful parameter for describing conductivity. In some cases T_e might not even exist.

In high pressure discharges, on the other hand, the existence of T_e is usually well founded. If the discharge is furthermore in LTE then equilibrium statistics(i.e. Eq.30) can be brought in to supply the value of n_e. For pure gases(e.g. H, He, Ne, Ar, etc.) poss-

*This is often considered to be the distinction between a "conductivity" and a "mobility" controlled discharge.

essing high ionization potentials, the n_e vs. T_e curve (e.g. see Fig.18) shows why thermal arcs usually do not exist under 7000°K.

The question of how a highly convectively-cooled arc column maintains its conductivity, therefore, boils down to how well the electrons are insulated from, but exist in the same volume as, the cool gas. Figures 55 and 56 indicate that the electrons having started from the cathode side with about 12000°K and then traversing a highly nonequilibrium 10 mm distance, are only cooled to about 9000°K. This unmistakable degree of insulation is the main reason for the ability of the column to carry current.

The high conductivities measured are quite above the computed values as shown in Fig.19. At higher temperatures the lower limits as indicated would result if the sharp peaks in J on the axis are smoothed off. Even then, this does not bring the conductivity completely in line with theory.

Very recently, Schweitzer and Mitchner* discussed the correction to the Spitzer and Härm conductivity when $\ln\Lambda$ is small, in accordance with the so-called unified

*Schweitzer, S. and Mitchner, M., AIAA J., 4, 1012-1019, (June, 1966).

theory*. The correction is indicated in Fig.60. Note that at $\ln\Lambda = 2.48$ the conductivity is infinite. When the correction is applied to our points at 12000°K ($\ln\Lambda = 3.8$) better agreement between theory and experiment is obtained.

3. Regarding the two-temperature conduction law, we see that Part(a) is verified for the first time in a high current arc discharge in pure gas. To discuss Part(b), we plot in Fig.61 the computed η as function of J and parametric in T_e and T_g. Also plotted are the experimental points of η vs E(the E lines in Fig.61 have -1 slope; those for E = 5, and 10 v/cm are shown). It is seen that Eq.42 is far from being met. To meet Eq.42 the arc current density and electric field must be about 10 times greater than observed.

It is clear that neither the J and E measured, nor the temperatures could have been subject to such large errors. We may conclude with some assurance that the relationship given by Eq.42 is invalid. This does not mean, however, that energy conservation is not observed - as will be seen in the following.

4. In the energy equation, Eq.27, the recombination

*Kihara,T. and Aono,O.,J.Phys.Soc.Japan, 18, 837-851, (1963).

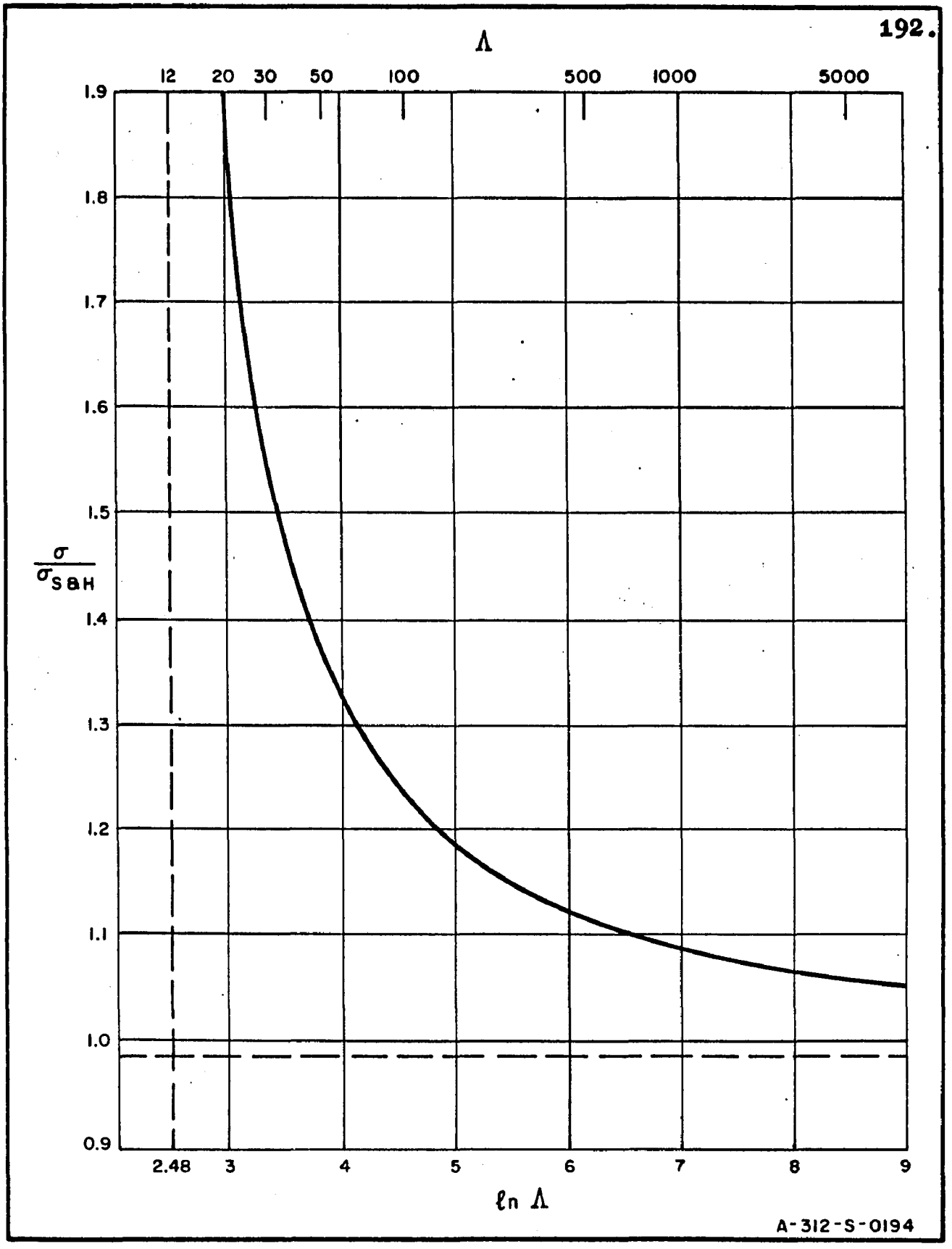

FIG. 60 ELECTRICAL CONDUCTIVITY CORRECTION ACCORDING TO SCHWEITZER AND MITCHNER

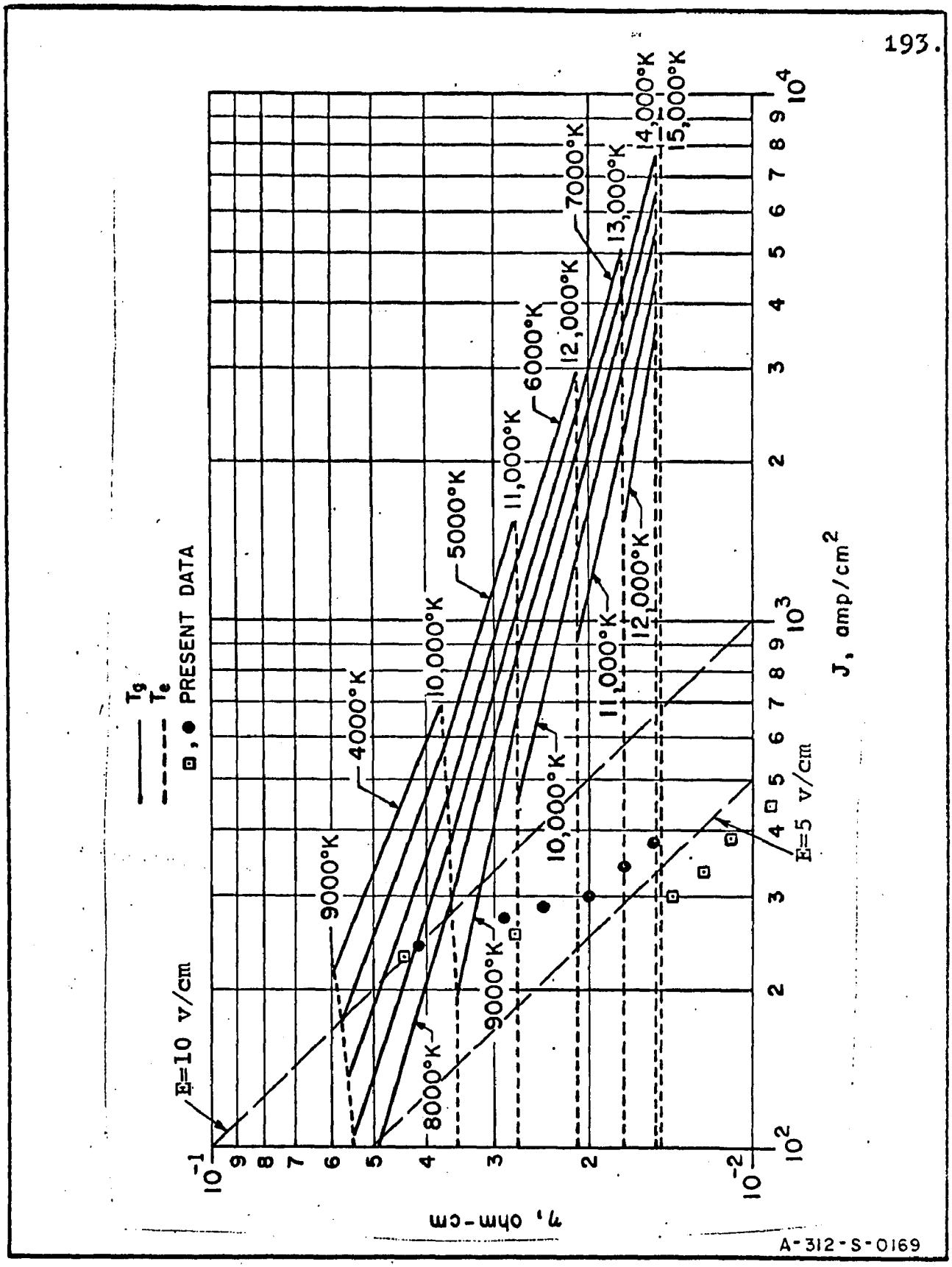

FIG. 61 ARGON RESISTIVITY vs. CURRENT DENSITY FOR A SIMPLE TWO-TEMPERATURE MODEL

term turns out to be quite insignificant since the ion flux from the anode is definitely limited by approximately the neutral gas velocity(the ion drift velocity due to E is much smaller) which is about 2000 cm/sec. From this, the maximum recombination in the entire arc may not be more than

$$e(n_i U_i A)_{anode} \approx 1.6\times10^{-19}\times10^{16}\times2000\times1$$
$$\approx 3.2 \text{ amp.}$$

Or, the total recombination power(max.):

$$3.2 \times 1.5 \cong 5 \text{ watt.}$$

The remaining terms on the left hand side of Eq.27 can also be seen to be negligible when the values of n_e, T_e as given in Figs.55, 56 are used.

Thus, we can say that either Eq.42 holds or energy balance will be grossly violated. The fact is, energy balance is closely satisfied because the convected energy of the gas,

$$p_g = \dot{m} \frac{dH}{dT_g} \frac{dT_g}{dz}$$

where $\frac{dH}{dT_g}$ is given by Fig.62, and the electrical energy input,

$$p_e = E\ J$$

as shown in Tables 6 and 7, are quite closely in agreement. Also tabulated are p_{ea} and p_{ei} from computations. We see that a good fraction of energy transfer from the electrons to the ions(and neutrals) can be accounted for by p_{ea}.

We must emphasize, the extremely large p_{ei} computed from theory is nowhere in evidence. From this we must conclude that the commonly used formula for p_{ei}(and ν_{ei}) appears to be invalid under present conditions.

Since reasonably good check is obtained for the conductivity, we further conclude that the collision frequencies appear to be different for momentum and for energy transfer. This is why Eq.42 is not satisfied because it is based on the same ν_{ei} for both types of transfer.

In reviewing the literature, we note that all existing theories for dense plasmas are only applicable to the order of the Debye screening theory(see Reference 53, p.73) while in the present setup(very low $\ln\Lambda$)

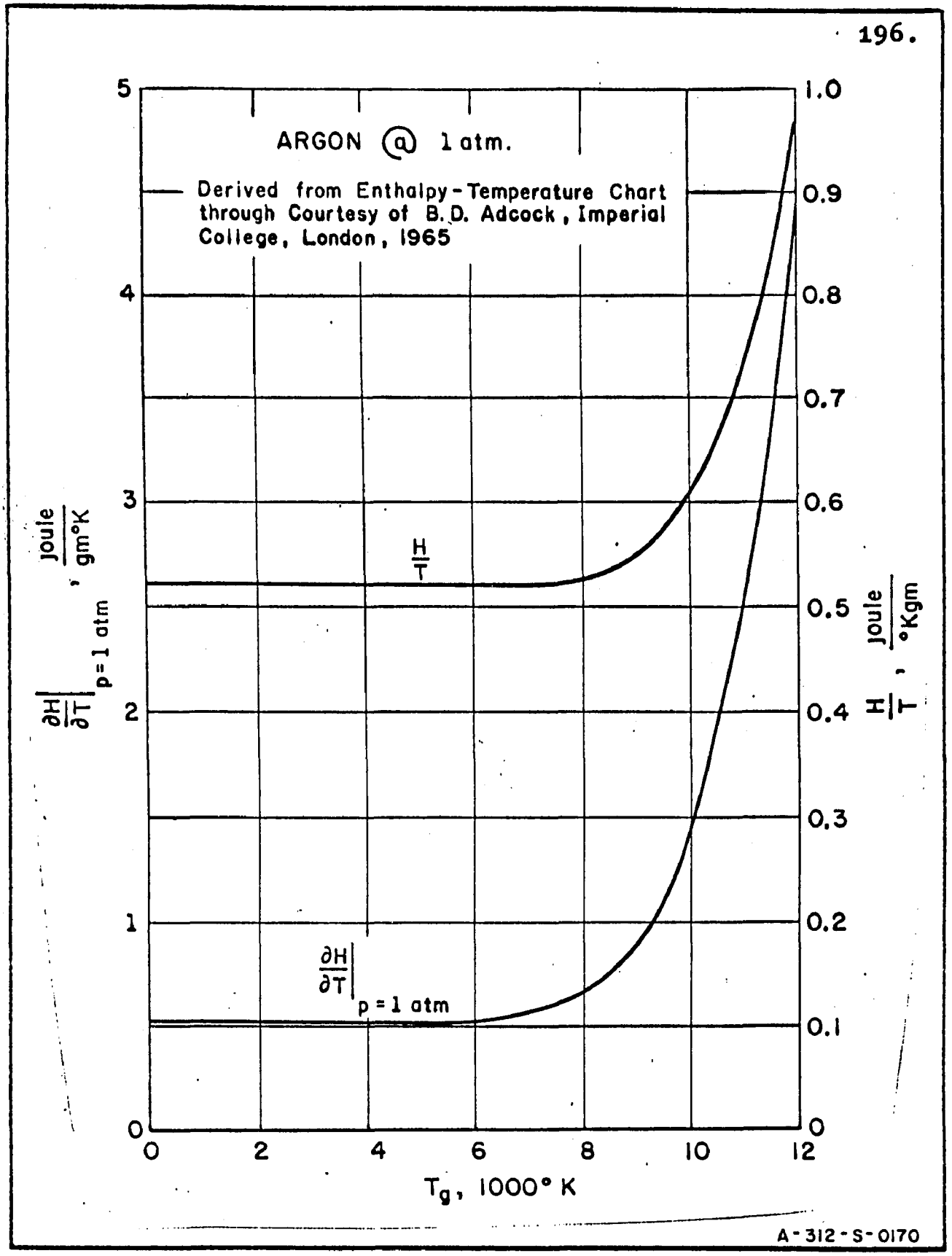

FIG. 62 ENTHALPY OF 1 ATM. ARGON

TABLE 6

Case I: 150 amp, 12.5 gm/min ($m = 0.2 \frac{gm}{cm^2\text{-sec}}$)

Z, mm	J, amp/cm^2	E, v/cm	T_e, 10^3 ^oK	T_g, 10^3 ^oK	dT_g/dZ, 10^3 ^oK/cm	$T_e - T_g$, 10^3 ^oK	n_e, 10^{16} cm^{-3}	n_a, 10^{18} cm^{-3}	P_g, kw/cm^3	P_e, kw/cm^3	P_{ea}, kw/cm^3	P_{ei}, kw/cm^3
1	220	10	9.25	5.0	17.5	4.3	0.7	1.42	1.82	2.2	0.610	2.33
2	260	7	9.75	6.6	13.2	3.2	1.2	1.08	1.58	1.82	0.660	4.7
3	280	4	10.25	7.7	11.3	2.4	2.0	0.92	1.43	1.12	0.760	8.25
4	320	4	10.5	8.8	10.0	1.7	2.5	0.81	1.66	1.28	0.620	8.0
5	350	4	10.9	9.7	8.3	1.2	3.5	0.73	1.95	1.4	0.590	9.1
6	375	4	11.2	10.4	5.5	0.8	4.3	0.71	1.98	1.5	0.495	8.25
7	400	4	11.3	10.8	3.3	0.5	4.6	0.68	1.52	1.6	0.321	5.6
8	425	4	11.3	11.1	2.0	0.2	4.6	0.66	1.07	1.7	0.125	2.3
9	440	4.4	11.3	11.2	1.3	0.1	4.6	0.66	0.76	1.93	0.062	1.2
10	470	4.5	11.3	11.3	0.8	0	4.6	0.65	0.47	2.03	0	0

COMPARISON OF MEASURED AND COMPUTED QUANTITIES

TABLE 7

Case II: 150 amp, 21.5 gm/min ($m = 0.35 \frac{gm}{cm^2\text{-sec}}$)

Z, mm	J, amp/cm^2	E, v/cm	T_e, 10^3 ^oK	T_g, 10^3 ^oK	dT_g/dZ, 10^3 ^oK/cm	$T_e - T_g$, 10^3 ^oK	n_e, 10^{16} cm^{-3}	n_a, 10^{18} cm^{-3}	P_g, kw/cm^3	P_e, kw/cm^3	P_{ea}, kw/cm^3	P_{ei}, kw/cm^3
1	250	10.5	8.8	3.0	11.4	5.8	0.44	2.46	2.04	2.63	0.83	1.31
2	265	9	9.1	4.2	11.0	4.9	0.6	1.75	2.0	2.39	0.72	2.0
3	275	8	9.4	5.3	10.8	4.1	0.84	1.39	1.96	2.2	0.71	3.12
4	290	6.5	9.7	6.3	10.25	3.4	1.15	1.17	1.87	1.89	0.71	4.6
5	320	5.8	10.0	7.4	10.0	2.6	1.55	0.995	2.1	1.86	0.66	6.13
6	330	6	10.3	8.3	9.35	2.0	2.1	0.89	2.39	1.98	0.65	8.25
7	345	6.5	10.5	9.2	9.3	1.3	2.5	0.8	3.12	2.24	0.47	7.4
8	370	6.5	10.75	10.2	7.8	0.55	3.0	0.72	4.45	2.4	0.22	4.3
9	400	6.5	10.9	10.8	4.6	0.1	3.5	0.68	3.7	2.6	0.05	1.44
10	420	6.5	11.1	11.1	2.3	0	4.0	0.66	2.14	2.73	0	0

COMPARISON OF MEASURED AND COMPUTED QUANTITIES

the number of electrons in a Debye sphere(see Fig.1) is as low as about 3. It would seem, the concept of screening loses validity and the encounter of an electron with an ion becomes much more complicated. Present results indicate that the ions are energetically rather well insulated from the electrons.

The electron-ion energy relaxation rate has been checked as a link in shock ionization of argon in the shock-tube work by Petschek and Byron(Reference 45). In that case, however, the energy transfer is from the ions to the electrons. It might not be directly comparable with the present case - even though the usual theory gives the same rate for both directions.

Dougal and Goldstein(Reference 19) employed microwave techniques to the study of electron-ion energy relaxation in low pressure afterglows. The agreement with theory is better than one order of magnitude. Significantly, they too observe noticeably longer relaxation time for the run with the lowest n_D.

For noble gas seeded with alkali metal vapor, the two-temperature model of electron conduction appears to have been confirmed(see, e.g. Reference 14). However, because of the usual low temperature(3000^{o}K), low seed concentration(0.005) and low n_e/n_a, even at $n_e = 10^{15}$ cm^{-3}, Coulomb collisions are secondary to electron-atom

collisions, and, no definite conclusion can be drawn as to the correctness of the Coulomb rates.

Chapter 7

CONCLUSION AND RECOMMENDATIONS

A. The postulated forced-convection-dominated, quasi one-dimensional arc column has, within a good approximation, been realized in a reasonably large region and verified by the experiments. In particular, this has permitted the steady-state measurement of the rates of energy equilibration among the nonequilibrium species.

B. The departure from local thermal equilibrium is shown to be significant and appears to follow the two-temperature(displaced Maxwellian distribution) model. The energy flows from the applied electric field to the electron gas and is then volume-transferred to the heavy particles through which it is finally convected down stream.

C. Present data indicate that the volume rate of energy transfer by electron-ion collision is considerably weaker than is commonly accepted. This weak coupling observed explains the case with which high degree of electron-heavy particle nonequilibrium can occur even in a dense arc discharge. Since existence of LTE has often been theoretically established on the basis of commonly accepted formulas, a re-examination of the

numerical criteria based on these formulas seems indicated.

In the present work, the theoretical electron-atom equilibration rate for argon, based on the Engelhardt and Phelps reduction, accounts for up to 50% of total of the experimental values. This can be quite different from that computed from a hard-sphere model - as has been done in the past.

D. Cross checking of experimental evidence confirms the essential correctness of the various techniques. This should lend more confidence to the use of transient probe techniques for dense plasmas.

E. In looking ahead, several interesting extensions of this research may be recommended:

(1) The same basic experimental setup may be applied to the study of other relaxation phenomena, as for example, electronic excitation of atoms or molecules.

(2) In the dark space some population inversion in the excited states must exist. This region therefore could conceivably be used to generate laser action. Because of the geometrical configuration, it appears that such a laser may indeed not possess optimum efficiency, but,

by the same token, it offers diagnostic conveniences that could further understanding of the laser mechanism at one end, and of energy transfer in plasma at the other end.

(3) Because many plasmas of engineering importance lie in the low $\ln\Lambda$ region, an appropriate plasma kinetic theory should be developed. This problem may not be easy. The number of interacting charged particles at any instant is neither just two nor infinitely many but a thorny "few" - enough to require solution of the many-body problem. On the other hand,it is inviting to design a scheme of generating nonequilibrium plasma of even lower $\ln\Lambda$ and to see if the electron-ion interaction actually approaches zero(superconducting) in the limit.

APPENDIX A*

PROOF THAT E IS RADIALLY INVARIANT

From the Maxwell equations for steady state, one obtains:

$$\nabla\cdot\vec{J} = 0$$

$$\nabla\cdot\vec{E} = \epsilon_o^{-1}(n_i - n_e)e$$

From $\vec{J} = \sigma(T)\cdot\vec{E}$, and the above equations:

$$\nabla\cdot\vec{J} = \nabla\cdot(\sigma(T)\vec{E})$$

$$= \sigma(T)\,\nabla\cdot\vec{E} + \vec{E}\cdot\nabla\,\sigma(T)$$

$$= \epsilon_o^{-1}\,\sigma(T)(n_i - n_e)e + \frac{d\,\sigma(T)}{dT}\vec{E}\cdot\nabla T = 0$$

Hence,

$$\vec{E}\cdot\nabla T = -(n_i - n_e)e \Big/ \epsilon_o \frac{d}{dT}(\ln \sigma(T))$$

When there is charge neutrality, the right side is zero and the electric field is orthogonal to the temperature gradient. In a fully developed column ∇T is radial. Hence, $\vec{E}$ must be axial, and radially invariant ($\because \nabla\times\vec{E}=0$).

* This derivation was apparently first shown by Thiene, P.G. in AFOSR-TN-59-947, Plasmadyne Corp. (25 Aug., 1959).

APPENDIX B

SPECTROGRAPHIC EVIDENCE*

Interesting confirmatory evidence for some of the conclusions reached in this study may be seen in spectrograms taken of an argon FTA positive column under conditions quite similar to those used in this study. Figure B1 shows a portion of the spectrum emitted by a thin axial increment(0.1mm) of the positive column at a distance of 12.7 mm from the anode. The Abel inversion of a chordal scan of the 6965Å line intensity showed the gas temperature in this volume element to be 9650°K, while the continuum intensity at 5000Å indicated an electron temperature a few hundred degrees higher.

An impressive qualitative feature of the spectrogram is the unusually high continuum intensity relative to the line intensities in this region. The appearance is more characteristic of argon arcs at high pressures than of a 1 atm. argon arc. The continuum arises mainly from electron-ion encounters of two types, namely free-free(Brehmstrahlung) and free-bound transitions (Kramers' radiation). Both types are proportional to the charged particle number density.

The appearance of the spectrum therefore implies

*From unpublished data supplied by C.Sheer.

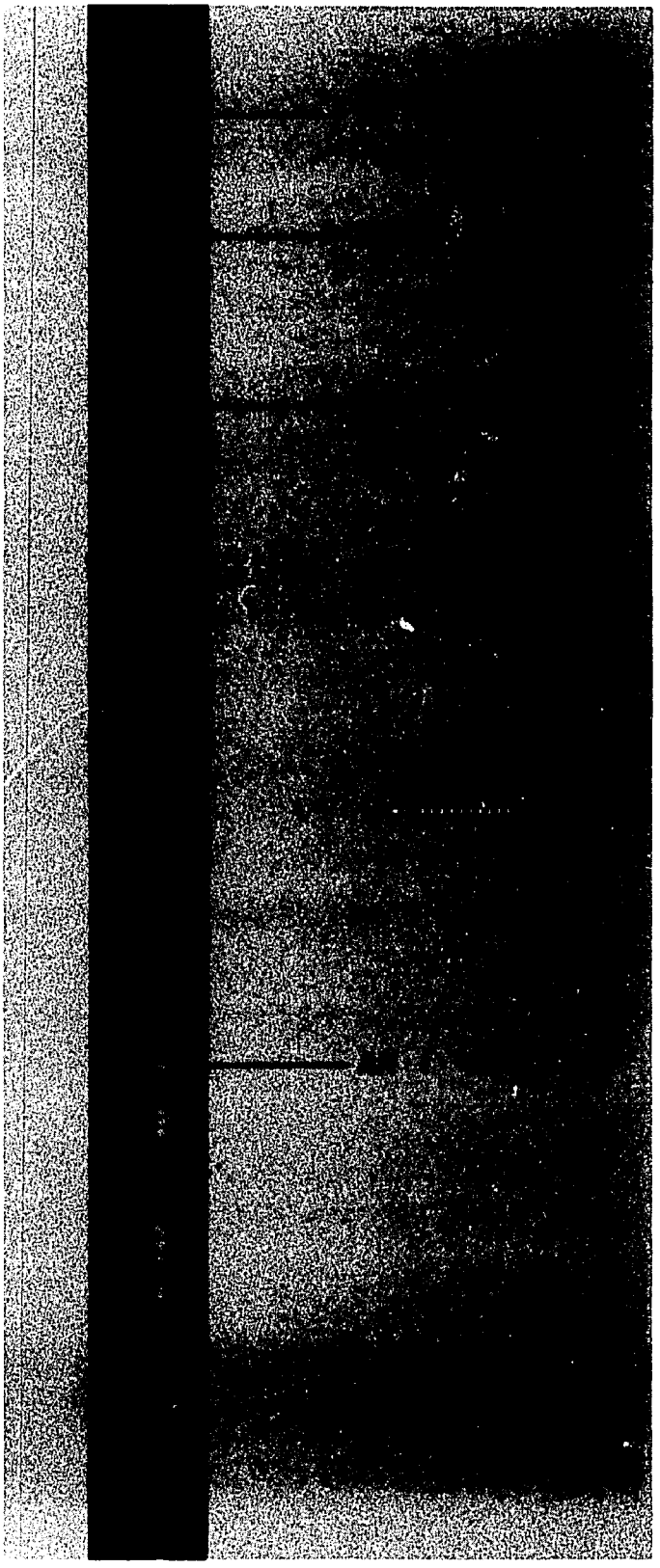

Fig.B1

an abnormally high electron(ion) density. This is borne out by calculating the ratio of the ion to neutral atom densities from the ratio of intensities of selected ion and neutral lines(marked in Fig.B1). The lines selected were among those of the argon spectrum for which the transition probabilities and other spectroscopic constants are known. The results of two such calculations showed the charged particle density to be some five times greater than predicted from the measured temperature. This tends to confirm the abnormally high electrical conductivity as reported in this dissertation.

APPENDIX C

VOLUME IONIZATION OF ARGON BY ELECTRON IMPACT

For a Maxwellian electron gas the speed distribution is a Rayleigh distribution:

$$f^s(c) = \frac{4n_e}{\sqrt{\pi}} \frac{c^2}{\bar{c}^2} \exp(-c^2/\bar{c}^2)$$

where $\bar{c}^2 = 2kT_e/m_e$ and c = speed of electron.

If $Q_i(c)$ is the ionization cross section of argon by electron impact, then, since the motion of argon atoms is negligible compared with that of the electrons, the rate of ionization in a unit volume is:

$$\Gamma_i = \int_0^\infty n_a \, c \, Q_i(c) \, f^s(c) \, dc$$

$$= \frac{4n_e n_a}{\sqrt{\pi}} \int_0^\infty Q_i(c) \left(\frac{c}{\bar{c}}\right) \exp-(c/\bar{c})^2 \, d\frac{c}{\bar{c}}$$

(Eq.C1)

For argon, the experimentally determined $Q_i(c)$ * can be represented by:

$$Q_i = 0 \qquad , \quad c^2 < E_i/B$$

*Brown,S.C., Basic Data of Plasma Physics, Technology Press of MIT - Wiley(1959), p 110.

$$Q_i = A(Bc^2 - E_i),\ cm^2 \quad ,\ c^2 \geqslant E_i/B \qquad \text{(Eq.C2)}$$

where $A = 27\times10^{-18}$

$B = 2.85\times10^{-16}$

$E_i = 15.755$

When Eq.C2 is inserted into Eq.C1 and the lower limit of integration properly taken care of, then Γ_i can be evaluated analytically by using the relations:

$$\int_x^\infty u^3\, e^{-u^2} du = \tfrac{1}{2}(x^2+1)e^{-x^2}$$

and

$$\int_x^\infty u^5\, e^{-u^2} du = (\tfrac{1}{2}x^4+x^2+1)e^{-x^2} \ .$$

As a result,

$$\Gamma_i = \frac{4n_a n_e AB\bar{c}}{\sqrt{\pi}}\left[\frac{E_i}{2B} + \bar{c}^2\right]e^{-E_i/B\bar{c}^2} \ ,cm^{-3}sec^{-1} \qquad \text{(Eq.C3)}$$

Note that Eq.C3 can be used to evaluate the rate of any collision process, e.g. electronic excitation of atoms, whose cross section may be approximated by the form given in Eq.C2.

APPENDIX D

BASIC CONSIDERATION OF TRANSIENT THERMOCOUPLE PROBE

Basically, all temperature probes are governed by heat transfer to and from the probe body, as schematically shown in Fig.D1. In steady-state probing, the probe temperature attains a value, $(T_p)_\infty$, which is generally different from the true hot gas temperature, T_g. This difference is accounted for by heat balance at the probe, involving conduction across the boundary layer and along the thermocouple wires and support, convection(since in general the hot gas is in motion with respect to the probe), and radiation interchange at the probe surface. A properly designed steady-state probe minimizes the boundary layer thermal resistance, $R_f = (hA)^{-1}$, and maximizes the conduction loss thermal resistance, R_o, along the thermocouple stem. In addition, radiative exchanges may be reduced by means of radiation shields. In practice, the various transfer coefficients from which the thermal resistances are evaluated are needed only to give small corrections and exact knowledge of these factors is generally unnecessary.

In contrast, referring to Fig.D2, transient probing of a high temperature gas requires the withdrawal of the probe at some time t_2, at which T_p is still

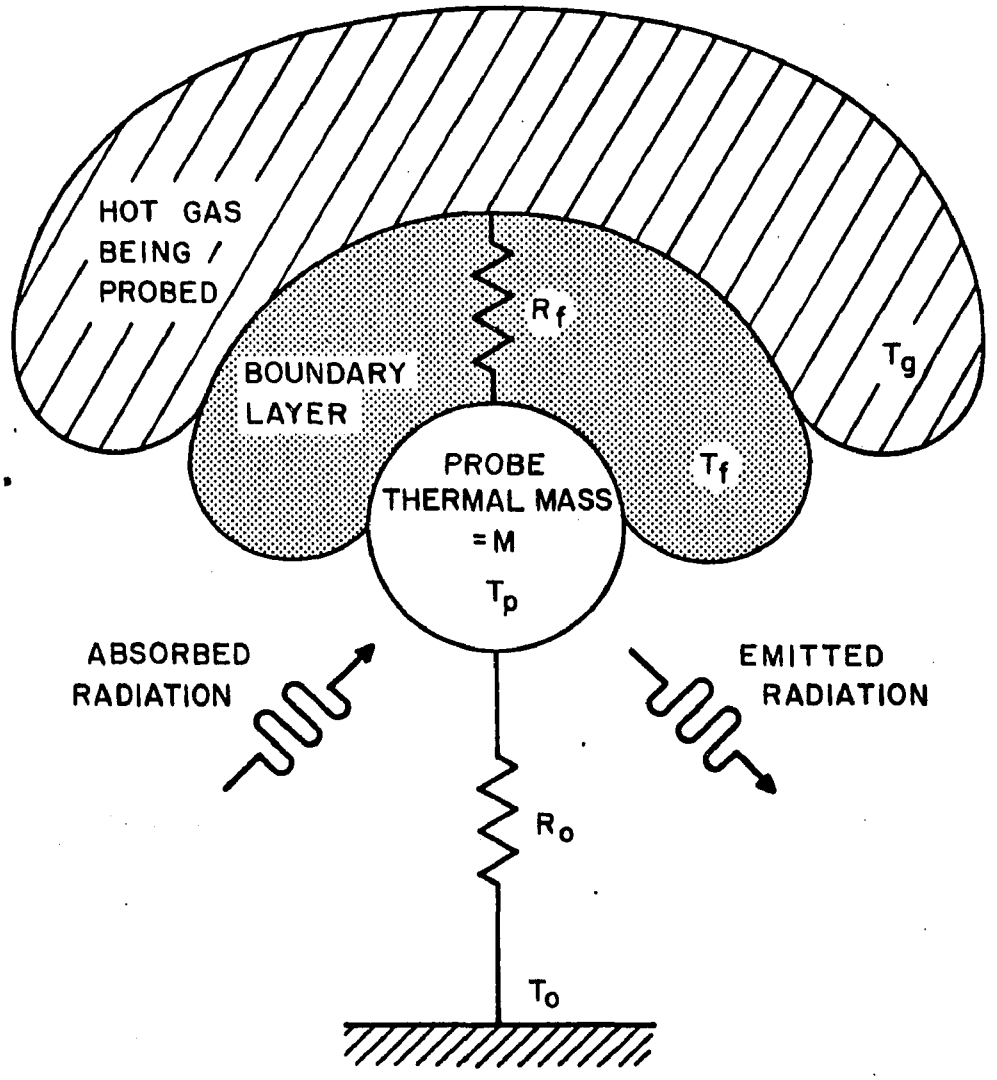

FIG. D1 SCHEMATIC REPRESENTATION OF HEAT TRANSFER BETWEEN PROBE AND ENVIRONMENT.

DRAWN | CHECKED | APPROVED

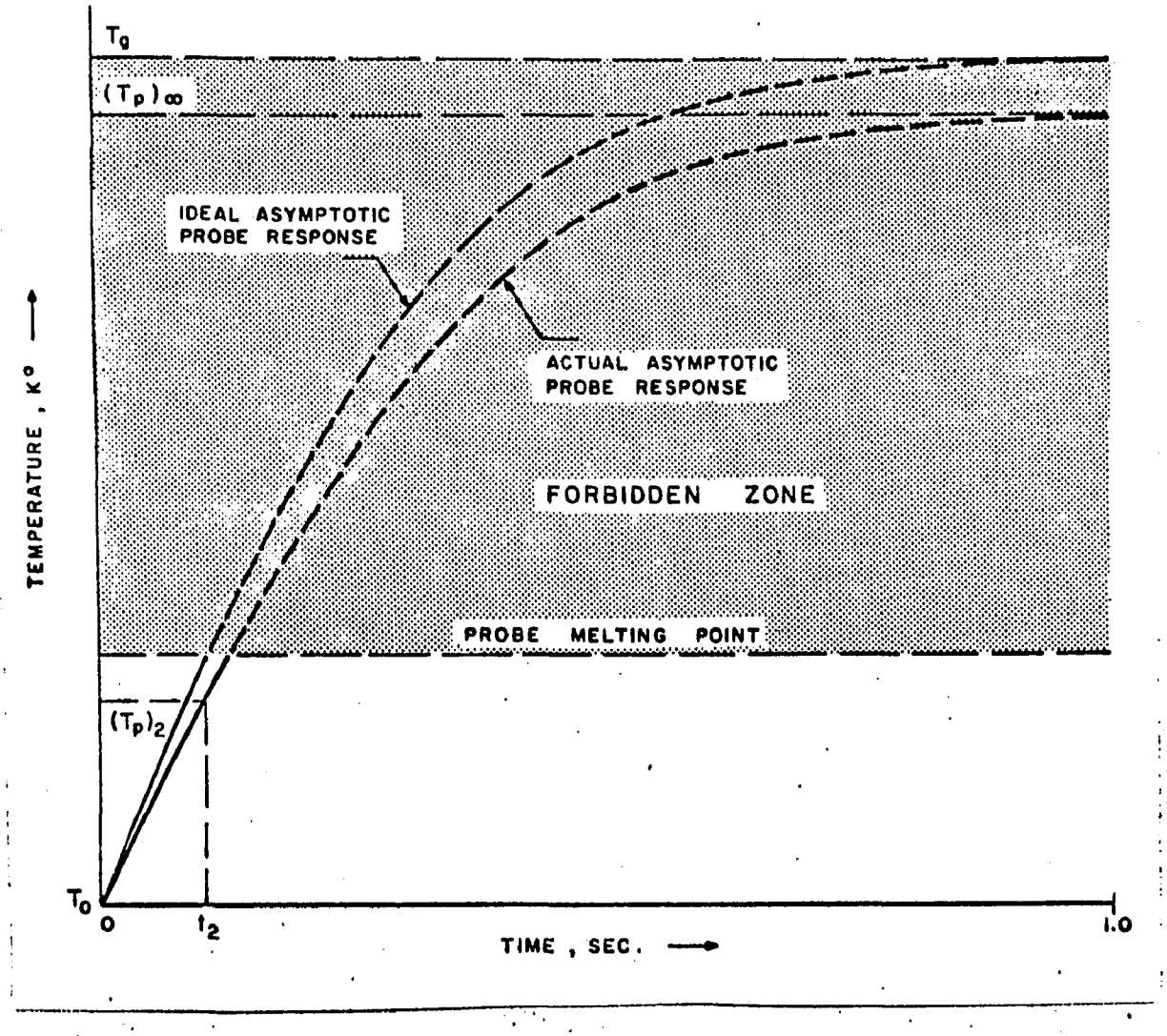

FIG. D2 IDEAL AND ACTUAL PROBE RESPONSE CURVES

sufficiently low to avoid thermal destruction; this defines the boundary of the large forbidden zone which cannot be utilized. To extract temperature information from such a limited probe history, the transfer coefficients assume paramount importance. It is therefore unavoidable that, in the transient measurement, the probe is used primarily as a heat-flux gauge.

If the material of the probe tip has sufficiently high thermal diffusivity that we may assume isothermal conditions to prevail at an instant, then we may relate the gas temperature, T_g, to the probe temperature, T_p, by means of the heat transfer equation in the following form:

$$\frac{T_g}{R_f} = M\frac{dT_p}{dt} + \left(\frac{1}{R_f} + \frac{1}{R_o}\right)T_p - \frac{T_o}{R_o} + \text{Radiative Transfer} \qquad \text{(Eq.D1)}$$

By using long slender lead wires and insulator, the conduction heat loss along the probe stem can be made negligible, so that Eq.D1 reduces to:

$$T_g = R_f M \frac{dT_p}{dt} + T_p + R_f(\text{Radiative Transfer}) \qquad \text{(Eq.D2)}$$

Equation D2 shows that T_g may be deduced from the meas-

ured quantitites, T_p and dT_p/dt, if the thermal resistance of the boundary layer, R_f, the thermal mass of the probe, M, and the radiative heat transfer are known. The radiative transfer term is usually made negligible by the use of a radiation shield. Since this would add undesired bulk to the probe and defeat one of the prime objectives of probe miniaturization, the use of a shield was not considered in this application. At moderate pressures($\sim$1 atm) and within the temperature range investigated(3000 to 12000^{o}K) the radiative heat transfer is nearly always minor compared to the convective heat transfer. This may be due in part to the low absorptivity of the platinum probe. In any case, examination of experimental probe outputs shows that, under most of the conditions prevailing, the radiation term may be neglected.

The thermal mass, M, is readily available from the probe dimensions, density and specific heat, all of which are accurately known for the probe material(Pt) used. The quantity of importance in determining T_g from Eq.D2 is R_f(or the heat transfer coefficient of the boundary layer, h). It is apparent that in deducing T_g with the aid of Eq.D2 we are using the probe to measure absolute heat flux. The infrequent use of heat flux gauges for obtaining gas temperatures is perhaps a reflec-

tion of the general state of uncertainty in the knowledge of h. As was shown in this research it is not always the case, and under appropriate conditions, the transient thermocouple probe may be used as a heat flux gauge to measure plasma temperature with acceptable precision and speed.

Because of our initial uncertainty as to the validity of estimating the required values of h, in the first application of the transient thermocouple probe, it was used to measure the ratio of the heat flux at two successive instants of time during its immersion in the plasma. Thus, neglecting the radiation term we have

$$T_g = (R_f M)_1 (\dot{T}_p)_1 + (T_p)_1 \qquad \text{(Eq.D3)}$$

$$T_g = (R_f M)_2 (\dot{T}_p)_2 + (T_p)_2 \qquad \text{(Eq.D4)}$$

where the subscripts, 1 and 2 denote two successive times on the probe response curve, e.g., just after insertion and just before withdrawal, respectively. Solving Eq.D3 and Eq.D4 for T_g, we obtain:

$$\dot{T}_g = \frac{K_{12} \frac{(\dot{T}_p)_1}{(\dot{T}_p)_2} (T_p)_2}{K_{12} \frac{(\dot{T}_p)_1}{(\dot{T}_p)_2} - 1} \qquad \text{(Eq.D6)}$$

$$= (T_p)_2 \frac{z}{z-1} \qquad \text{(Eq.D6)}$$

where $z = K_{12}(\dot{T}_p)_1/(\dot{T}_p)_2 = T_g/(T_g-(T_p)_2)$. It is evident that z is the critical parameter in the determination of T_g. This may be emphasized by taking the variation of T_g with respect to z, arriving at

$$-\frac{\Delta T_g/T_g}{\Delta z/z} = \frac{1}{z-1} .$$

The result is shown in Fig.D3 with $-(\Delta T_g/T_g)/(\Delta z/z)$ (appropriately labelled the "error amplification", E_z) plotted against $(T_p)_2/T_{ref}$ and parametric with T_g/T_{ref}, T_{ref} being any convenient reference number in ^oK. Since we have made $(T_p)_1 = 0$, $(T_p)_2$ represents the temperature difference (call it Δ_{12}) between the two instants of time at which the measurements are taken. We see then, that, at small $(T_p)_2$, i.e. at small Δ_{12}, errors in z are amplified much more than at large $(T_p)_2$. In fact, $\lim_{\Delta_{12}\to 0}(E_z) = \infty$, and $\lim_{\Delta_{12}\to T_g}(E_z) = 0$. It is not surprising that as more of the forbidden zone is opened up for data taking the determination of T_g becomes correspondingly more accurate. It is important to note that E_z is a figure of demerit of the flux ratio process of

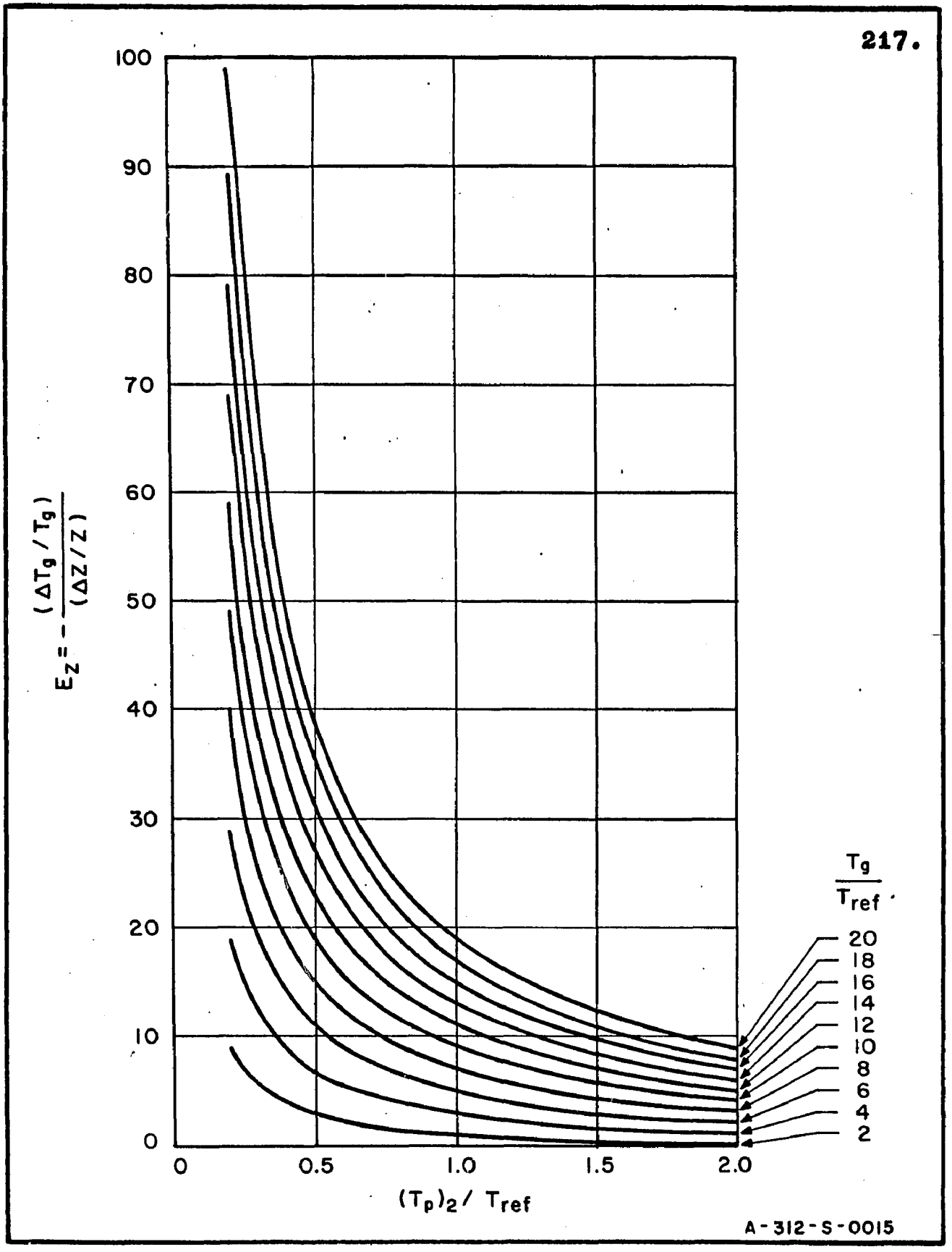

FIG. D3 ERROR AMPLIFICATION FACTOR VS. MAXIMUM PROBE TEMPERATURE FOR VARIOUS GAS TEMPERATURES.

data reduction and because it ranges from 0 to ∞ the accuracy of the flux ratio method can be either more or less than that of the absolute flux method. To locate the break-even point, let $\Delta(R_f, M, \dot{T}_p)$ be the combined error in $R_f M \dot{T}_p$ in Eq.D2 and, the temperature error, for the absolute case

$$\left.\frac{\Delta T_g}{T_g}\right|_{abs} = \frac{\Delta(R_f, M, \dot{T}_p)}{R_f M \dot{T}_p} = \epsilon$$

Now,

$$z = \frac{(R_f M \dot{T}_p)_1}{(R_f M \dot{T}_p)_2}$$

and, at best

$$\frac{\Delta z}{z} = \epsilon$$

whence we gather that when E_z is somewhat less than unity the two methods will have comparable accuracy. Admittedly, this does not include the effects of radiation error but this can be shown to degrade the ratio method even further at the transition point. Therefore, to favor the ratio method a little, we take $E_z = 1$, which makes $z = 2$, and observe from Eq.D6 that

$$(T_p)_2 = \tfrac{1}{2}(T_g)$$

represents the dividing point.

Thus, as far as transient thermocouple probes are concerned, the proper domain of the absolute flux method(i.e., data reduction by Eq.D2) is above twice the melting point of the probe material. On the other hand, some advantage is gained by using the flux ratio method(Eq.D5) in the domain between the probe melting point and twice this value. It therefore follows that the absolute flux method, which involves the simplest data reduction process, is in fact the preferred method od measurement over almost the entire temperature range of interest(3000 to 12000^{o}K). Of course, at very high temperature, e.g., $>$ 12000^{o}K, a practical upper limit is imposed on the absolute flux method by the fact that energy transfer processes become increasingly complex in this range and are presently not well understood.

REFERENCES

(1) Ahtye,W.F., NASA TN D-2611(Jan.,1965).

(2) Allis,W.P., "Motions of Ions and Electrons", Encyclopaedia of Physics, Vol.21, Springer-Verlag(1956).

(3) Amdur,I. and Mason,E.A., Phys.Fluids, 1, No.5, 370-383(Sept.-Oct.,1958).

(4) Biondi,M.A., Atomic Collision Processes, McDowell, M.R.C., Editor, Wiley(1964), pp 491-509.

(5) Bond,J.W.jr., Las Alamos Sci.Lab.Rept. LA-1693 (July 1, 1954).

(6) Bott,J.F., Phys.Fluids, 9, No.8, 1540-1547(Aug., 1966).

(7) Boulegue,G. et al, Proc. 2nd. United Nations International Conf. on Peaceful Uses of Atomic Energy, Vol.31(1958), p 242.

(8) Brown,S.C., Basic Data of Plasma Physics, Technology Press of MIT - Wiley(1959).

(9) Byron,S., Stabler,R.C. and Bortz,P.I., Phys.Rev. Letters, 8, No.9, 376-379(May 1, 1962).

(10) Cahn,J.H., Phys.Rev., 75, No.2, 293-300(1949).

(11) Chapman,S. and Cowling,T.G., The Mathematical Theory of Non-uniform Gases, Cambridge Univ. Press(1952).

(12) Chen,C.J., Tech.Rept.No.32-707, Jet Propulsion Lab., California Inst. of Tech.(Dec. 30, 1964).

(13) Cohen,I.M., Phys.Fluids, 6, No.10, 1492-1499(1963).

(14) Cool,T.A. and Zukoski,E.E., Phys.Fluids, 9, No.4, 780-796(April,1966).

(15) D'Angelo,N., Phys.Rev., 121, No.2, 505-507(Jan.15, 1961).

(16) Delcroix,J.-L., Introduction to the Theory of Ionized Gases, Interscience(1960).

(17) DeVoto,R.S., Rept.No.SU AA217, Inst. for Plasma Research, Stanford Univ.(Feb.,1965).

(18) Denbigh,K., The Principles of Chemical Equilibrium", Cambridge Univ. Press(1964).

(19) Dougal,A.A. and Goldstein,L., Phys.Rev., 2nd.Ser., 109, No.3, 615-624(Feb.1, 1958).

(20) Emmons,H.W., Modern Developments in Heat Transfer, Ibelle,W., Editor, Academic Press(1963), p401.

(21) ———, Tech.Rept.No.23, Engineering Sciences Lab., Harvard Univ.(Dec.,1965).

(22) ———, and Land,R.I., Phys.Fluids, 5, No.12, 1489-1500(Dec.,1962).

(23) Finkelnburg,W. and Maecker,H., "Electric Arc and Thermal Plasma", Encyclopaedia of Physics , Vol.22, Springer-Verlag(1956).

(24) Grey,J., Jacobs,P.F. and Sherman,M.P., Rev.Sci. Instr., 33, No.7, 738-741(1962).

(25) ——, and Jacobs,P.F., AIAA 3rd Aerospace Sci. Meeting, Paper No.66-73(1966).

(26) Griem,H.R., Plasma Spectroscopy, McGraw-Hill(1964).

(27) Gryzinski,M., Phys.Rev., 115, No.2, 374-383(July 15, 1959).

(28) Gusinow,M.A., Gerardo,J.B. and Verdeyen,J.T., Phys.Rev., 149, No.1, 91-96(9 Sept.,1966).

(29) Handbook of Chemistry and Physics, Chemical Rubber Publishing Co.

(30) Hasted,J.B., Physics of Atomic Collisions, Butterworths(1964), p 54.

(31) Hirschfelder,J.O., Curtis,C.F. and Bird,R.B., Molecular Theory of Gases and Liquids, Wiley (1954).

(32) Kerrebrock,J.L., Engineering Aspects of Magneto-hydrodynamics, Mannal and Mather, Editors, Columbia Univ.Press(1962).

(33) Kramers,H.A., Phil.Mag., 6th.Ser., 46, 836-871 (1923).

(34) Kutateladze,S.S. and Borishanskii,V.M., A Concise Encyclopedia of Heat Transfer, Pergamon Press (1965), p 138.

(35) Langmuir,I. and Mott-Smith,H.M., General Electric Rev., 27, 499, 538, 616, 762, 810(1924).

(36) Lin,S.C., Resler,E.L. and Kantrowitz,A., J.Appl. Phys., 26, 95-109(1955).

(37) Loeb,L.B., Basic Processes of Gaseous Electronics, Univ.of California Press, Berkeley(1960).

(38) Lyman,F.A., AIAA J., 4, No.6, 1128-1130(June,1966).

(39) Morris,J.C., Bach,G.R. and Yos,J.M., ARL Rept. 64-180, Aerospace Research Labs.(Oct.,1964).

(40) Morse,T.F., Phys.Fluids, 6, No.10, 1420-1427(1963).

(41) Nestor,O.H. and Olsen,H.N., Soc.Ind.and Appl.Math., 2, 200-207(1960).

(42) Pai,S.-I., Viscous Flow Theory, Vol.I. Laminar Flow, Van Nostrand(1956).

(43) Pain,H.J. and Smy,P.R., J.Fluid Mech., 9, 390 (1960).

(44) ——,—— and ——,——, J.Fluid Mech., 10, 51 (1961).

(45) Petschek,H. and Byron,S., Annals of Physics, 1, 270-315(1957).

(46) Plasma Jet Technology, NASA SP-5033(Oct.,1965).

(47) Prandtl,L. and Tietjens,O.G., Fundamentals of Hydro- and Aeromechanics, Dover(1957), p 151.

(48) Raezer,S.D. and Olsen,H.L., Temperature Its Measurement and Control in Science and Industry, Vol.3, Part 2, Reinhold Publ.Co.(1962),p901.

(49) Rose,D.J. and Clark,M.jr., Plasmas and Thermonuclear Fusion, Wiley(1961), p 158.

(50) Sheer,C., Cooney,J.A. and Rothacker,D.L., AIAA J., 2, 483-489(1964).

(51) ———, et al, Tech.Note No.1, Vitro Laboratories (June 16, 1961).

(52) ———, Kennedy,J.M. and Tschang,P.S., ARL Rept. 63-150, Aerospace Research Labs.(Aug.,1963).

(53) Spitzer,L.jr., Physics of Fully Ionized Gases, Interscience(1956), p 78.

(54) ————, and Härm,R., Phys.Rev., 89, 977-981(1953).

(55) Stine,H.A. and Watson,V.R., NASA TN D-1331(Aug., 1962).

(56) Su,C.H. and Lam,S.H., Phys.Fluids, 6, No.10,

1479-1491(1963).

(57) Tannenbaum,B.S., Tech.Memo.T-453, Research Div., Raytheon Co.(March 21, 1963).

(58) Temme,M.I. and Giedt,W.H., ARL Rept.174, Aerospace Research Labs.(Dec.,1961).

(59) Tolman,R.C., Principles of Statistical Mechanics, Oxford Univ.Press(1938), p 95.

(60) Tschang,P.S., AIAA J., 3, 849-852(1965).

(61) ————, ARL Rept.65-95, Aerospace Research Labs. (May,1965).

(62) ————, "Measurement of plasma temperature by transient thermocouple probe", 130th.meeting of the Electrochemical Society, Philadelphia, Oct.9-14, 1966(Abstract No.220).

(63) Unsöld,von A., Annalen der Physik, 33, 607-616 (1938).

(64) Vlasov,A.A., Many-Particle Theory and its Application to Plasma, Gordon & Breach, New York (1961), p 374. Original Russian, 1950.

VITA

Pin-Seng Tschang was born in , on . He graduated from Chung Ling High School, Penang in 1953 and received from Oregon State University, Corvallis, Oregon the B.S. degree in Electrical Engineering(Communications) and the M.S. degree in Mechanical Engineering(Aerodynamics) in 1958 and 1959, respectively. While at Oregon State, he was variously the recipient of the Oregon State Tuition Scholarship and the Engineering Experimental Station Fellowship. From 1959 to 1962, he was an Instructor at Newark College of Engineering, Newark, New Jersey. Since 1962, he has joined the Electronics Research Laboratories of Columbia University, New York, N.Y. where he now holds the position of Senior Research Engineer. The experimental portion of his doctoral dissertation research was carried out at the Electronics Research Laboratories as part of several U.S. Air Force research contracts. The rest of the research was done at Newark College of Engineering, including the exploratory phase with the partial support of the Newark College of Engineering Research Foundation.